Carrier multipath mitigation in linear combinations of Global Navigation Satellite Systems measurements

Ramin Moradi

A thesis submitted for the degree of Doctor of Philosophy of the Imperial College London

Centre for Transport Studies
Department of Civil and Environmental Engineering
Imperial College London,
London,
United Kingdom

September 2014

Acknowledgements

Firstly, I would like to express my appreciation to my primary supervisor Professor Washington Yotto Ochieng who has been a constant source of support, knowledge and encouragement. His academic support has helped guide this thesis onto the correct path and enabled it to reach its desired aim. I would like to thank Dr Wolfgang Schuster, my second supervisor, for providing invaluable technical advice and research guidance, and for providing a friendly discussion environment around my work throughout the course of my research. I would further like to thank Dr. Shaojun Feng my third supervisor for his most helpful advice, especially during the early stage of the research. Special thanks go to my friend and colleague Dr Khalid Nur who provided me with invaluable support throughout the research, especially during the late stage with structuring and reviewing this thesis. I would also like to thank my colleague and friend Mr Altti Jokinen for supporting me from the first day of the research and helping me solve programing issues with admirable patience.

I am as ever, especially indebted to my parents for their love and encouragement in pursuing my path towards knowledge during the ups and downs of my life. To my father, Mr Mohammad Ali Moradi, who inspired me to sacrifice for knowledge. To my mother, Fatemah Entezari, who sacrificed everything in her life to support me in achieving all my goals. Special thanks go to my wife Mrs Razieh Musavi who supported me patiently throughout the research. She was the one who stood by me through the good and bad times. Last but not least, I would like to thank my three lovely children Ali, Kawsar and Mahdi who fill my life with love. I dedicate this thesis to them to encourage them to pursue the path to knowledge and I pray to Allah Almighty to support them like he supports me all the time.

Declaration of Contribution

During the research presented in this thesis, I have received advice from my supervisors, Prof. Washington Y. Ochieng, Dr. Wolfgang Schuster and Dr. Shaojun Feng. Their contributions were in line with the role defined by Imperial College London for supervisors. Furthermore, I had discussions with various colleagues, researchers and academics relevant to the research presented in this thesis. However, they have minor roles and none constituted a significant input to the research. Given the above, I hereby declare that apart from the statutory role played by the supervisors, the work presented in this thesis has been carried out by myself.

Copyright Declaration

Abstract

Global Navigation Satellite Systems (GNSS) are the main systems that provide positioning, navigation and timing at a global level. They are being used in numerous applications in different sectors including transport, military, oil & gas, agriculture as well as location based services.

A significant number of these applications require centimetre-level positioning accuracy, a challenging feat due to the many error sources that affect GNSS measurements. These include errors at the satellite, propagation medium, and receiver levels. Most of these errors can be mitigated by modeling, or by exploiting their spatial and temporal correlation characteristics. However, multipath errors, which result from the combination of the direct signal with reflected signals in the vicinity of the receiver antenna, are difficult to model and therefore, difficult to mitigate. Furthermore, high accuracy positioning applications typically rely on linear combinations of measurements at different frequencies (e.g. L1 and L2 in the case of the Global Positioning System) to mitigate frequency-dependent errors such as ionospheric errors (i.e. ionosphere free combination) or otherwise facilitate position calculation (e.g. Wide Lane observable). The multipath errors associated with such combinations are significantly larger than those of individual signals.

The dependency of the multipath error on the environment and its low level in single frequency measurements (i.e. up to quarter of wavelength) makes modelling and mitigating it very difficult. Current techniques attempt to mitigate multipath errors for measurements at each individual frequency, independently of the error at other

frequencies, even when linear combinations of measurements are used. The literature review carried out in this thesis has drawn three main conclusions regarding carrier multipath mitigation. Firstly, existing carrier multipath mitigation techniques are inaccurate, impractical or not effective. Secondly most of the practical techniques attempt to mitigate the error by de-weighting the measurements which are most prone to the multipath error (i.e measurement at low elevation). Thirdly, existing weighting techniques are oversimplified and do not reflect the error level accurately.

In this research and for the first time, carrier multipath errors have been studied directly at the linear combination level. This is by exploiting the dispersive nature of multipath errors in order to model and correct them. New carrier multipath mitigation techniques applicable to linear combinations of measurements have been developed in this thesis on the basis of a new error model and a new observable referred to as the IFM (Inter-Frequency carrier Multipath). The IFM is computed from carrier phase measurements at two different frequencies, and corresponds to the combined multipath errors of those signals. In addition to multipath mitigation, this observable has various other applications.

The well-defined relationship between the IFM and carrier multipath errors is used in this thesis to develop multipath mitigation techniques based on two approaches: multipath correction and measurement weighting. The new mitigation techniques are applicable to linear combinations of observations such as Wide Lane (WL) and Ionosphere Free (IF) carrier phase measurements in double differenced mode.

The new multipath mitigation techniques have been validated using real data and the results compared with those obtained using the elevation weighting technique. The results show that the new methods developed in this thesis improve the mean error of horizontal position by up to 33% when using the IF combination. The results also show improvements of up to 78% in the time it takes to resolve ambiguities when using the WL combination.

To my Children

Ali, Kawsar and Mahdi

Table of Contents

List of Figures

List of Tables

Nomenclature

AOD	Age Of Data
AR	Axial Ratio
ARNS	Aeronautical Radio Navigation Service
BOC	Binary Offset Carrier
CDMA	Code Division Multiple Access
CEP	Circular Error Probable
CS	Commercial Service
CSNAS	Chinese Satellite Navigation Augmentation Systems
DD	Double Difference
DOP	Dilution of Precision
EDM	electronic distance measurement
EGNOS	European Geostationary Navigation Overlay Service
ESA	European Space Agency
FDMA	Frequency Division Multiple access
FOC	Full Operation Capability
GAGAN	GPS Aided Geo Augmented Navigation
GBAS	Ground Based Augmentation System
GEO	Geo stationary Orbit
GNSS	Global Navigation Satellite Systems
GPS	Global Positioning System
HDOP	Horizontal Dilution of Precision
ICAO	International Civil Aviation Organization
IF	Ionosphere Free
IFB	Inter-Frequency Biases
IFI	Inter-Frequency Ionospheric error
IFM	Inter Frequency carrier Multipath
IGS	International GPS Service
IGSO	Inclined Geosynchronous Satellites Orbits
IMFM	Inter Multiple Frequency carrier Multipath
IPP	Ionospheric Pierce Point
JPL	Jet Propulsion Laboratory
KF	Kalman Filter
LAMBDA	Least-squares AMBiguity Decorrelation Adjustment
LHCP	Left-Hand Circular Polarized
LOS	Line Of Sight
MEDLL	Multipath Estimation Delay Lock Loop
MEO	Medium Earth Orbit
MFIF	Multipath Free IF

MFWL	Multipath Free WL
ML	Maximum Likelihood
MSAS	Multi-functional Satellite Augmentation System
NL	Narrow Lane
NLOS	Non-Line-Of-Sight
OS	Open Service
PDOP	Position Dilution of Precision
PPP	Precise Point Positioning
PPS	Precise Positioning Service
PRN	pseudorandom noise
PRS	Public Regulated Service
RHCP	Right-Hand Circular Polarized
RNP	Required Navigation Performance
RTK	Real Time Kinematic
SAR	Search and Rescue Service
SBAS	Satellite Based Augmentation System
SDCM	Russian System of Differential Correction and Monitoring
SEP	Spherical Error Probable
SLM	Single Layer Mapping
SoL	Safety-of-Life
SPS	Standard Positioning Service
STD	total slant delay
TDOP	Time Dilution of Precision
TEC	Total Electron Content
TECU	TEC units
TOA	time of arrival
TTAF	Time To Ambiguity Fixing
UERE	User Equivalent Range Error
VDOP	Vertical Dilution of Precision
VHF	Very High Frequency
WAAS	Wide Area Augmentation System
WL	Wide Lane
ZHD	Zenith Hydrostatic Delay
ZWD	Zenith Wet Delay

Chapter 1

INTRODUCTION

Positioning and navigation are increasingly important in our daily lives. Positioning technologies play an important role in supporting a wide range of applications with different accuracy requirements. Despite the maturity of current technologies, positioning for applications with stringent positioning and navigation performance requirements remains a challenge. The work presented in this thesis addresses this challenge. This chapter defines the context of the thesis through a brief background followed by the aim and objectives. It highlights the main contributions of this thesis and concludes with its structure.

1.1 Background

Positioning and navigation have a wide variety of applications in different sectors including transport, military, oil & gas, agriculture and location based services. These applications vary significantly in terms of their accuracy requirement (GALA 2000). The accuracy requirements range from mm-level in the case of surveying and structural monitoring to km-level for maritime navigation. This thesis addresses the challenging requirements of the former, i.e. high accuracy applications.

Over the past twenty years, Global Navigation Satellite Systems (GNSS) technology has become the main means for providing positioning, navigation and timing all over the world. GNSS has taken over from terrestrial positioning systems in many sectors due to the many advantages, including low cost and global coverage. By the end of this decade, the modernisation of GPS (USA) and GLONASS (Russia) will be complete, and Galileo (EU) and COMPASS (China) will have achieved Full Operation Capability (FOC). Despite the many advantages, GNSS also has a number of challenges to overcome including the need for better error mitigation. Extensive research is ongoing to address these challenges in order to achieve better performance in terms of accuracy and the other RNP parameters.

GNSS error sources can generally be classified into satellite errors, propagation medium errors and receiver errors. The satellite errors include ephemeris errors, satellite clock errors and hardware delays. The propagation medium errors are the result of atmospheric (ionospheric and tropospheric) disturbances, other unintentional interference

(e.g. multipath) and intentional interference. Receiver errors include receiver clock errors, hardware delays and noise (Kaplan and Hegarty 2006). Most of these errors are mitigated by one of four methods: the application of error models, the use of additional measurements (e.g. to correct the receiver clock errors), the application of measurement combination in different frequencies, the application of differential corrections, which exploit the spatial and temporal correlation characteristics of some of the errors (Leick 2004). Among the error sources, multipath is particularly challenging due to two main reasons. Firstly, its complex dependence on the local environment, which makes modeling difficult and secondly, its low spatial correlation characteristics making it unfeasible to apply the differential concept.

To date, different multipath mitigation techniques have been developed, each with significant limitations. Current techniques include the mitigation at the receiver antenna, mainly by exploring the GNSS signal polarization which changes after a single reflection. A GNSS antenna with higher sensitivity to the right-handed polarization rejects a reflected signal to some extent. However, the ability of an antenna to suppress a reflected signal depends on the satellite elevation angle. In addition, if a signal is reflected for a second time it is converted back to the original polarization. Therefore, a signal reaching the receiver is typically still contaminated with multipath errors when using this technique. Different signal processing techniques have been developed to mitigate the residual multipath at the receiver after passing the antenna (Moernaut and Orban 2008; McGraw and Braasch 1999; Sahmoudi and Landry 2008). However, the application of

signal processing techniques to mitigate short delay multipath errors caused by reflections from nearby objects, is very difficult, resulting in measurements typically being contaminated with short delay multipath. Such a level of residual multipath is acceptable for low accuracy positioning and navigation applications. However, it is not sufficient for high accuracy positioning applications (GALA 2000).

Different multipath mitigation techniques have been developed to mitigate residual multipath errors (Lau and Cross 2007b, 2006; Wieser and Brunner 2000; Lau and Cross 2007a). However, these are either not effective or not practical in common operational environments. Therefore, the residual multipath errors in the measurement domain are typically mitigated by applying stochastic models, such as the elevation based stochastic model. However, these models tend to be over-simplistic and are unable to accurately capture the multipath environment (Barnes et al. 1998). Furthermore, high accuracy applications typically rely on linear combinations of measurements at different frequencies (e.g. L1 and L2 in the case of GPS) to mitigate frequency-dependent errors such as ionospheric errors (i.e. ionosphere free combination) or otherwise facilitate the positioning calculation (e.g. Wide Lane observable). The drawback is that such combinations considerably increase the residual multipath errors.

1.2 Aim and objectives

Given the issues identified above, the aim of this thesis is to develop an effective and practical multipath mitigation technique for linear combinations of measurements for

high accuracy positioning applications. The thesis focusses on static applications, with a high level consideration of the transferability of the developed technique to dynamic applications.

In order to achieve this aim, the following research objectives have been formulated:

1. Identify the target GNSS positioning applications based on their challenges and vulnerability to multipath errors.
2. Review the positioning techniques applicable to the applications and identify their limitations focusing on multipath errors.
3. Carry out a detailed review of different multipath mitigation techniques, quantify their performance and identify their strengths and weaknesses.
4. Model the multipath errors focusing on the target applications.
5. Investigate the prospect of forming a new observable from GNSS measurements, representative of the multipath condition.
6. Develop new multipath mitigation techniques based on the new observable for the target applications.
7. Validate the new techniques using real data representative of common operational environments for the target applications.

1.3 Research contributions

This research distinguishes itself in the domain of carrier phase multipath error mitigation, by mitigating the error directly in the linear combinations of measurements as opposed to each individual frequency separately. In line with the identified aim and objectives, the thesis makes the following novel contributions in the field of carrier multipath modelling and mitigation.

1. Solution of the issue of carrier phase multipath error directly in the measurements formed by linear combinations as opposed to individual frequency measurements. This new approach has resulted in the introduction of a novel carrier multipath error model for linear combinations.
2. Successful resolution of the difficulty of isolating the carrier multipath error by introducing the Inter Frequency carrier Multipath (IFM) observable, derived from raw carrier phase measurements. The IFM observable is directly related to the carrier multipath error in the measurements. Therefore, it can be used for carrier multipath error modelling and mitigation.
3. Development of new carrier phase multipath mitigation techniques based on the IFM observable. The new techniques are able to detect the carrier multipath error level and mitigate the error in the linear combinations by

either correcting the measurements or applying a more accurate weighting. These new techniques have been validated for carrier multipath mitigation in the Ionosphere Free (IF) and Wide Lane (WL) combinations.

The research conducted in this thesis resulted in several publications which are listed here:

a) Moradi R, Schuster W, Feng S, Jokinen A, Ochieng W (2014) The carrier-multipath observable: a new carrier-phase multipath mitigation technique. GPS Solutions:1-10. doi:10.1007/s10291-014-0366-8
b) Moradi R, Schuster W, Feng S, Ochieng W (2013) A New Carrier Phase Multipath Mitigation Technique for Ionosphere-free Combination. In: Proc. ION-ITM 2014, Institute of Navigation, San Diego, California, January 27 - 29 2014b. 2014, pp 562 – 567
c) Moradi R, Schuster W, Feng S, Ochieng W (2013) Reducing GPS Wide Lane Ambiguity Resolution Time: A Novel Carrier Phase Multipath Mitigation Technique. In: Proc. ION-ITM-2013, Institute of Navigation, San Diego, California, January 29 - 27 2013. pp 343 – 350

In addition, the next journal paper has been submitted to GPS Solutions and is under review:

Moradi R, Schuster W, Feng S, Jokinen A, Ochieng W (2014) Inter frequency carrier multipath based stochastic model for Wide Lane observable, GPS Solutions (under review)

1.4 Outline of the thesis

The thesis is composed of 8 chapters starting with the introduction. The remainder of the thesis is structured as follows:

Chapter 2: *GNSS applications and overview*

This chapter provides an overview of the applications of relevance to this thesis and the existing and near-future Global Navigation Satellite Systems (GNSS). The latter is addressed in terms of operational concept, measurement types and error sources.

Chapter 3: *GNSS augmentation*

The different GNSS augmentation systems are discussed in this chapter with a focus on their capability to support high positioning accuracy applications. In this respect both code phase and carrier phase based augmentation techniques are discussed.

Chapter 4: *Multipath error*

This chapter details the impacts of multipath on different GNSS measurements and discusses the existing multipath mitigation techniques along with their strengths and limitations.

Chapter 5: *Carrier multipath mitigation in linear combinations*

In this chapter, the importance of mitigating carrier multipath error in linear combinations is justified by making an analytical comparison of the error in linear combinations with the error in individual frequency measurements. The error in linear combinations is modelled and a new carrier multipath observable is derived. Based on the new observable new multipath mitigation techniques are developed.

Chapter 6: *Carrier multipath mitigation in IF combination*

This chapter defines the test cases and data collection methodology. The multipath mitigation techniques developed in chapter 5 are applied to the IF combination using the test cases and data, with the aim of decreasing the positioning error.

Chapter 7: *Carrier multipath mitigation in WL observable*

In this chapter the multipath mitigation techniques are tested in the mitigation of carrier multipath error in the wide lane observable, with the aim of decreasing the ambiguity resolution time.

Chapter 8: *Conclusions, implementations and future work*

This chapter discusses the implementation issues of the new multipath mitigation techniques. Conclusions are made and future research and development for improved IFM estimation and IFM-based multipath mitigation techniques are discussed.

Chapter 2

GNSS APPLICATIONS AND OVERVIEW

The past twenty years have witnessed a revolution in the development of positioning and navigation technologies, with the dominance of the Global Navigation Satellite Systems (GNSS). The GNSS revolution has been driven by the multitude of existing and newly emerging GNSS applications. GNSS provides positioning and timing services in any place near the Earth with relatively lower cost. Despite their many advantages, GNSS also suffer from a number of drawbacks which limit their use for some applications. Extensive research effort is on-going to improve the performance of existing GNSS in order to unlock further applications limited by the current systems.

The first part of this chapter provides a non-exhaustive list of GNSS applications with emphasis on a subset of applications targeted in this thesis. The second part provides an overview of GNSS covering its operational concept, system architecture, signal

characteristics and error sources, as well as the mathematical models required to estimate the user position. The current status of the different GNSS is discussed also.

2.1 GNSS positioning applications

GNSS positioning applications can be categorized based on various criteria such as the user group (e.g. transport, agriculture, security, leisure), operational environment (i.e. rural, urban, dense urban or indoor) or the Required Navigation Performance (RNP) in terms of accuracy, integrity, continuity and availability (GALA 2000). In this thesis, positioning applications are categorized based on their accuracy requirements, into two groups, low-accuracy and high-accuracy applications.

2.1.1 LOW-ACCURACY POSITIONING APPLICATIONS

Low accuracy applications are defined in this thesis as requiring position accuracy at the level of one metre or lower, and include a large number of applications such as vehicle navigation, air navigation, fleet management, wild animals tracking, forestry and route guidance (GALA 2000). The applications in this category can be supported largely by the use of the current GNSS along with existing error mitigation techniques.

2.1.2 HIGH-ACCURACY POSITIONING APPLICATIONS

High accuracy applications require positioning accuracy at the decimeter level or better. Such applications are very diverse and include surveying, geodynamics, reference frame maintenance, atmospheric monitoring and orbit determination of low Earth orbiting satellites, discussed in the next subsections. Given the more stringent accuracy requirements of these applications, more advanced error mitigation techniques are required. Therefore, this thesis addresses error mitigation with a particular focus on carrier multipath errors. This is due to the difficulties in detecting and mitigating such errors.

2.1.2.1 Surveying

Surveying was one of the first high accuracy applications of carrier phase GNSS which typically requires cm-level positioning accuracy. The use of GNSS in surveying is due to their numerous advantages over terrestrial surveying techniques. Such advantages include faster data collection and less required equipment and labor forces. However, carrier multipath produces an error in the calculated position or delays achieving the required accuracy. Therefore, the GNSS antenna must be located far enough from any obstructions to avoid multipath error. However, it is not always possible to locate the antenna in a favorable place. Furthermore, multipath error due to reflection from ground is also of great concern in surveying by GNSS. Therefore, measurements from low

elevation satellites are usually discarded to avoid such an error. This is not desirable as it reduces the number of measurements. Therefore, an effective carrier multipath mitigation technique will improve surveying by GNSS (Rao 2010).

2.1.2.2 Geodynamics

Geodynamics is a branch of Geophysics which deals with the dynamics of the earth such as monitoring the earth tectonic plates and changes in active volcanos. Monitoring tectonic plates movement improves the prediction of earthquakes while monitoring changes in volcanos enables accurate prediction of their eruption. The monitoring of such events requires the estimation of velocity and position at the cm-level accuracy and at a global scale for the case of tectonic plate movements. The use of high accuracy GNSS in geodynamics improves the accuracy of events prediction and overcomes the limitations of existing applied technologies such as the electronic distance measurement (EDM) (Segall and Davis 1997). However, the carrier multipath error is the main remaining error source which prevents achieving the required accuracy in geodynamic applications (Puchrik et al. 2014).

2.1.2.3 Reference frame maintenance

Terrestrial reference frames require accurate measurements of selected points located on the Earth surface. Existing global, continental and national reference frames

are maintained by monitoring GNSS stations spread in the target areas. In this application, high accuracy relative positioning between stations is of great importance. The required accuracy for reference frame maintenance is in the order of centimtres, achievable using GNSS carrier phase measurements. Therefore, the used GNSS monitoring stations must be free from carrier multipath error. This requires a reliable carrier multipath detection technique for reference frame maintenance.

2.1.2.4 Atmospheric monitoring

Meteorologists extract water vapor content of the lower part of the atmosphere from GNSS measurements to conduct numerical weather prediction. Furthermore, GNSS is used to monitor the ionosphere, including storms, other ionospheric disturbances, and scintillation, as well as other space weather. Such information can be utilized in communications, space science and earthquake forecasting. The accuracy requirement for atmospheric monitoring using GNSS measurements is at the level of decimetres or even centimetres (Notarpietro et al. 2012; GALA 2000). Achieving such level of accuracy requires an effective technique for carrier multipath mitigation.

2.1.2.5 Orbit determination of low earth orbiting satellites

Orbit determination of low earth orbiting satellites has several applications. Examples include geoid determination and mapping of the Earth's gravity field which

require knowledge of the satellite position with cm-level accuracy or better (GALA 2000; Swatschina). While such a high accuracy requirement can be achieved using a GNSS receiver, there is a need for multipath mitigation. Such multipath arises from the satellite body and its solar arrays (Rim and Schutz 2002).

2.1.2.6 Summary of applications

This section has provided a non-exhaustive list of high-accuracy positioning applications and the potential of GNSS to satisfy their requirements. A more comprehensive review of various other high-accuracy applications are provided in (GALA 2000; Jenkins and Caswell 2007). In order for GNSS to support the high accuracy requirements of these applications, it is important to mitigate the effects of the different GNSS error sources including carrier multipath error. This is a challenging task, as discussed in Section 2.3.

2.2 GNSS Overview

Currently GPS (USA) and GLONASS (Russia) are the main operational GNSS. It is expected that by the end of this decade Galileo (EU) and COMPASS (China) will also achieve Full Operation Capability (FOC). Despite various differences (discussed in Section 2.2.2), these GNSS share a number of common characteristics, including their main operational concept, system architecture, extracted measurements and error sources.

This section discusses these common characteristics (Section 2.2.1) and the various systems currently in operation or under construction (Section 2.2.2). Their error sources are discussed in Section 2.3.

2.2.1 GNSS OPERATIONAL CONCEPT AND ARCHITECTURE

Each GNSS consists of 3 main segments: space, control and user segments. The space segment consists of a set of satellites, each of which generates and transmits ranging signals and navigation messages to the user receiver. The Navigation message contains the necessary information to compute the range. This information includes transmission time and the satellite position or Keplerian parameters from which the satellite position is calculated at the time of signal transmission. The ranging signal has a spreading code also known as the pseudorandom noise (PRN) code, which consists of chip units. One chip is the minimum interval between two transitions in the code. The chipping rate of the spreading code determines the spread of energy of the signal across the frequency band, impacting the range estimation accuracy. Higher chipping rates spread the energy over wider frequency bands, leading to better rejection of narrow band interference. The PRN code modulates an RF carrier signal with a frequency that is dependent on the signal and the GNSS. A given constellation should provide at least 4 operational satellites in view at any point of interest on the Earth. The reasons for this number are explained later in this section.

The Control segment is also known as the ground segment and consists of a network of monitoring stations installed at carefully selected locations worldwide. The main activities of the control segment are to monitor and control (including command) the satellite constellation. It also predicts and updates the satellite navigation message.

The user segment is composed of a receiver capable of decoding the range signals transmitted by the satellites. Based on the transmission times by each satellite in view, it computes the ranges and the position of the receiver. Once the signal has been received by the antenna and pre-processed, the main functions of a GNSS receiver are acquisition, tracking and calculation of the position and time. The acquisition function identifies the satellites from which the signals have been received. It also makes rough estimation of the received signal parameters such as carrier frequency and code phase (chip number). The tracking function refines the parameters obtained in the acquisition phase and tracks changes in these parameters continuously as long as it receives the signal. The receiver decodes the navigation message from the received signal and performs the necessary operations to calculate the position and time (Kaplan and Hegarty 2006).

Position determination by GNSS is based on the trilateration/multilateration concept in which the 3D position of a point is determined by measuring its distance/range to three or more reference points with known positions. GNSS satellites act as reference points and each range measurement defines a sphere centred at the satellite centre of mass or satellite antenna phase centre. If measurements were errorless, three such spheres would intersect, defining the receiver position. The distance measurements in GNSS are

achieved using the time of arrival (TOA) concept in which the travel time of a radio signal from a transmitter to a receiver is measured. By scaling the travel time by the speed of the signal, the distance between the transmitter and receiver is calculated. A GNSS system typically provides two types of range measurements known as code phase and carrier phase measurements. Code phase measurements estimate the satellite signal arrival time by correlating the received PRN code with a locally generated copy at the receiver. The travel time of the satellite signal is estimated from the difference between the signal transmission and reception times, which must be precisely known. Both satellite and receiver clocks may be biased with regard to the GNSS system time. Satellite clocks are very stable and have readily available correction parameters. Hence, the satellite clock bias is assumed to be zero at this point, and the code phase measurement *P* can be represented as:

$$P = \rho - cdt_k \tag{2.1}$$

where ρ is the true range between satellite and receiver, c is speed of light and dt_k is the receiver clock error.

In addition to code phase measurements, a GNSS receiver is also able to measure accurately carrier phase differences between epochs of times. By accumulating the phase differences, carrier phase measurements are obtained. From these measurements, range measurements can be calculated, which are significantly more accurate than code phase measurements. However, this requires the number of complete cycles, referred to as

integer ambiguities (N), to be resolved. High accuracy (i.e. centimtre level) positioning is achieved using carrier phase measurements. Carrier phase measurements are discussed in more detail in Chapter 3.

2.2.2 EXISTING AND NEAR FUTURE GNSS

2.2.2.1 GPS

The Global Positioning System (GPS) provides a 24-hour positioning and timing service worldwide. It was built and is being operated and maintained by the US government, with Full Operational Capability (FOC) since 1995. GPS was designed to have 21 active and 3 spare satellites in 6 orbital planes which are equally spaced at the equator with 60 degrees separation. However, there are usually more than 24 operational satellites although the extra satellites are not part of the core constellation. In Jun 2011 a GPS constellation expansion was completed with 6 satellites being relocated and 3 extra satellites became part of the constellation. As a result, the GPS constellation became a 27-slot constellation. The orbital inclination at the equator is 55 degrees. GPS satellites are located about 20200km above the Earth in near-circular orbits. The nominal period of a GPS satellite in its orbit is 11 hours and 58 minutes which is half of a sidereal day. Each GPS satellite passes the same place on the Earth after one sidereal day (approximately 24 hours).

GPS is designed to provide two levels of service: Standard Positioning Service (SPS) and Precise Positioning Service (PPS). According to specification the SPS provides horizontal and vertical accuracies better than 9m and 15m 95% of the time (DoD 2008).

GPS signals are transmitted on two radio frequencies: L1 (1575.42 MHz) and L2 (1227.60 MHz). Furthermore, each GPS satellite transmits two unique spreading codes, the open coarse acquisition code (C/A) and the encrypted precision code (P(Y)), using a technique referred to as Code Division Multiple Access (CDMA) (Kaplan and Hegarty 2006). The C/A code has a length of 1023 chips with a chipping rate of 1.23 MHz which results in the code being repeated every 1ms. In contrast, the P code has a potential length of $2.3547 * 10^{14}$ chips with a chipping rate of 10.23MHz. The P sequence is truncated at the end of the week (Saturday/Sunday midnight), resulting in $6.1871 * 10^{12}$ chips. The C/A code is modulated on the L1 carrier while the P code is modulated on both the L1 and L2 carriers.

Each GPS satellite has a known unique spreading code. They use a transmitting technique called as code division multiple access (CDMA) in which different transmitters use different code and share a common frequency (Kaplan and Hegarty 2006).

2.2.2.1.1 GPS modernization

Modernization of GPS was announced in 1999 with the promise of adding two new civil signals, L2C and L5. The L2C signals are relayed on the L2 carrier for non-safety of life applications. The L5 frequency is designed to operate in the Aeronautical

Radio Navigation Service (ARNS) band, at 1176.45MHz, for safety-of-life applications. In addition to the new civil signals, a military signal, the M code, are designed for transmission on the L1 and L2 frequencies, separated spectrally from the civil signals. The M code is used for PPS and provides better resistance against interference, more robust acquisition, increased accuracy and better security compared to the P(Y) code. The first satellite in Block IIF containing all the signals including L5 was launched in 2010. GPS L1 and L2 signals are BPSK modulated, while the modernized signals use the Binary Offset Carrier (BOC) modulation, which has sharper correlation peaks (Kaplan and Hegarty 2006).

2.2.2.2 GLONASS

The Global Navigation Satellite System (GLONASS) was originally developed by the Soviet Union to provide both civil and military services. It is currently owned and operated by the Russian Federation. It was designed to have 21 active satellites in 3 orbital planes with an additional spare satellite in each orbital plane. The satellites are uniformly distributed in each plane. The orbital period is 11 hours and 15 minutes. Each satellite passes the same point on the earth after 8 sidereal days. With 21 satellites, at least 4 satellites should be visible over 97% of the Earth's surface at any time. According to the Russian Federal Space Agency Information Analytical Centre, from March 2014, 24 GLONASS satellites were "in operation" in addition to three "spare" satellites. The orbits of the GLONASS satellites are circular at 19100km above the Earth's surface with

an inclination of 64.8 degrees to the equator. According to the Russian System of Differential Correction and Monitoring (SDCM), as of 23 January 2012, the position accuracies obtained by GLONASS were worse than the accuracies obtained by GPS for 4 selected monitoring stations (at 95% probability). GLONASS provided the positions with horizontal errors between 4 and 7m and vertical errors between 10 and 15m. On the other hand, GPS provided position errors between 2 and 4m in the horizontal direction and 5 to 9m in the vertical direction for the same stations (SDCM 2012).

GLONASS uses the Frequency Division Multiple Access (FDMA), where all satellites use the same PRN code modulated at different frequencies. FDMA is more robust against narrow band interference as only those satellites transmitting in this band are affected. On the other hand, for the CDMA technique where all satellites operate on the same frequency, narrow band interference has the potential to block the signals on all satellites. The disadvantage of using FDMA is that it requires more complex receivers, capable of processing a multitude of frequencies. GLONASS L1 signals are transmitted using different frequency channels. The frequencies are obtained as:

$$1602MHz + n * 0.5625MHz$$

where n is the satellite frequency channel number and takes integer values from 7 to 6. A receiver on the Earth's surface is not able to receive signals from satellites having the same orbit and separated by 180 degrees known as antipodal satellites. Hence, every antipodal satellite pairs have the same frequency channel. Similarly, the frequencies of the L2 signals are obtained as:

$$1246MHz + n * 0.4375MHz$$

where *n* can also take integer values ranging between -7 and 6.

Similar to GPS, GLONASS has a C/A code for civil use and a P code for military use. The C/A code has a rate of 0.511 Mchips/s. The code length is 511 chips and repeats every 1ms. The P code rate is 5.11 Mchips/s and the code length is 33,554,432 chips. The code is truncated resulting in repetition rate of 1Hz. The acquisition of the P code is more difficult than the C/A code due to the 511 million different code phase possibilities. Therefore, it is common to first acquire the C/A code to narrow down the search possibilities before attempting to acquire the P code (Kaplan and Hegarty 2006).

2.2.2.2.1 GLONASS modernization

The GLONASS modernisation program includes the introduction of the CDMA signal on an L3 band carrier. This has the benefit of facilitating increased interoperability with the other GNSS. In addition, the introduction of new signals will provide services for additional applications which require measurements at two or three frequencies. Currently, most of the GLONASS satellites are of the GLONASS-M design with civil signals transmitting in the FDMA mode on the L1 and L2 bands. The next generation of GLONASS satellites, known as GLONASS-K started transmission in February 2011 in the L1, L2 and L3 bands. The L1 and L2 carriers are modulated in the FDMA mode as before, while the signal in the L3 band is modulated in the CDMA mode. The next step

for GLONASS modernisation will be started after launching the first GLONASS-K2 satellite, scheduled for 2015. GLONASS-K2 will transmit FDMA signals in the L1 and L2 bands. In addition, CDMA signals will be transmitted on L1, L2 and L3 (GPSWold 2011).

2.2.2.3 Galileo

GALILEO is being built by the European Space Agency (ESA). It has been designed to have 30 satellites with 27 operational and 3 active spares located in 3 circular orbits at 23222km above the Earth. The satellites orbits are inclined at 56 degrees to the equatorial plane. The orbital period is 14 hours and 7 minutes. Galileo is designed to provide good coverage up to 75 degrees in latitude north and south of the equator (Avila-Rodriguez, 2008). The large number of satellites with active spares in addition to the constellation optimisation provide a better availability than all other constellations. The first Galileo experimental satellite called GIOVE-A was launched on 28 December 2005. It was followed with the launch of the second experimental satellite GIOVE-B. According to the European GNSS Service Centre, there were 4 GIOVE satellites in orbit as of February 2014. Galileo is expected to reach FOC by the end of the decade.

Similar to GPS, Galileo uses the CDMA technique. It will provide various services, namely Open Service (OS), Safety-of-Life Service (SoL), Commercial Service (CS), Public Regulated Service (PRS) and Search and Rescue Service (SAR). The OS is transmitted at the same frequency as GPS L1. The Galileo L1 frequency consists of three

channels (L1-A, L1-B and L1-C). Access to L1-A is restricted to Public Regulated Service (PRS). The other two channels, L1-B and L1-C are known as data and pilot signals respectively. The data signal contains the navigation message and the pilot is used for range calculation. According to the Galileo Mission High Level Definition, the OS will provide horizontal and vertical accuracies better than 15m and 35m 95% of the time. (ESA 2002)

The Galileo signal modulation has been improved over that of the GPS signals by using the Binary Offset Carrier (BOC) modulation technique. This also ensures that the main peaks of the Galileo signal have minimal interference with the GPS L1 signal. The BOC modulation, in addition to the code and carrier, has a third component referred to as the subcarrier (excluding data). The subcarrier is a square wave type. A BOC modulation is identified as BOC (m, n) where m and n are the subcarrier frequency in units of 1.023MHz and code chipping rate in units of 1.023 MHz respectively. For example BOC(1,1) which is used in L1-OS signals has a subcarrier frequency of 1.023MHz and a code chipping rate of 1.023MHz (Borre et al. 2007). The code length in L1-B (data channel) is 4092 chips (four times the GPS CA code length) which has a repetition period of 4ms. Using such a long code provides better separation between wanted and unwanted signals, due to better cross correlation performance. The L1-C (pilot channel) code is made of a primary code of 4092 chips and a secondary code of 25 chips. The secondary code extends the repetition period of the L1-C code to 100ms.

2.2.2.4 Beidou/Compass

The BeiDou Navigation System (BDS) is an extension to the Chinese regional system known as BeiDou-1. The BeiDou-1 system consists of 3 Geo stationary Orbit (GEO) satellites launched between 2000 and 2003 and provides regional positioning services in China (Samama 2008). The BeiDou-1 requires two-way communication between the central control station and the user receiver via GEO satellites.

BDS, also known as COMPASS, is currently under development with a future constellation of 5 geostationary orbit satellites, 27 Medium Earth Orbit (MEO) satellites and 3 Inclined Geosynchronous Satellites Orbits (IGSO) satellites. The development of the BDS will be completed in two steps. The target of the first step was to achieve regional coverage over China and neighboring areas. The second step targets global coverage of the system. The first step has been completed after the successful launch of 5 GEO satellites and 8 non-GEO satellites between 2007 and 2012. The altitude of the GEO satellites is 35,786km. The MEO satellites are at an altitude of 21,528km above the earth with an orbital inclination of 55 degrees to the equator. The IGSO satellites have also an inclination of 55 degrees at an altitude of 35,786km. In December 2012 the system started its services for the Asia-Pacific region. Global coverage is expected to be achieved by 2020. According to the BeiDou Navigation Satellite System official website, BDS open service will provide a position accuracy of about 10m.

The multiplexing technique used by BDS signal is CDMA similar to GPS. BDS transmits its signals over 4 different bands. The modulation technique used is BPSK. The

system will provide two levels of services which are free civilian and restricted ones. The open service signal known as B1I consists of code and navigation message modulated on a carrier with frequency of 1561.098 MHz. The B1I ranging code has a length of 2046 chips with a chip rate of 2.046Mcps (BDS 2014).

2.2.2.5 GNSS summary

In addition to the modernisation of GPS and GLONASS, a large number of new signals will be transmitted by Galileo and BDS in the near future. Multiple systems and signals will provide opportunities to create linear combinations of signals with different frequencies and error characteristics, enabling amongst others to better mitigate errors that are frequency dependent including those induced by the ionosphere and multipath. Although multiple GNSS systems with improved signal structures will bring significant benefits, there are also significant GNSS error sources which must be addressed in order to achieve high accuracy positioning.

2.3 GNSS error sources

The position accuracy obtained by a GNSS depends heavily on the magnitude of the different error sources affecting the estimation of the range measurements. Dedicated efforts are ongoing to model and mitigate these error sources. The errors can be classified into satellite errors, propagation medium errors and receiver errors. In addition to the

error sources, satellite geometry in relation to the receiver measured by Dilution of Precision (DOP) parameter also affects the performance of positioning by GNSS. In this section the main GNSS errors are presented and common ways of dealing with them are discussed. This is followed by a discussion of the DOP parameters.

2.3.1 SATELLITE ERRORS

There are three main error sources associated with GNSS satellites: satellite clock, satellite hardware delay and ephemeris errors.

2.3.1.1 Satellite clock errors

For a receiver to accurately estimate the GNSS signal travel time and hence the range measurement, it is imperative to know the signal transmission time based on the GNSS time with a high accuracy. Although very stable atomic clocks are used in the GNSS satellites, deviation of the satellite clock from the system time can be as large as 1ms, causing an error of 300km in the range measurements. Therefore, satellites broadcast clock parameters to the user via the navigation message from which the receiver calculates the satellite clock correction. After correcting the clock error, the residual range error for the GPS satellite lies between 0.3-4m depending on the satellite type and the Age Of Data (AOD) (i.e. the time since the data was uploaded from the control segment). The accuracy of the correction is best at zero AOD and deteriorates

gradually with time. When the AOD reaches 24 hours, the range error becomes typically between 1-4m. The 1-sigma satellite clock error averaged over AOD in 2004 for GPS constellation was 1.1m (Kaplan and Hegarty 2006).

2.3.1.2 Satellite hardware delay

Satellite signal generation is accomplished by passing the signal through an electronic path, which causes delays in the signal. The delay is different for signals at different frequencies and is referred to as group delay bias. Therefore, it must be taken into account if linear combinations of measurements are formed from different frequencies. The GPS broadcast clock correction compensates for the L1 and L2 group delay bias with the assumption of using Ionosphere Free combination. This combination of measurements is formed to mitigate the ionospheric effect on the measurement and will be discussed in Section 1.4. The group delay bias for GPS L1 and L2 could be as large as 2.4m (2 sigma) (Kaplan and Hegarty 2006).

2.3.1.3 Ephemeris error

The accurate calculation of the receiver position requires an accurate knowledge of the satellite positions. The satellite position data or ephemeris can be broadcast to users in the navigation message either directly, as in the case of GLONASS, or through a set of orbital parameters, as in GPS. Ephemeris are predicted at ground stations and uploaded to

each satellite. Errors in modelling the satellite orbit lead to residual satellite position errors. The effective pseudorange error due to the satellite position error is the projection of the satellite position error vector to the satellite-receiver vector, and is of the order of 0.8m (1 sigma). The accuracy of the broadcasted ephemeris improves over time. More accurate ephemeris products of GPS and GLONASS are collected by the international GNSS service from a global network of GNSS reference stations. The ephemeris products are available at the IGS Analysis Centres over the Internet and through private service providers (Kaplan and Hegarty 2006).

2.3.2 PROPAGATION MEDIUM ERRORS

This group of error sources affects the GNSS signals between the satellites and receivers. They correspond to atmospheric effects and other interference, including multipath.

2.3.2.1 Atmospheric effects

In the context of signal propagation at GNSS frequencies, the atmosphere consists of two main layers: ionosphere and troposphere. Each layer affects signal propagation in different ways, including signal refraction, signal bending, modulation delay, carrier phase advance, and scintillation. Of these signal bending can be ignored because the

range errors in the measurements from satellites with an elevation above 5 degrees (the only ones typically used to compute the user position) are negligible.

2.3.2.1.1 Ionospheric error

The ionosphere layer extends from approximately 50 to 1500 km above the Earth. It contains ions including free electrons (negatively charged), positively charged atoms and molecules. The total number of free electrons in the propagation path in the column of unit area ($1m^2$) is called Total Electron Content (TEC). The TEC along the signal path between the satellite and receiver in TEC units (TECU), equivalent to $10^{16} electron/m^2$ is:

$$TEC = \int_r^s N_e ds$$

2.2

where N_e is the electron density in $electron/m^3$. The ionospheric error (in units of length) of an electromagnetic wave with a frequency of f passing through the ionosphere can be approximated as:

$$I_{error} = \frac{40.30}{f^2} TEC$$

2.3

The free electrons in the ionosphere layer advance carrier phase and delay code phase measurements by the same amount of range error. Depending on the electron density, the ionospheric error for GNSS signals may reach tens of meters. The electron density (N_e) is a function of time and place. N_e is relatively low and flat at night and varies approximately sinusoidally during the day, peaking at around 2.00 PM. This behavior of the ionospheric error occurs under stable ionospheric conditions and is captured by the Klobuchar model (Angrisano et al. 2011):

$$I_t = F\left(DC + A\cos\left(\frac{2\pi(t - t_0)}{P}\right)\right) \quad 2.4$$

Where I_t is the ionospheric delay at the time of day *t*, *F* is the oblique factor related to satellite geometry, *DC* is the amplitude of the daily cosine component, $t_0$is the peak time of the daily error which is 14:00 local time in seconds and *P* is the period of the cosine component.

For GPS, the parameters for calculating the ionospheric error using the Klobuchar model are broadcast by the satellites in the navigation message. Up to 60% of the ionospheric error can be corrected using this model (Leick 2004). Other GNSS may use different ionospheric models and include the required parameters in their navigation message. For example, Galileo uses a more advanced ionospheric model known as NeQuick (Bidaine and Warnant 2011). The performance of the NeQiuck model is still under investigation. (Angrisano et al. 2011) has shown that the NeQuick model provides

slight improvements compared to the Klobuchar model. Unlike GPS and Galileo, GLONASS does not include any ionospheric parameters in its navigation message.

The TEC is usually specified in terms of a vertical column and the error obtained from equation 2.3 is the vertical ionospheric error. The error magnitude for other elevations can be obtained by using different mapping functions such as the Single Layer Mapping (SLM) function (Komjathy and Langley 1996; Mannucci et al. 1998). In this function it is assumed that all the free electrons are concentrated in an infinitesimal spherical layer around the earth. The SLM expresses the relstionship between the vertical and slant TEC values based on:

$$SLM = \frac{1}{\cos(z')} \tag{2.5}$$

where z' is the geocentric zenith distance at the Ionospheric Pierce Point (IPP). IPP is defined as the intersection of the signal with the ionospheric layer at height of 350 km. The angle z' is obtained from the geocentric zenith distance z at the height of the receiver based on:

$$z' = \arcsin\left(\frac{R}{R+H} sin(z)\right) \tag{2.6}$$

where R is the mean radius of the earth (approximately 6371km) and H is the height of the assumed single layer usually set between 350 to 450km. A value of 428.8km is suggested by (Schaer 1999) as the optimum value.

If measurements at two frequencies are available, based on equation 2.3 the first order of the ionospheric error which accounts for about 99% of the total error can be removed by forming appropriate linear combinations, as discussed in detail in Sections 2.4.1 and 2.4.2.

2.3.2.1.2 Tropospheric error

The troposphere is the lowest atmospheric layer and extends from 0km to 50km above the earth's surface. The existence of natural gases in the troposphere causes signals to be refracted. The troposphere behaves as a non-dispersive medium for signals with frequencies lower than 30GHz, i.e. the refraction of the signal is independent of the signal frequency. The signal delay in the tropospheric layer (T) can be divided into two parts, hydrostatic or dry (T_h) and wet (T_w) as:

$$T = T_h + T_w$$

The hydrostatic component causes zenith delays (ZHD) of about 240 cm at sea level. ZHD can be calculated accurately in the receiver based on the atmospheric pressure, using for example, the commonly used Saastamoinen model (Leick 2004):

$$ZHD_{[m]} = \frac{0.0022768 P_{0_{[mbar]}}}{1 - 0.00266 \cos 2\varphi - 0.00028 H_{[km]}}$$

2.7

where P_0 is the pressure calculated at the receiver, H is height and φ is the latitude of the receiver.

The wet component at zenith (ZWD) causes delays of up to 40 cm. The ZWD is more difficult to calculate because the water vapor content is temporally and spatially correlated. Mendes and Langley propose the following model for the ZWD (Mendes and Langley 1998):

$$ZWD_{[m]} = 0.0122 + 0.00943\, P_{wv,0[mbar]}$$

2.8

where $P_{wv,0[mbar]}$ is the surface partial water vapour pressure. The problem with this model is that it is based on measurements on the Earth's surface, with for example, water vapour that may be significantly different from that in the upper layers.

Mapping functions are required to obtain the slant tropospheric delays (delay at elevations other than the zenith), from ZHD and ZWD. An example of mapping function is Black and Eisner's mapping function:

$$m(E) = \frac{1.001}{\sqrt{0.002001 + \sin^2(E)}}$$

2.9

where E is the satellite elevation angle. The total slant delay (STD) is then calculated as:

$$STD = ZHD.m(E) + ZWD.m(E) \quad 2.10$$

According to (Kaplan and Hegarty 2006) the residual tropospheric delay after applying equation 2.10 is a 0.2m (1-sigma).

2.3.2.2 Interference

The low power GNSS signal is vulnerable to intentional and unintentional interference which can result in degraded navigation accuracy or complete loss of receiver tracking. Intentional interference includes jamming and spoofing. Unintentional interference is the result of any transmissions in the same L band frequency as GNSS. Numerous devices exist that transmit in this band. Depending on the interference characteristics, different mitigation techniques may be used. For example, narrowband and pulse radio frequency interference can be mitigated by spectrum excision techniques in which the narrow band interference is reduced below the noise level. However, this technique also suppresses the GNSS signal.

Mitigation of wideband interference can be achieved by gain steering the antenna main lobe towards the satellites and the nulls towards the source of interference (e.g. a jammer). A directional antenna consisting of several antenna elements may be used for

this purpose. However, these antennas tend to be bulky and require additional signal processing functions. Due to these limitations, directional antennas are mainly used in military receivers (Kaplan and Hegarty 2006).

2.3.2.3 Multipath

Multipath error is a common problem in positioning using GNSS in which the signal is reflected off surrounding objects and combined with the direct signal at the antenna. If the signal arrives at the receiver via additional paths other than the direct line of sight, the accuracy of the range calculated by the receiver is degraded. Figure 2.1 illustrates a typical multipath situation.

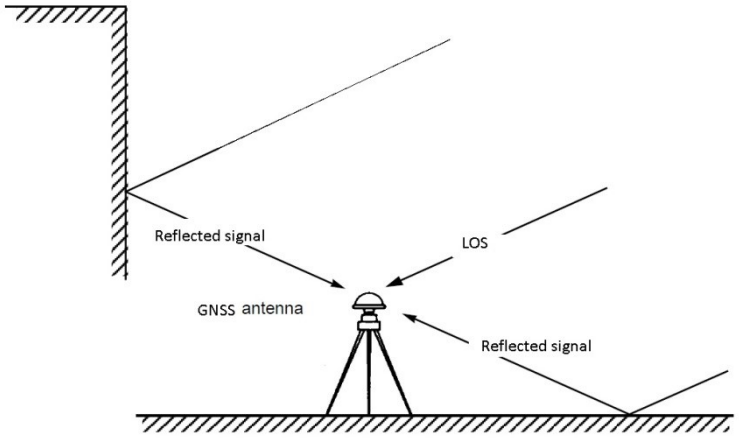

Figure 2.1: Multipath geometry

In some scenarios, the direct signal from the satellite is blocked by an obstruction and the receiver only detects reflected signals. This is referred to as Non-Line-Of-Sight (NLOS). In this thesis, it is assumed that the direct signal is always available, i.e. NLOS reception is not considered. For a receiver with wide bandwidth, a typical code multipath error level is 0.2m (1-sigma) in a benign environment. The corresponding error in carrier phase measurement is 0.02m (Kaplan and Hegarty 2006). Multipath errors and their mitigation techniques are discussed in detail in Chapter 4.

2.3.3 RECEIVER ERRORS

Receiver errors can be due to receiver internal clock errors, hardware delay and noise within the receiver circuitry.

2.3.3.1 Receiver clock errors

In order to keep costs low, receiver clocks used tend to be cheap and significantly less accurate than satellite clocks. In order to correct this error, the receiver clock error is usually assumed to be unknown and solved for alongside the 3D position parameters. Therefore, at least 4 range measurements are required.

2.3.3.2 Receiver hardware delay

The GNSS signal is delayed while passing through the antenna, analog circuits and digital processing units until the measurements are obtained. The delay can be as large as 1 microsecond (~ 300 m in range) if a long cable is used between the antenna and receiver. For similar signals at the same frequency the delay is the same. A common delay does not have an impact on positioning performance since it is estimated as part of the receiver clock error. However, it is obviously relevant in timing applications. The receiver hardware delay may be different for signals in different frequencies. If a linear combination of measurements is formed from signal in different frequencies, the delay can also be ignored since it is common for every individual combination of the same type (Kaplan and Hegarty 2006).

2.3.3.3 Receiver noise

Induced noise by the receiver tracking loop is one of the error sources for code and carrier phase measurements. The noise depends on different factors such as the power of the received signal, antenna design, technique used for analog-to-digital conversion and the correlation process. In modern receivers, and under nominal conditions, this error is of the order of decimetres or less (1-sigma) for code phase measurements. The error magnitude for carrier phase measurements is of the order of millimetres (1-sigma) (Kaplan and Hegarty 2006).

2.3.4 ERROR BUDGET

Based on the different error sources discussed in this chapter the error budget for GNSS stand-alone can be constructed. The error in the position obtained by GNSS is a function of both the User Equivalent Range Error (UERE) and the receiver-satellite geometry. Table 2.1 shows a typical error budget in the code phase measurement obtained from a GPS single frequency receiver. The total error is obtained by using the root-sum-square of all the errors, under the assumption that the individual errors are uncorrelated and normally distributed (Kaplan and Hegarty 2006).

The high error value of the ionosphere-induced error in Table 2.1 highlights the advantages of using linear combinations of measurements, as they significantly reduce this type of error.

Table 2.1: Error budget for GPS L1 C/A code (UERE)

Error	*1 σ error [m]*
broadcast clock	*1.1*
L1 P(Y)-L1 C/A group delay	*0.3*
Broadcast ephemeris	*0.8*
Ionopheric error	*7.0*
Tropospheric error	*0.2*
Multipath	*0.2*
Receiver noise	*0.1*
Total (root-sum-squared)	*7.1*

2.3.5 DILUTION OF PRECISION

In addition to the GNSS error sources, the accuracy of the position is also affected by the relative geometry of the satellites with respect to the receiver. This geometry is measured in terms of the Dilution of Precision (DOP). DOP can be interpreted as a factor transforming the errors in the measurement domain to errors in the position domain. A high value of DOP reflects a poor satellite geometry scenario. If σ is the total user equivalent range error (UERE), the 3-D Position DOP (PDOP), Horizontal DOP (HDOP), Vertical DOP (VDOP) and Time DOP (TDOP) can be obtained respectively as:

$$PDOP = \frac{\sqrt{\sigma_E^2 + \sigma_N^2 + \sigma_U^2}}{\sigma} \quad 2.11$$

$$HDOP = \frac{\sqrt{\sigma_E^2 + \sigma_N^2}}{\sigma} \quad 2.12$$

$$VDOP = \frac{\sigma_U}{\sigma} \quad 2.13$$

$$TDOP = \frac{\sigma_t}{\sigma} \quad 2.14$$

where σ_E, σ_N and σ_U are the standard deviation of the position estimate east, north and up components respectively and σ_t is standard deviation of the receiver clock error estimate in seconds (Kaplan and Hegarty 2006).

2.4 GNSS point positioning

The receiver obtains the signal propagation time by comparing the signal transmission time with the signal reception time (measured by the receiver clock). By scaling the signal propagation time by the speed of light, the range is obtained. However, the cheap clocks used in GNSS receivers are typically biased with respect to the system time. This bias induces errors in the range measurements, which are therefore referred to as pseudorange measurements. In the position calculation the receiver clock bias is considered as an unknown as discussed in Section 2.3.3.1, which is then solved together

with the position parameters. Therefore, at least 4 range measurements are needed. Ranges can be obtained from code and carrier phase measurements by the receiver using digital signal processing techniques. According to (Leick 2004) point positioning generally refers to the estimation of receiver antenna coordinates and receiver clock errors on the basis of code phase measurements with a standalone receiver. In point positioning, carrier phase measurements may, but do not have to, be used to smooth the code phase measurements. Satellite coordinates and clocks are obtained from the navigation message, atmospheric errors are corrected through modelling while hardware delays, residual satellite clock errors and multipath are neglected. In the presence of multiple frequencies, the ionospheric error may also be mitigated by forming linear combinations of measurements at different frequencies. Since ionospheric error mitigation can be achieved with a standalone receiver, it is also discussed as a point positioning technique in this thesis.

In the following subsections, the required mathematical models for positioning using code and carrier phase measurements are presented. Throughout the thesis, a superscript identifies the satellite and a subscript identifies the receiver. The carrier frequencies L1 and L2 are represented by subscript 1 and 2 respectively. The true satellite and receiver times are identified by $\hat{t}^p$and $\hat{t}_k$respectively which are different from the measured times of $t^p$and t_k by $dt^p$and dt_k respectively.

2.4.1 CODE PHASE MEASUREMENT MODELS

In addition to the clock error, there are other errors that affect the range measurements. Taking into account the main GNSS errors introduced in Section 2.3, the code phase measurement model from satellite p to receiver k can be written as (Leick 2004):

$$P_{k,f}^{p}(t_k) = \rho_k^p(\hat{t}^p) - cdt_k + cdt^p + I_{k,f}^{p}(t_k) + T_k^p(t_k) + \delta_{k,f,C}^{p}(t_k) + M_{k,f,C}^{p}(t_k) + \varepsilon_{f,C} \quad 2.15$$

where

t_k is the receiver nominal time which differs from the system time by dt_k,

$\hat{t}^p$ is the satellite true time which differs from satellite nominal time by dt^p,

I the ionospheric delay,

T the tropospheric delay,

δ the code hardware delay,

M the code multipath error and

the subscript C defines the code related variables.

In equation 2.15, variables which are frequency dependent have been identified by the subscript f. For simplicity, in this thesis the satellite and receiver dependency on time are omitted and code phase measurements are expressed as:

$$P_f = \rho - cdt_k + cdt^p + I_f + T + \delta_{f,C} + M_{f,P} + \varepsilon_{f,C}$$

2.16

If dual frequency measurements are available, code phase measurements from two frequencies can be combined to form Ionosphere Free (IF) code phase measurements by utilizing the dispersive nature of the ionosphere. In such a combination, first order ionospheric errors which accounts for 99% of the total error are eliminated. Code phase measurements from two frequencies are multiplied by the square of their correspondent frequencies and subtracted from each other to form the IF combination:

$$f_1^2 P_{f1} - f_2^2 P_{f2} = f_1^2\left(\rho - cdt_k + cdt^p + I_{f_1} + T + \delta_{f_1,C} + M_{f_1,P} + \varepsilon_{f_1,C}\right) - f_2^2\left(\rho - cdt_k + cdt^p + I_{f_2} + T + \delta_{f_2,C} + M_{f_2,C} + \varepsilon_{f_2,C}\right)$$

2.17

From equation 2.3:

$$f_1^2 I_{f_1} = f_2^2 I_{f_2}$$

Therefore, in Equation 2.17, the ionospheric terms are eliminated. After reordering, the ionosphere free code phase measurement (P_{IF}) is optained:

$$P_{IF} = \alpha_P P_{f1} - \beta_P P_{f2} = \rho - cdt_k + cdt^p + T + \delta_{IF,C} + M_{IF,P} + \varepsilon_{IF,C}$$

2.18

where

$$\alpha_{IF,P} = \frac{f_1^2}{f_1^2 - f_2^2}$$

and

$$\beta_{IF,P} = \frac{f_2^2}{f_1^2 - f_2^2}$$

Note that the multipath errors and noise from each individual frequency are also combined during the formation of the IF combination.

2.4.2 CARRIER PHASE MEASUREMENT MODELS

The carrier phase measurement in units of cycles can be expressed as:

$$\varphi_{k,f}^{p}(t_k) = \frac{f}{c}\rho_k^p(\hat{t}^p) - N_k^P - fdt_k + fdt^p - I_{k,f}^p(t_k) + \frac{f}{c}T_k^p(t_k) + \delta_{k,f,\varphi}^p(t_k) + m_{k,f,\varphi}^P(t_k) + \varepsilon_{f,\varphi} \quad 2.19$$

where subscript φ stands for units of cycles and m is the carrier multipath error. Note that the ionospheric error is negative, i.e. the ionosphere advances the carrier. The simplified notation of equation 2.19 is used throughout this thesis:

$$\varphi_f = \frac{f}{c}\rho - N_f - fdt_k + fdt^p - I_{f,\varphi} + \frac{f}{c}T + \delta_{f,\varphi} + m_{f,\varphi} + \varepsilon_{f,\varphi} \quad 2.20$$

The carrier phase measurements in the units of length (Φ) can be obtained by multiplying the right-hand-side of equation 2.20 with the carrier wavelength:

$$\Phi_f = \rho - \lambda_f N_f - cdt_k + cdt^p - I_{f,\Phi} + T + \delta_{f,\varphi} + m_{f,\Phi} + \varepsilon_{f,\Phi}$$

2.21

Similar to the IF code phase measurements, IF carrier phase measurements can be obtained from measurements at two different frequencies, thereby eliminating any first order ionospheric errors. Carrier phase measurements at two frequencies in units of cycles are multiplied by their correspondent frequencies and subtracted from each other:

$$f_1\varphi_{f_1} - f_2\varphi_{f_2} = f_1\left(\frac{f_1}{c}\rho - N_f - f_1 dt_k + f_1 dt^p - I_{f_1,\varphi} + \frac{f_1}{c}T + \delta_{f_1,\varphi} + m_{f_1,\varphi} + \varepsilon_{f_1,\varphi}\right)$$
$$-f_2\left(\frac{f_2}{c}\rho - N_f - f_2 dt_k + f_2 dt^p - I_{f_2,\varphi} + \frac{f_2}{c}T + \delta_{f_2,\varphi} + m_{f_2,\varphi} + \varepsilon_{f_2,\varphi}\right)$$

2.22

If the IF combination is expressed in terms of the *f1* frequency, equation 2.22 is multiplied by:

$$\frac{f_1}{f_1^2 - f_2^2}$$

which leads to the following ionospheric-free combination in units of cycles:

$$\varphi_{IF} = \alpha_{\varphi}\varphi_{f_1} - \beta_{\varphi}\varphi_{f_2}$$

$$= \frac{f_1}{c}\rho + \alpha_{\varphi}N_{f1} - \beta_{\varphi}N_{f2} - dt_k - f_1 dt_k + f_1 dt^p + \frac{f_1}{c}T + \delta_{\varphi,IF} + m_{\varphi,IF} + \varepsilon_{\varphi,IF}$$

2.23

where

$$\alpha_{IF,\varphi} = \frac{f_1^2}{f_1^2 - f_2^2}$$

and

$$\beta_{IF,\varphi} = \frac{f_1 \ f_2}{f_1^2 - f_2^2}$$

Note that integer ambiguities are multiplied by non-integer values. Therefore, the ambiguity in IF is no longer an integer. Ionospheric-free combinations for carrier phase measurements in the units of length (Φ_{IF}) can be formed by multiplying the right-hand side of Equation 2.23 by the wavelength of the f_1 signal:

$$\Phi_{IF} = \frac{c}{f_1}\left(\frac{f_1}{c}\rho + \alpha_{\varphi}N_{f1} - \beta_{\varphi}N_2 - f_1 dt_k + f_1 dt^p + \frac{f_1}{c}T + \delta_{\varphi,IF} + m_{\varphi,IF} + \varepsilon_{\varphi,IF}\right)$$

2.24

which leads to:

$$\Phi_{IF} = \rho + \alpha_{\Phi}N_{f1}\lambda_{f1} - \beta_{\Phi}N_{f2}\lambda_{f2} - cdt_k + cdt^p + T + \delta_{\Phi,IF} + m_{\Phi,IF} + \varepsilon_{\Phi,IF}$$

2.25

where

$$\alpha_{\mathrm{IF},\Phi} = \frac{f_1^2}{f_1^2 - f_2^2}$$

and

$$\beta_{\mathrm{IF},\Phi} = \frac{f_2^2}{f_1^2 - f_2^2}$$

The IF combination contains increased multipath errors and noise, similar to the IF code phase measurements. The relation between the multipath errors associated with single frequency measurements and the IF combination are discussed in detail in Chapter 5.

2.4.3 GNSS STATE ESTIMATION

Parameters such as position coordinates are typically estimated using the least squares or Kalman Filter (KF) approach. In static applications, the least squares technique is often used, while the KF approach can be used in general cases where the parameter vector may change with time (Leick 2004). These are discussed in detail in the following subsections.

2.4.3.1 Least square estimation

In the least squares method, the relation between the set of range measurements and the position solution is approximated by a linear system. The range measurements are not linearly related to the position solution. Therefore, in least square estimation of the position solutions, the pseudorange equation given by Equation 2.1 must be linearised. In this section, least square estimation of position solutions is presented briefly.

If P_j is the user range from the jth satellite, $c$the speed of light, t_u is the time offset, **s** the jth satellite position vector and **u** the user position vector:

$$P_j = \sqrt{(x_j - x_u)^2 + (y_j - y_u)^2 + (z_j - z_u)^2} + ct_u = f(x_u, y_u, z_u, t_u)$$

If we know the approximate position of the user $(\hat{x}_u \hat{y}_u \hat{z}_u)$ and have an estimate of the time bias $\hat{t}_u$, an approximate pseudorange can be calculated:

$$\hat{P}_j = \sqrt{(x_j - \hat{x}_u)^2 + (y_j - \hat{y}_u)^2 + (z_j - \hat{z}_u)^2} + c\hat{t}_u = f(\hat{x}_u, \hat{y}_u, \hat{z}_u, \hat{t}_u)$$

If:

$$x_u = \hat{x}_u + \Delta x_u$$

$$y_u = \hat{y}_u + \Delta y$$

$$z_u = \hat{z}_u + \Delta z_u$$

$$t_u = \hat{t}_u + \Delta t_u$$

We can write:

$$f(x_u, y_u, z_u, t_u) = f(\hat{x}_u + \Delta x_u, \hat{y}_u + \Delta y, \hat{z}_u + \Delta z_u, \hat{t}_u + \Delta t_u)$$

The last equation can be rewritten using a Taylor series expansion to a first order differential about the approximate position and receiver clock offset (linearization).

$$f(\hat{x}_u + \Delta x_u, \hat{y}_u + \Delta y, \hat{z}_u + \Delta z_u, \hat{t}_u + \Delta t_u) = f(\hat{x}_u, \hat{y}_u, \hat{z}_u, \hat{t}_u)$$
$$+ \frac{\partial f(\hat{x}_u, \hat{y}_u, \hat{z}_u, \hat{t}_u)}{\partial \hat{x}_u} \Delta x_u + \frac{\partial f(\hat{x}_u, \hat{y}_u, \hat{z}_u, \hat{t}_u)}{\partial \hat{y}_u} \Delta y_u$$
$$+ \frac{\partial f(\hat{x}_u, \hat{y}_u, \hat{z}_u, \hat{t}_u)}{\partial \hat{z}_u} \Delta z_u + \frac{\partial f(\hat{x}_u, \hat{y}_u, \hat{z}_u, \hat{t}_u)}{\partial \hat{t}_u} \Delta t_u$$

After derivation, we obtain:

$$\frac{\partial f(\hat{x}_u, \hat{y}_u, \hat{z}_u, \hat{t}_u)}{\partial \hat{x}_u} = \frac{-(x_j - \hat{x}_u)}{\sqrt{(x_j - \hat{x}_u)^2 + (y_j - \hat{y}_u)^2 + (z_j - \hat{z}_u)^2}}$$

$$\frac{\partial f(\hat{x}_u, \hat{y}_u, \hat{z}_u, \hat{t}_u)}{\partial \hat{y}_u} = \frac{-(y_j - \hat{y}_u)}{\sqrt{(x_j - \hat{x}_u)^2 + (y_j - \hat{y}_u)^2 + (z_j - \hat{z}_u)^2}}$$

$$\frac{\partial f(\hat{x}_u, \hat{y}_u, \hat{z}_u, \hat{t}_u)}{\partial \hat{z}_u} = \frac{-(z_j - \hat{z}_u)}{\sqrt{(x_j - \hat{x}_u)^2 + (y_j - \hat{y}_u)^2 + (z_j - \hat{z}_u)^2}}$$

$$\frac{\partial f(\hat{x}_u, \hat{y}_u, \hat{z}_u, \hat{t}_u)}{\partial \hat{t}_u} = c$$

If

$$\hat{r}_j = \sqrt{(x_j - \hat{x}_u)^2 + (y_j - \hat{y}_u)^2 + (z_j - \hat{z}_u)^2}$$

$$P_j = \hat{P}_j - \frac{x_j - \hat{x}_u}{\hat{r}_j} \Delta x_u - \frac{y_j - \hat{y}_u}{\hat{r}_j} \Delta y_u - \frac{z_j - \hat{z}_u}{\hat{r}_j} \Delta z_u + c\Delta t_u$$

$$\hat{P}_j - P_j = \frac{x_j - \hat{x}_u}{\hat{r}_j} \Delta x_u + \frac{y_j - \hat{y}_u}{\hat{r}_j} \Delta y_u + \frac{z_j - \hat{z}_u}{\hat{r}_j} \Delta z_u - c\Delta t_u$$

For convenience, we introduce the following new variables:

$$\Delta P_j = \hat{P}_j - P_j$$

$$a_{xj} = \frac{x_j - \hat{x}_u}{\hat{r}_j}$$

$$a_{yj} = \frac{y_j - \hat{y}_u}{\hat{r}_j}$$

$$a_{zj} = \frac{z_j - \hat{z}_u}{\hat{r}_j}$$

So the simplified equation is:

$$\Delta P_j = a_{xj}\Delta x_u + a_{yj}\Delta y_u + a_{zj}\Delta z_u - c\Delta t_u$$

For j from 1 to 4 the system of equations can be expressed as:

$$\Delta \boldsymbol{P} = \boldsymbol{H}\Delta \boldsymbol{x} \qquad 2.26$$

where:

$$\Delta \boldsymbol{P} = \begin{bmatrix} \Delta P_1 \\ \Delta P_2 \\ \Delta P_3 \\ \Delta P_4 \end{bmatrix} \mathbf{H} = \begin{bmatrix} a_{x1} a_{y1} a_{z1} 1 \\ a_{x2} a_{y2} a_{z2} 1 \\ a_{x3} a_{y3} a_{z3} 1 \\ a_{x4} a_{y4} a_{z4} 1 \end{bmatrix} \Delta \boldsymbol{x} = \begin{bmatrix} \Delta x_1 \\ \Delta y_2 \\ \Delta z_3 \\ -\mathrm{c}\Delta t_{u4} \end{bmatrix}$$

The solution for equation 2.26 is obtained as:

$$\Delta\hat{\boldsymbol{x}} = \boldsymbol{H^{-1}}\Delta\boldsymbol{P} + \boldsymbol{\varepsilon}$$

2.27

In order to account for differences in the error magnitudes between measurements, they are allocated different weights. The solution using weighted least squares is obtained as:

$$\Delta\hat{\boldsymbol{x}} = (\boldsymbol{H^{-1}WH})^{-1}\boldsymbol{H^{-1}W}\Delta\boldsymbol{P}$$

2.28

where $\boldsymbol{W}$ is a diagonal matrix with reciprocal of measurement variances as it elements (Kaplan and Hegarty 2006).

2.4.3.2 Kalman filter process

In this thesis, the KF approach is used to estimate the state parameters due to versatility, ease of implementation and optimum performance. The Kalman filter requires a state transition model, which defines the relationship between the old and new state vectors:

$$\mathbf{x}_{\mathrm{k}}^{-} = \boldsymbol{\Phi_{k-1}}\boldsymbol{x}_{k-1} + \boldsymbol{w}_k$$

2.29

In equation 2.29 $\boldsymbol{\Phi}$ represents the state transition model. The white noise $(\boldsymbol{w}_k)$ is added to the model in order to add some flexibility to the model. This allows the

parameters to change slightly from one epoch to another. $\boldsymbol{w}_k$ is also referred to as system noise or process noise which is assumed to have a normal distribution $\boldsymbol{w}_k \sim (\boldsymbol{0}, \boldsymbol{Q}_{wk})$.

The corresponding covariance matrix is predicted using the state model:

$$\boldsymbol{Q}_k^- = \boldsymbol{\Phi}_{k-1} \boldsymbol{Q}_{k-1} \boldsymbol{\Phi}_{k-1}^T + \boldsymbol{Q}_{wk}$$

If measurements such as ranges are non-linear with respect to the state vector (such as position coordinates), the measurements can be linearised about a nominal trajectory (approximate state). Another approach is to linearise the measurements about the predicted trajectory. This means that the state vector is predicted first, followed by the prediction of the ranges using the state model ($\boldsymbol{H}$):

$$\boldsymbol{y}_k^- = \boldsymbol{H}_k \boldsymbol{x}_k^-$$

On the basis of the predicted ranges, the innovation vector, which is the difference between the predicted range measurement and observed range measurement, is obtained as:

$$\boldsymbol{v}_k = \boldsymbol{y}_k - \boldsymbol{y}_k^-$$

The innovation vector is then weighted by the KF gain ($\boldsymbol{K_k}$):

$$\boldsymbol{K_k = Q_k^- H_k^T \left(H_k Q_k^- H_k^T + R_k\right)^{-1}}$$

where, $\boldsymbol{R_k}$ is the measurement covariance matrix. The state vector and covariance matrix are then obtained as:

$$\boldsymbol{x_k = x_k^- + \ K_k v_k}$$

$$\boldsymbol{Q_k = (I - K_k H_k) Q_k^-}$$

In the Kalman process explained above it is assumed that $\boldsymbol{w_k}$ and $\boldsymbol{v_k}$ are mutually independent and white noise. This requires the errors at each epoch to be independent from the previous epoch. $\boldsymbol{w_k}$ and $\boldsymbol{v_k}$ are also assumed to be independent of the initial states (Leick 2004)**.**

The power of the KF approach is that it uses all the earlier measurements and current measurements to optimally estimate the current state, independently of the number of instantaneous measurements available. Additionally, the current state is estimated even during a period of lack of measurements. The KF approach also allows taking into consideration additional information to help the state estimation, such as maximum range measurements for base stations or different models for errors such as multipath. However, in KF an initial state estimate, the state transition model and error distributions are needed. These are often not well-known. Hence, the model may not be accurate resulting in divergence, long convergence time or noisy solutions.

2.5 Summary

This chapter has provided an overview of various GNSS applications with a focus on the high accuracy applications. Subsequently an overview of GNSS has been provided, focussing on their general operational concept and architecture. A description of the constellations and signal attributes of the different GNSS is provided along with their current operational status. The main GNSS error sources, their effect on GNSS signals and the common ways of dealing with such errors were discussed.

The last section of this chapter discussed the principles of GNSS point positioning. In this regard, it presented code and carrier phase measurement models, as well as the least squares and KF approaches to estimate the user receiver state parameters.

Based on the discussions in this chapter and the GNSS errors summarised in Table 2.1, it is clear that the point positioning does not fulfil the requirements for high accuracy positioning applications. Therefore, more advanced positioning techniques are required. Such techniques are discussed in Chapter 3.

Chapter 3

GNSS AUGMENTATION

Chapter 2 presented the different GNSS applications classified into low-accuracy and high-accuracy applications, and highlighted the latter as the focus of this thesis. The chapter then provided an overview of the different GNSS including their operational concept, architecture and error sources. On the basis of the GNSS error budget, it was concluded that basic GNSS positioning cannot support high accuracy applications. Therefore, this chapter presents the augmentation systems developed to improve the performance of GNSS, by mitigating the effects of some of the error sources, and assesses their ability to support high accuracy applications. The integration of GNSS with terrestrial sensors is not considered in this thesis.

All the GNSS augmentation systems are based on the Differential GNSS (DGNSS) operational concept (Kaplan and Hegarty 2006). DGNSS can be classified based on different criteria such as the measurement type (code or carrier phase), the

service area (i.e. local area, regional area and wide area) or the positioning method (i.e. absolute or relative positioning) (Kaplan and Hegarty 2006). The remainder of this chapter describes the DGNSS operational concept and the different DGNSS which are classified here based on the measurement type (i.e. code based and carrier based techniques). It assesses the ability of these systems to satisfy the requirements of the high-accuracy applications identified in Chapter 2. Section 3.1 presents the DGNSS concept, Section 3.2 discusses the different code-phase DGNSS while Section 3.3 discusses the carrier-phase based systems. The chapter provides concluding remarks in Section 3.4.

3.1 Differential GNSS

The DGNSS concept exploits the spatial error correlation between two receivers separated by a given distance, also referred to as baseline. The concept is based on correcting the correlated errors at the receiver with an unknown location (rover) with those extracted from, and broadcast by, another receiver at a known location (reference station). The reference station(s) may provide different types of information to the rover and improve its solution. The information can be transmitted using different data links, such as radio links or over the internet and include:

- Corrections to the raw pseudorange and carrier phase measurements or corrections to the satellite ephemeris and clock.

- Raw reference station measurements
- Integrity data which indicate the health status of visible satellites and/or the accuracy statistics of the corrections provided
- Various auxiliary data, such as the reference station position (Kaplan and Hegarty 2006)

In general, DGNSS measurements can be based on single differencing between two receivers, single differencing between two satellites, double differencing between two receivers and two satellites. The single and double differencing techniques are discussed in more detail in Section 3.2.3.

3.2 Code based techniques

Augmentation systems in this category primarily rely on code phase measurements to calculate the position of the rover. In this section the Ground Based Augmentation System (GBAS), the Satellite Based Augmentation System (SBAS) and code based relative positioning are discussed briefly as respective examples of the regional, wide-area and local DGNSS.

3.2.1 GBAS

GBAS is a local augmentation system which supports for example, civil aviation operations at an airport level. These are the approach, landing, departure and surface movement phases of flight. Such a GBAS consists of a ground sub-system and an aircraft sub-system. The Ground sub-system's task is to provide the aircraft with the approach path data and corrections and integrity information for the satellites in view. It consists of at least two GNSS reference stations which collect the necessary measurements to calculate pseudorange differential corrections and integrity information. The ground sub-system data are then broadcast via a Very High Frequency (VHF) data link. Aircrafts within the GBAS coverage area receive the corrections and may use them to compute their positions with better accuracy and integrity than a point positioning service. However, the presence of multipath at the ground reference stations may create large errors and degrade the performance of GBAS (Kaplan and Hegarty 2006).

3.2.2 SBAS

Unlike GBAS, SBAS provides differential corrections and integrity information to users over a wide area via geostationary satellites. Although primarily designed for aviation applications, with suitable receivers it can be utilized for other applications. SBAS consists of monitoring (reference) stations spread over large regions (typically the size of a continent), central processing facilities, satellite uplink facilities and one or more

geostationary satellites. The GNSS signal is received by the monitoring receivers which provide code and carrier phase measurements to the central processing facilities. The central processing facilities generate the corrections for satellite orbit and clock errors. In addition, for each satellite the vertical ionospheric delay errors and integrity information are generated. The wide-area differential corrections (for satellite orbit, clock and ionospheric delay) and integrity messages are then transmitted to a geostationary satellite via uplink facilities where the message is modulated. The geostationary satellite broadcasts these messages to the users (Kaplan and Hegarty 2006). Examples of SBAS are:

- The US Wide Area Augmentation System (WAAS)
- The European Geostationary Navigation Overlay Service (EGNOS)
- The Multi-functional Satellite Augmentation System (MSAS) developed by Japan
- The Indian GPS Aided Geo Augmented Navigation (GAGAN) designed to provide augmentation to GLONASS and GPS
- The Russian System of Differential Correction and Monitoring (SDCM) which is currently under development to cover Russia and provide augmentation to GPS and GLONASS and,
- The Chinese Satellite Navigation Augmentation Systems (CSNAS).

The SBAS performance requirements, defined by International Civil Aviation Organization (ICAO), are accuracies of 16m and 4-6m for horizontal and vertical

directions respectively (95%). This level of accuracy is required for category I precision approach flight operations. Although SBAS considerably improves the position accuracy compared to the standard positioning service, it hardly meets the performance requirements defined by ICAO with currently available signals (Kaplan and Hegarty 2006). In addition, the presence of multipath errors in the monitoring and user receivers degrades the overall system accuracy (Wanninger and Wallstab-Freitag 2007).

3.2.3 CODE BASED RELATIVE POSITIONING

Code based relative positioning is based on differencing the code phase measurements of a rover and reference station receiver to mitigate the correlated errors. Therefore, the rover position is determined relative to the known reference station position.

The single differenced code phase measurements (ΔP) between receivers *k* and *m,* at the frequency *f* is based on the code phase measurement model introduced in Chapter 2:

$$\Delta P_f = \rho_{km} - cdt_{km} + I_{km,f} + T_{km} + \delta_{km,f} + M_{km,f} + \varepsilon_{km,f} \quad 3.1$$

where the subscript km refers to the differenced values between the two receivers. In Equation 3.1 the satellite clock errors and satellite hardware delays have been removed. Ionospheric and tropospheric errors are also mitigated by single differencing to

some extent, depending on the degree of correlation of these errors (i.e. horizontal distance and relative atmospheric conditions) between the two receivers.

The single differenced code phase measurements can be differenced across two satellites to generate double differenced code phase measurements. From Equation 3.1, double differenced code phase measurements between receivers *k* and *m* and across satellites *p* and q are generated as:

$$\nabla\Delta P_f = \rho_{km}^{pq} + I_{km,f}^{pq} + T_{km}^{pq} + M_{km,f}^{pq} + \varepsilon_{km,f}^{pq} \quad 3.2$$

where the pq superscript refers to the differencing between the measurements from two satellites. Double differencing further eliminates receiver clock errors and hardware delays as shown in Equation 3.2.

It is common to apply this type of DGNSS in post processing mode while GBAS and SBAS are real time applications (Sabatini and Palmerini 2008). Although differencing is effective in mitigating the correlated errors between receivers, it also increases multipath errors and noise, which can be a significant weakness of this approach.

3.2.4 SUMMARY

The positioning performance of code-based DGNSS techniques is dependent upon the level of error correlation between two receivers. They eliminate satellite clock and

hardware delays as well as user receiver errors and, under favorable conditions, these techniques tend to reduce errors associated with the troposphere and ionosphere. However, these techniques are not effective in mitigating code multipath errors and receiver noise due to the local nature of these errors. Differencing techniques in fact magnify these errors, potentially up to several metres. Therefore, code based differential techniques alone are not able to fulfill the requirements of high accuracy positioning applications and carrier phase measurements must be utilized for such applications. Carrier phase based technique are discussed in the next section.

3.3 Carrier based techniques

This class of differential techniques relies primarily on carrier phase measurements where the accuracy improves significantly compared to code based techniques. However, a carrier phase measurement is ambiguous and the initial integer ambiguity must be estimated in addition to other parameters. In this section the two main carrier based DGNSS techniques are discussed: Precise Point Positioning (PPP) and relative positioning.

3.3.1 PRECISE POINT POSITIONING

PPP is a technique that enables centimetre-level position accuracy using standalone receivers (Kouba and Heroux 2000). It requires dual frequency measurements

to create Ionospheric-Free (IF) observables, as well as precise ephemeris and satellite clock corrections. These corrections are provided by different organizations such as the International GPS Service (IGS), Jet Propulsion Laboratory (JPL) and Veripos. The carrier phase ionospheric-free observable ambiguities are not integers. Therefore, a float solution is typically used in PPP, which is not as accurate as a fixed solution, and suffers from relatively longer convergence time. Multipath error in PPP is one of the main limiting factors in achieving centimeter-level positioning. Multipath errors (code and carrier) in linear combinations of measurements, such as the IF combination, are considerably larger than those for single frequency measurements. For example, carrier multipath errors are of the order of centimetres in single frequency measurements and increase to decimetres in IF combinations (see Chapter 5).

In addition to the atmospheric errors, satellite clock and orbital errors, there are other errors which affect PPP positioning. Satellite antenna effects and phase windup errors are the main ones and are discussed briefly in this section.

3.3.1.1 Satellite antenna effects

The broadcast ephemeris is based on the satellite antenna phase centre, consistent with the measurements made in the receiver. On the other hand, the IGS GPS precise satellite coordinates and clock products are based on the satellite centre of mass. Therefore, the satellite phase centre offset from the centre of mass must be applied to the measurements when the IGS products are used. The phase centre offset of each individual

satellite is known and the orientation of the offset vector must be monitored as the satellite orbits the earth.

3.3.1.2 Phase wind-up corrections

The GPS signal has circular polarisation, in which the electric field vector rotates. Therefore, carrier phase measurements in the receiver depend on the relative orientation of the satellite and receiver antennas. Rotation of either of the antennas may change the carrier phase measurements by up to one cycle (19 cm in length in the case of GPS L1), an effect known as “phase wind-up”. During stationary conditions, the receiver antenna does not rotate but the satellite antenna is rotates to direct the satellite solar panels towards the sun. As the satellite rotates around the earth it is subjected to slow and rapid rotations. The latter may reach one cycle in less than half an hour. The phase wind-up effect is negligible when using differencing techniques. However, its effect due to the rapid rotations is significant for un-differenced point positioning techniques such as PPP, resulting in decimetre-level positioning errors. Therefore, it must be corrected in the measurements. Fortunately, most of the IGS analysis centres apply this correction in their orbital/clock products since 1994.

3.3.1.3 PPP Summary

PPP is able to achieve centimetre-level positioning accuracy if reliable error corrections are available. However, it suffers from long convergence time, of the order of 10-30 minutes or even more with current techniques. This long convergence time is not acceptable for most of the high accuracy positioning applications. Therefore, other techniques are required, such as carrier phase relative positioning, discussed in the next section.

3.3.2 CARRIER-BASED RELATIVE POSITIONING

This technique applies the differential concept and is commonly used in surveying and can achieve centimetre level accuracy if the horizontal distance between the two receivers is sufficiently small. An example of carrier based relative positioning is the Real Time Kinematic (RTK) technique in which the Double Difference (DD) carrier phase observable is used as the primary measurements. Carrier phase single differenced measurements ($\Delta\varphi$) between receivers *k* and *m* at frequency *f* are obtained from the carrier phase measurement model:

$$\Delta\varphi_f = \frac{f}{c}\rho_{km} - N_{km,f} - f dt_{km} - I_{km,f,\varphi} + \frac{f}{c}T_{km} + b_{km,f,\varphi} + m_{km,f,\varphi} + \varepsilon_{km,f,\varphi} \quad 3.3$$

The single differenced carrier phase measurements are then differenced across two satellites to create DD carrier phase measurements. From Equation 3.3 the DD carrier phase observable is derived as:

$$\nabla\Delta\varphi_f = \frac{f}{c}\rho_{km}^{pq} - N_{km,f}^{pq} - I_{km,f,\varphi}^{pq} + \frac{f}{c}T_{km}^{pq} + m_{km,f,\varphi}^{pq} + \varepsilon_{km,f,\varphi}^{pq}$$

3.4

Double differencing eliminates receiver clock errors and hardware delays. However, carrier multipath errors and noise are increased. It should be noted that the integer ambiguity remains an integer after double differencing.

Integer ambiguity resolution is discussed in the next subsection. This is followed by a discussion of the effect of wavelength on ambiguity resolution (Section 3.3.2.2) and the effect of the receiver loss of lock (Section 3.3.2.3), resulting in cycle slips.

3.3.2.1 Integer ambiguity resolution

Carrier phase measurements are ambiguous due to the unknown integer number of carrier cycles between the satellite and the receiver. The process of ambiguity resolution is based on a least squares adjustment of a linearised carrier phase model, which can be generalised as:

$$y = Aa + Bb + e$$

3.5

where, *y* is usually the so called observed-minus-computed measurement vector, a the vector of ambiguities, b a vector of all other unknowns such as baseline components and atmospheric corrections and e the noise vector. *A* and *B* are design matrices for a and b respectively.

After taking into account the integer constraints of the ambiguities, the integer least-squares minimisation can be represented as:

$$\min_{a,b}(y - Aa - Bb)^{*}Q_{y}^{-1}(y - Aa - Bb), \;\; with\; a \in Z^{m}, b \in R^{3} \tag{3.6}$$

Unfortunately, there is no direct method for solving the constrained minimization expressed by Equation 3.6. Therefore, it has been suggested by (Teunissen 1995) to solve the integer-least square in three steps:

In the first step, Equation 3.6 is solved by relaxing the integer condition. In other words $a \in Z^{m}$ is replaced by $a \in R^{m}$. The outputs of solving the unconstrained least squares are real-valued ambiguities and other parameters in the vector *b* in addition to the variance covariance matrix:

$$\begin{bmatrix}\hat{a}\\ \hat{b}\end{bmatrix}, \begin{bmatrix}Q_{\hat{a}} & Q_{\hat{a},\hat{b}}\\ Q_{\hat{b},\hat{a}} & Q_{\hat{b}}\end{bmatrix}$$

In the second step, the integer least squares estimate of ambiguities ($\check{a}$) is solved, represented as:

$$\min_{a}(\hat{a}-a)^{*}Q_{\hat{a}}^{-1}(\hat{a}-a)\,,with\ a\in Z^{m}$$

3.7

In the third step, a fixed solution for the parameters in vector b ($\check{b}$) is obtained based on:

$$\check{b}=\ \hat{b}-Q_{\hat{b},\hat{a}}-Q_{\hat{a}}^{-1}(\hat{a}-\check{a})$$

3.8

The conversion of the real-valued ambiguities to integer values is known as ambiguity resolution (step 2) and can be achieved based on different techniques. The Ambiguity rounding, searching and Least-squares AMBiguity Decorrelation Adjustment (LAMBDA) is an example of such techniques. These are discussed in the subsequent sections.

3.3.2.1.1 Rounding

The easiest way to resolve the ambiguities is to round the estimated float ambiguities to their nearest integer values. This approach needs good estimation of the float solution which can be achieved for data from many satellites and observations over long time periods. In such situations, the float ambiguities are typically very close to integer values and their variances are small. The requirement to collect measurements for a long time is a limitation for this approach and in some situations, it is necessary or

desirable to fix the ambiguities as fast as possible. However, with smaller numbers of observations, the estimated float ambiguities are not necessarily close to integer values, making this approach non-viable (Teunissen et al. 2002).

3.3.2.1.2 Searching

This technique searches for different sets of ambiguities within a boundary and checks the least squares residual. Each least squares solution provides float ambiguities together with a variance-covariance matrix. If $\hat{\boldsymbol{a}}$ is the vector of float and $\boldsymbol{a}$ is the vector of integer ambiguities and $\boldsymbol{Q}_{\hat{\boldsymbol{a}}}$ is the variance-covariance matrix of the ambiguities, the ambiguity search ellipsoid is developed as:

$$[\hat{\boldsymbol{a}} - \boldsymbol{a}]^{\boldsymbol{T}} \boldsymbol{Q}_{\hat{a}}^{-\boldsymbol{1}} [\hat{\boldsymbol{a}} - \boldsymbol{a}] \leq \chi^2 \qquad 3.9$$

where χ^2 is a positive constant value determining the search size. The search ellipsoid is centered at $\hat{\boldsymbol{a}}$ and its shape is governed by $\boldsymbol{Q}_{\hat{\boldsymbol{a}}}$. Since ambiguities are correlated with each other, the covariance matrix $\boldsymbol{Q}_{\hat{\boldsymbol{a}}}$ is far from diagonal, which results in an ellipsoidal search space. The search band depends on the accuracy of the measurements and if it is within 10 wavelengths ($\pm$2m in L1), the search for integers over ± 10 must be performed. With 4 ambiguities, the number of searches would be 21^4. The integer ambiguity vector $\boldsymbol{a}$ which satisfies 3.9 is selected as the candidate set. After

selecting the candidate sets, a statistical test such as the ratio test is executed to choose the correct ambiguity set. The down side of this technique is the high computation effort it requires (Teunissen et al. 2002; Leick 2004; Kaplan and Hegarty 2006).

3.3.2.1.3 Lambda technique

Most of the ambiguity resolution techniques are based on searching (i.e. LAMBDA). Float ambiguities are highly correlated, resulting in an extremely elongated search space. Searching for correct ambiguities in an ellipsoidal space is less efficient than in a spherical space. The core of the lambda technique is to improve the searching technique by pushing the ellipsoidal search space towards a spherical one. In this technique, the search space is transformed by applying the so called Z transformation on the float ambiguities and the corresponding covariance matrix:

$$\hat{z} = Z^T \hat{a} \tag{3.10}$$

$$Q_{\hat{z}} = Z^T Q_{\hat{a}} Z \tag{3.11}$$

The Z matrix must be chosen such that the transformed ambiguities are as decorrelated as possible, which transforms the covariance matrix closer towards a diagonal matrix. If the Z matrix is integer and volume preserving, after the Z transformation, the minimisation problem becomes:

$$\min_{z}(\hat{z}-z)^T Q_{\hat{z}}^{-1}(\hat{z}-z),\ \ z \in Z^n$$

3.12

which is solved based on:

$$(\hat{z}-z)^T Q_{\hat{z}}^{-1}(\hat{z}-z) \leq \chi^2$$

3.13

In an ideal case, the transformation results in a complete diagonal covariance matrix and the solution for 3.7 is obtained by simply rounding the elements in $\hat{z}$ to their nearest integer value. However, achieving a perfect diagonal covariance matrix is not possible due to the integer requirements of the Z matrix. Therefore, some kind of search technique must be applied. The integer least squares of the transformed ambiguities can be estimated using sequential conditional least-squares adjustment. In this process the search is carried out by placing bounds on the individual ambiguities:

$$(\hat{z}_1 - z_1)^2 \leq \sigma_{z1}^2 \chi^2$$

$$\left(\hat{z}_{2|1} - z_2\right)^2 \leq \sigma_{z_{2|1}}^2 (\chi^2 - (\hat{z}_1 - z_1)^2/\sigma_{z_1}^2)$$

...

$$\left(\hat{z}_{n|N} - z_n\right)^2 \leq \sigma_{z_{n|N}}^2 (\chi^2 - \sum_{j=1}^{n-1} \frac{\left(\hat{z}_{j|J} - z_j\right)^2}{\sigma_{z_{j|J}}^2})$$

3.14

where the notation $\hat{z}_{i|I}$ denotes the least squares estimate of the transformed ambiguity z_i, conditioned on the previous ambiguities from z_I with $I = 1, \ldots, (i-1)$. Note that all integers which satisfy Equation 3.13, also satisfy Equation 3.14.

The integer least squares solution for the transformed ambiguities ($\check{z}$) is then transformed back to obtain $\check{a}$:

$$\check{a} = Z^{-T}\check{z}$$

The fixed solution to the parameters are then obtained based on 3.8 (Teunissen et al. 1996).

The LAMBDA technique considerably improves the ambiguity search by decorrelating the ambiguities. However, the existence of multipath errors in the double difference carrier phase measurements results in biased estimates of the float solutions. This makes ambiguity resolution more difficult, even with high performance techniques such as LAMBDA.

3.3.2.2 Wavelength effect on ambiguity resolution

Carrier phase measurements at different frequencies provide opportunities to create new observables by combining their measurements. Searching for the correct ambiguities within a distance boundary is faster for longer wavelengths due to having less possible searching options (Kaplan and Hegarty 2006). A carrier phase observable

obtained from the linear combination of other carrier phase measurements in units of carrier cycles can be expressed as:

$$\varphi_{LC} = k_1\varphi_1 + k_2\varphi_2 + \cdots + k_n\varphi_n \quad 3.15$$

where φ_{LC} is the new observable, φ_i and k_i are the component observables and corresponding scale factors respectively.

The wavelength of the new observable in relation to its component signal observables is:

$$\lambda_{LC} = \frac{1}{\frac{k_1}{\lambda_1} + \frac{k_2}{\lambda_2} + \cdots + \frac{k_n}{\lambda_n}} \quad 3.16$$

where λ_{LC} is the wavelength of the linear combination and λ_i is the wavelength of the n^{th} component. Therefore, using different values of k creates new observables with different wavelengths. Commonly, observables with large wavelengths are used before resolving ambiguities to facilitate the search process. Following ambiguity resolution, smaller wavelengths may be used to improve position accuracy. The Wide Lane (WL) and Narrow Lane (NL) observables are such linear combinations in common use. The WL observable is obtained using Equation 3.15 with k_1 and k_2 equal to 1 and -1 respectively.

It is possible to calculate the WL observable in units of length similar to the single frequency measurements. In doing so, firstly the WL observable is formed based on Equation 3.15:

$$\varphi_{WL} = \varphi_{f_1} - \varphi_{f_2}$$

3.17

From carrier phase measurement model (Equations 2.19) and Equation 3.17, the WL observable in units of cycles is obtained as:

$$\varphi_{WL} = \frac{f_1}{c}\rho - \frac{f_2}{c}\rho - N_{f1} + N_{f2} + \frac{f_1}{c}V_{f1} - \frac{f_2}{c}V_{f2}$$

3.18

where V_{f1} and V_{f2} represent the combined errors and noise in units of length in L1 and L2 frequencies respectively. In order to convert the observable to the units of length, the right side of Equation 3.18 is multiplied by the WL wavelength ($\frac{c}{f_1 - f_2}$):

$$\Phi_{WL} = \frac{c}{f_1 - f_2}\left(\frac{f_1}{c}\rho - \frac{f_2}{c}\rho - N_{f1} + N_{f2} + \frac{f_1}{c}V_{f1} - \frac{f_2}{c}V_{f2}\right)$$

3.19

$$\Phi_{WL} = \rho - \alpha_{WL}N_{f1}\lambda_1 + \beta_{WL}N_{f2}\lambda_2 + \alpha_{WL}V_{f1} - \beta_{WL}V_{f2}$$

3.20

where

$$\alpha_{WL} = \frac{f_1}{f_1 - f_2}$$

and

$$\beta_{WL} = \frac{f_2}{f_1 - f_2}$$

According to Equation 3.16, the wavelength of the WL observable is approximately 0.86 m, considerably larger than the wavelength of the L1 and L2 observables. This improves the search process. However, multipath errors and noise are considerably higher in the WL observable in comparison to the L1 and L2 carrier phase measurements.

3.3.2.3 Carrier cycle slips

If the receiver loses its carrier phase tracking, the carrier phase measurement jumps suddenly by an integer number. This sudden jump, referred to as a cycle slip, may occur for example, due to obstruction of a satellite. Cycle slips may occur for a short period of time between epochs or longer. If cycle slips are not fixed, the fixed and float solutions diverge rapidly. Although it is possible to correct cycle slips, it is easier to detect them and exclude the affected satellite. Cycle slips can be detected based on

various test observables, such as raw carrier phase measurements, single and double differenced carrier phase measurements, by:

- Fitting a low-order polynomial on the time series of the tested observable and screening the residuals after the fit.
- Predicting the test observable with the Kalman filter and screening the difference between the predicted and observed values.
- Differencing the first or higher order test observables between epochs and screening the outliers.

If a cycle slip is detected, the affected satellite is ignored for a short time. After a predetermined time period, it is assumed that the satellite is back to normal and integer ambiguity resolution is attempted again for the affected satellite (Kaplan and Hegarty 2006; Leick 2004; Rizos 1997).

3.4 Summary

This chapter has presented the main characteristics of the different GNSS augmentation systems which improve the performance of standalone GNSS using the differential GNSS concept. The chapter has described the operational concepts of code-based (GBAS, SBAS and code-based relative positioning) and carrier-based (PPP and relative positioning) augmentation systems. Code-based augmentation systems cannot

satisfy the requirements of high accuracy positioning applications. On the other hand, carrier-based differential techniques have the potential to achieve a higher availability of cm-level position accuracy if the effect of multipath can be dealt with effectively. Chapter 4 discusses in detail the multipath error in GNSS and the state-of-the-art techniques used for its mitigation.

Chapter 4

MULTIPATH ERROR

Chapter 3 highlighted that multipath errors can significantly degrade the GNSS positioning accuracy required for high accuracy applications. Although the modernisation of GNSS and their augmentations have improved the mitigation of many of the error sources, they have had little effect on multipath errors, which remain significant and sometimes the dominant error in high accuracy positioning (Kaplan and Hegarty 2006).

Multipath affects both code and carrier phase measurements. For code phase measurements, the bias in the range calculation due to multipath leads to a direct bias in the position estimation. For carrier phase measurements, fluctuations in the range estimation due to multipath may result in a bias of the initial ambiguity, which then leads to a widening of the ambiguity search space. As a result, the required time for ambiguity resolution increases. Furthermore, multipath errors may lead to incorrect ambiguity

resolution and positioning errors of the order of a several centimetres (Kubo and Yasuda 2003).

Section 4.1 presents an analytical model of GNSS signals contaminated with multipath. In order to mitigate these errors, an understanding of the impact on the receiver measurements is required and is discussed in Section 4.2. This is followed in Section 4.3 by a detailed literature review of existing multipath mitigation techniques, with a focus on carrier phase multipath, given the context of this thesis. Finally, Section 4.4 concludes chapter.

4.1 Model of multipath-contaminated GNSS signals

A direct single-path GNSS signal $r_d(t)$ can be represented at the receiver as the complex envelop of the transmitted signal $x(t)$ as follows:

$$r_d(t) = \alpha_0 x(t - \tau_0) e^{-j\phi_0} e^{j2\pi f_c \tau_0} \quad 4.1$$

where f_c is the carrier frequency, τ_0 the propagation time of the signal from the satellite to the receiver, α_0 the amplitude of the received signal and ϕ_0 the carrier phase of the received signal. The zero subscript indicates the direct signal. The transmitted signal $x(t)$ is generally formed from the modulation of code *C(t)* and data *D(t)* signals. In the Galileo system and GPS III satellites, a rectangular subcarrier with a frequency equal to or higher than the code chip rate is also added to $x(t)$. Such a modualtion scheme is

known as Binary Offset Carrier (BOC) modulation. The addition of this subcarrier improves system interoperability between GPS and Galileo. In addition, the BOC modulation expands the signal frequency band, resulting in a narrower correlation peak. This improves the performance of the tracking loop at the receiver, and also multipath mitigation.

If a GNSS signal is reflected from *N* objects before reaching the antenna, *N* copies of the signal $r(t)$ are superimposed on the direct signal with different propagation times, carrier phases and amplitudes. Such a signal can be represented in the baseband as:

$$r(t) = \alpha_0 x(t-\tau_0) e^{-j\phi_0} e^{j2\pi f_c \tau_0} + \sum_{n=1}^{N} \alpha_n x(t-\tau_n) e^{-j\phi_n} e^{j2\pi f_n \tau_n} \quad 4.2$$

where *n* indicates the nth reflected signal and f_n is the received frequency of the nth reflected signal related to the carrier frequency. The motion of the satellites, receiver and reflecting surfaces causes the parameters in Equations 4.1 and 4.2 to vary as a function of time. This time dependency is omitted here for the sake of simplicity, but needs to be taken into consideration in the multipath analysis. The use of different notations for the direct (f_c) and reflected (f_n) signal frequencies is necessary because the relative motion between the satellite, reflector and receiver is different from between the satellite and receiver. This difference creates a different Doppler frequency for each path. The existence of reflected signals with considerably different frequencies does not create a problem for the receiver because it loses its correlation with the direct signal and can be

resolved by the receiver. Therefore, it is safe to assume that the direct signal and reflected replicas have the same frequency. Based on this assumption, Equation 4.2 is commonly rewritten with new parameters that relate the direct path to the reflected paths:

$$r(t) = \alpha_0 e^{-j\tilde{\phi}_0}\left(x(t-\tau_0) + \sum_{n=1}^{N} \tilde{\alpha}_n e^{-j\tilde{\phi}_n} x(t-\tau_0-\tilde{\tau}_n)\right) \quad 4.3$$

where $\tilde{\alpha}_n$ is the ratio of the multipath amplitude to the direct signal amplitude (damping factor), $\tilde{\tau}_n$ the propagation time difference between the direct signal and reflected one and $\tilde{\phi}$ the carrier phase of the different signal components.

Reflection from a smooth surface such as standing water or glass is called specular reflection. For L band signals if the height of the roughness of the surface is less than a few centimeters and the surface is large enough with consistent electrical properties, a specular reflection occurs. In contrast, reflection from a rough surface causes diffused multipath. Most of the multipath analysis is done based on specular reflection although a perfect specular reflection is rare in real life (Kaplan and Hegarty 2006).

In summary a multipath signal is characterized by different parameters like *time delay*, *amplitude* and *phase*, all relative to the Line Of Sight (LOS) direct path signal. The *time delay* of a multipath signal is caused by the signal travelling an additional distance relative to the LOS signal. The nature of the reflecting surface structure determines the related *amplitude* of the multipath signal while the reflecting/diffracting properties of the surface together with the additional path length determine the relative *phase* of the

multipath signal (Hannah 2001). If the relative amplitude is constant as in specular reflection, the error for a given multipath delay varies with the multipath phase. The maximum and minimum multipath error as a function of multipath delay with a given relative amplitude represents the multipath error envelope (Kaplan and Hegarty 2006). Such an error envelope is commonly used for analysing the receiver performance in multipath mitigation.

4.2 Impact of multipath on the receiver

The effect of multipath is mainly on the signal tracking function in the receiver, and less so on the signal acquisition and message demodulation. However, in severe multipath conditions, the acquisition and data demodulation may also be affected (Kaplan and Hegarty 2006). The focus of this thesis is on the effect of multipath on the tracking function. GNSS measurements are calculated in the receiver by correlating the received signal $r(t)$ with a locally generated signal $e^{-j\theta}x(t)$. If there is no multipath, the statistical mean of the correlation result is:

$$\bar{\lambda}(\tau) = \alpha_0 e^{-j(\tilde{\phi}_0-\theta)} R_x(\tau-\tau_0) \tag{4.4}$$

where $R_x(\tau-\tau_0)$ is the correlation function. If reflected signal(s) exist, the correlation function becomes the sum of the ideal correlation function and the correlation

function due to the reflected signal(s). The composite correlation function, $\hat{R}_x(\tau - \tau_0)$ with a direct signal and one multipath component can be represented as:

$$\hat{R}_x(\tau - \tau_0) = R_x(\tau - \tau_0) + \tilde{\alpha}_1 e^{-j\tilde{\phi}_1} R_x(\tau - \tau_0 - \tilde{\tau}_1) \quad 4.5$$

The multipath (indirect) signal always arrives later at the receiver than the direct signal due to the longer distance of travel. This indirect signal changes the correlation shape in the receiver. If the delay is sufficiently long (e.g. two chips) the receiver is able to resolve the multipath, because the peak of the correlation function is not distorted and the tracking loop is able to track the correct correlation peak between the locally generated signal and the direct signal. However, the receiver will not be able to resolve short delay multipath due to reflections from nearby objects. This causes the tracking loop to track the composite signal.

The effect of the multipath signal on the autocorrelation function of the GPS CA signal is illustrated in Figure 4.1. The top panel represents the square correlation function of a locally generated signal with the direct signal. The second, third and fourth panels represent the squared correlation functions in case of one reflection path delayed by 0.1 micro seconds with phase shift of zero, 90 and 180 degrees respectively (Kaplan and Hegarty 2006).

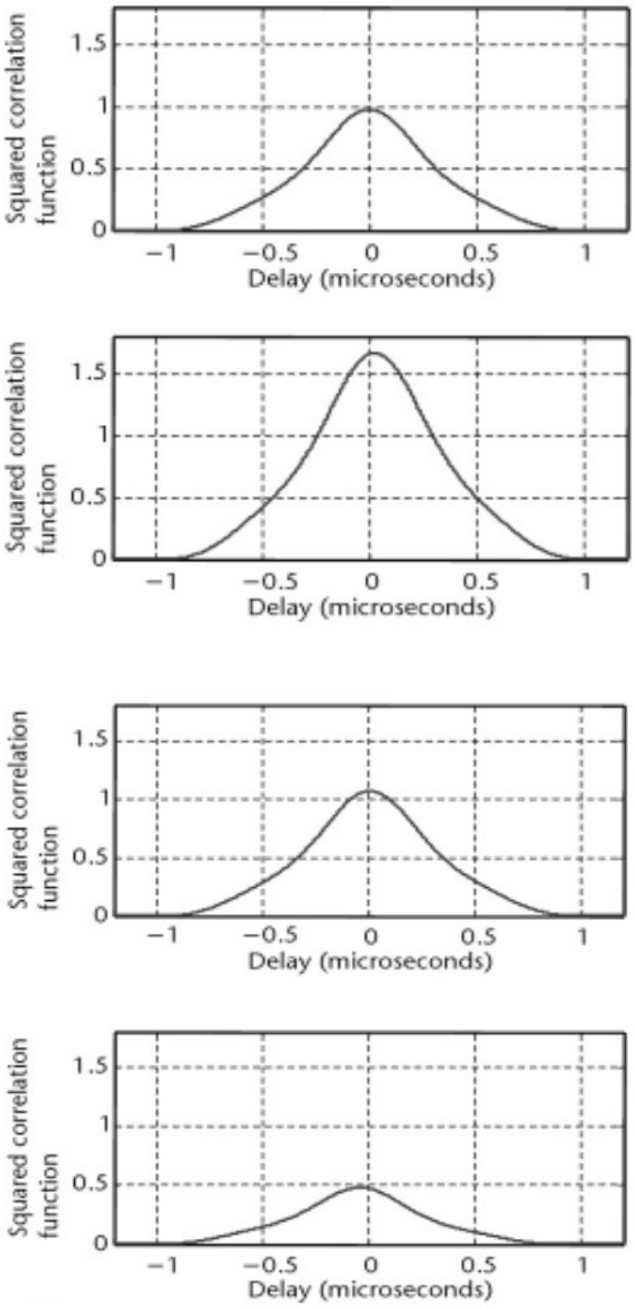

Figure 4.1: Multipath effect on the correlation function. First panel; no multipath; second panel: one reflected signal with zero phase shift; third panel: one reflected signal with a 90 degree phase shift; fourth panel: one reflected signal with a 180 degree phase shift (Kaplan and Hegarty 2006)

4.2.1 IMPACT OF MULTIPATH ON CODE PHASE MEASUREMENTS

To obtain code phase measurements, the locally generated code is shifted in time to achieve optimal correlation with the received signal. The correlation value is used by a discriminator function to adjust the local code with the incoming code and estimate the time delay from which the so called code phase measurement is obtained. A common code discriminator function used in GNSS receivers is the Early correlator (E) minus Late correlator (L) values (E-L). The Early correlator value is the correlation between the incoming code and an early version of the locally generated code. The Late correlator value is the correlation value between the incoming code and a late version of the locally generated code. In the presence of multipath, the time delay is estimated by correlating the composite signal with locally generate code(s), which results in code phase measurement errors, a phenomenon known as code multipath error. The impact of multipath on code phase measurements can be up to half a chip equivalent to a range error of about 150 meters for the GPS C/A code (Groves 2008). The error can be positive or negative depending on the phase (Kaplan and Hegarty 2006). Figure 4.2 shows the code multipath error envelope for the BPSK-R(1) signal (GPS CA code) using 4 MHz and 24 MHz precorrelation bandwidths, and the BPSK-R(10) code with a 24 MHz precorrelation bandwidth. In all three cases, the difference between the early version of the locally generated code (E) and the late one (L) is 50 ns, equivalent to 0.05 chips in the GPS CA code (narrow correlator).

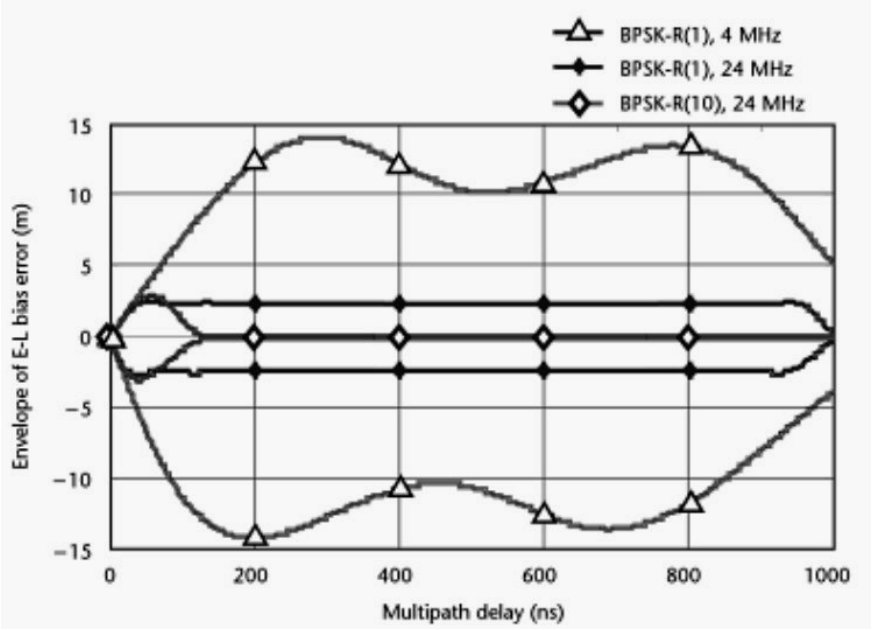

Figure 4.2: Code multipath error envelope (Kaplan and Hegarty 2006)

As shown in Figure 4.2, a higher chip rate decreases the multipath error significantly. Therefore, using an optimum GNSS code is a key factor to mitigate code multipath errors. In addition the spacing of the Early-Late correlator may also affect the performance. This effect is discussed in more detail in Section 4.3.2.1.

4.2.2 IMPACT OF MULTIPATH ON CARRIER PHASE MEASUREMENTS

The estimation of carrier phase measurements is also affected by multipath. The phase angle of the multipath-contaminated signal in the receiver is estimated from the composite correlation function by:

$$\psi = \tan^{-1}\left(\frac{Imaginary\left(\hat{R}_x(\tau-\tau_0)\right)}{Real\left(\hat{R}_x(\tau-\tau_0)\right)}\right)$$

4.6

where:

$$Imaginary\left(\hat{R}_x(\tau-\tau_0)\right) = \tilde{\alpha}_1 R_x(\tau-\tau_0-\tilde{\tau}_1)sin\tilde{\phi}_1$$

4.7

and

$$Real\left(\hat{R}_x(\tau-\tau_0)\right) = R_x(\tau-\tau_0) + \tilde{\alpha}_1 R_x(\tau-\tau_0-\tilde{\tau}_1)cos\tilde{\phi}_1$$

4.8

For relatively small multipath delays, $\tilde{\tau}_1$ can be neglected. Therefore, from Equations 4.6, 4.7 and 4.8, the carrier phase measurement is obtained as:

$$\psi = \tan^{-1}\left(\frac{\tilde{\alpha}_1 R_x(\tau-\tau_0)sin\tilde{\phi}_1}{R_x(\tau-\tau_0) + \tilde{\alpha}_1 R_x(\tau-\tau_0)cos\tilde{\phi}_1}\right)$$

4.9

If the carrier phase of the direct path is defined as zero, ψ is the carrier phase error caused by multipath which is referred to as the carrier phase multipath error. The maximum carrier phase multipath error happens when $\frac{\partial\psi}{\partial\tilde{\phi}_1} = 0$. In this case the maximum error is $\pm\sin^{-1}\tilde{\alpha}_1$ (Leick 2004). This means the maximum value is function of damping

factor only. This will result in a maximum carrier phase multipath error of $\frac{\pi}{2}$ radian, or one quarter of the wavelength when damping factor is one.

Figure 4.3 shows the carrier phase multipath error envelope for the BPSK-R(1) (GPS CA signal) using 4 MHz and 24 MHz precorrelation bandwidths and for the BPSK-R(10) code with a 24 MHz precorrelation bandwidth. The correlator spacing used in this figure is 50 ns.

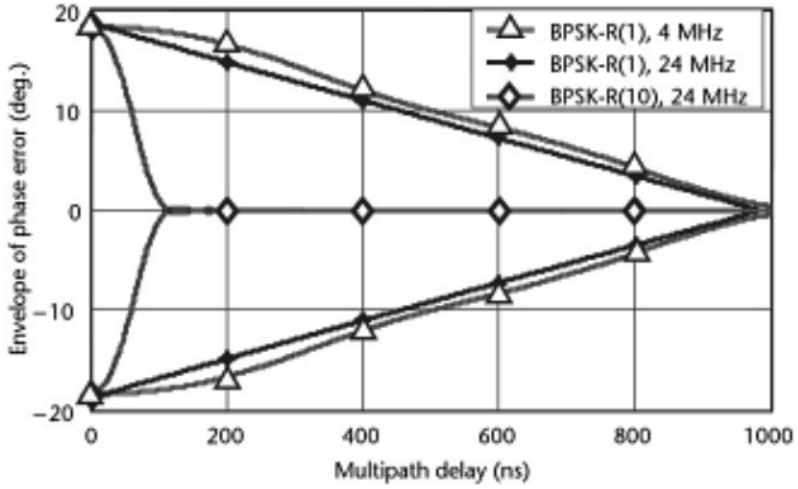

Figure 4.3: Carrier phase multipath error envelope (Kaplan and Hegarty 2006)

It is clear from Figure 4.3 that using higher code rates is very effective in achieving better carrier phase multipath mitigation in the receiver. Different Early-Late correlator spaces may also affect the performance. This effect is discussed in more detail in Section 4.3.2.1.

4.3 Multipath mitigation techniques

Despite the multitude of existing and emerging multipath mitigation techniques, multipath remains a major limiting factor for GNSS high accuracy positioning applications.

One common method of multipath mitigation is antenna siting or removing and modifying reflector surface in the vicinity of the antenna. For example, placing the antenna near the ground in an open area reduces the code multipath error significantly due to smaller errors in short-delay multipath (Figure 4.2) (Kaplan and Hegarty 2006). However, according to Figure 4.3 this is not the case for carrier multipath error. In contrast to code-multipath mitigation, it is better to raise the antenna to decrease the elevation angle of the reflected signal and hence, decrease the gain in the multipath direction (Kaplan and Hegarty 2006). However, this will increase the code multipath error due to reflection from the ground. Multipath mitigation by antenna siting is not the focus of this thesis and is not discussed further.

The rest of this section reviews the state-of-the-art multipath mitigation techniques, with a focus on carrier multipath errors. Existing multipath mitigation techniques can be classified into *antenna-based*, *signal-processing* and *measurement-processing* techniques. These are discussed in the following sections and their limitations identified.

4.3.1 ANTENNA-BASED TECHNIQUES

A number of *antenna-based* techniques have been developed to address the issue of multipath. The main techniques involve the use of antennae with a high sensitivity to Right-Hand Circular Polarized (RHCP) signals, choke-ring-ground-plane antennae and antenna arrays. These are discussed below along with their strengths and weaknesses.

4.3.1.1 Sensitivity to RHCP and Axial Ratio

The change in the polarization of the circular polarized signals after a single reflection can be used to mitigate multipath. All the current main GNSS transmit RHCP signals. Therefore, GNSS antennae are designed with a high sensitivity to RHCP signals and a low sensitivity to Left-Hand Circular Polarized (LHCP) signals. This property significantly reduces the multipath effect from all signals with an odd number of reflections. However, in practice it is not possible to design a perfect RHCP antenna which fully suppresses Left-Hand Circular Polarized (LHCP) signals. Generally, the quality of a Circular Polarized antenna (a special case of an elliptical polarized antenna) can be identified using the Axial Ratio (AR) parameter. AR is the ratio of the major axis of the polarisation ellipse to the minor axis (Galuscak–OM6AA and Hazdra 2006):

$$AR = \frac{Major\ axis}{Minor\ axis} \tag{4.10}$$

or

$$AR = 20 \log \frac{Major\ axis}{Minor\ axis} \quad 4.11$$

Good circular polarisation antennae should have an AR close to 1dB in broadside (looking straight up from the antenna) increasing with decreasing elevation angles. A high performance antenna should have an AR of 3 to 6 dB at an elevation angle of 10 degrees. Mitigating the reflected signal at high elevation angles is easier due to the relatively smaller AR value. At lower elevation angles (e.g. resulting from reflections from the ground), the AR is increasing, resulting in poor mitigation performance. In summary, this technique is not very effective since most of the reflections occur at low elevation angles (Moernaut and Orban 2008).

4.3.1.2 Choke ring ground plane antenna

Low elevation reflections can be mitigated within the antennae by reducing their gain at low elevation angles. The *choke ring ground plan*e antenna has been used for many years for this purpose. It is made of a single billet of aluminum and 3 to 5 cocentric ring structures. The choke rings create a high impedance surface which prevents the propagation of surface waves near the antenna. The ground plane suppresses the reflected signal from the ground. This technique is very effective in mitigating low elevation

reflected signals but at the same time the low elevation LOS signal reception is also degraded (Kunysz 2003). In kinematic or dynamic applications where the attitude of the antenna is not fixed, the use of such an antenna is limited, because it may remove the high elevation LOS signal when the ground plane is not horizontal. The other limitations of using choke ring ground plane antennae are their size and weight, making them difficult to be used in the majority of applications (Lim et al. 2010).

4.3.1.3 Directional antenna

The use of directional antennae is also referred to as *antenna array*. A combination of multiple antenna elements arranged in a certain configuration is able to achieve a gain in one direction and suppresses the signal from other directions through signal processing techniques. By adding a spatial dimension, the antenna array is able to distinguish between the LOS and unwanted signals, such as multipath and radio interference. The performance of the *antenna array* depends on the number of antenna elements, space between elements, as well as the amplitude and phase applied to each antenna element. Increasing the number of elements and element spacing leads to higher directivity of the array. However, element spacing of more than half of the wavelength results in increasing the side lobe amplitudes close to the level of the main lobe which is undesirable.

In addition to varying the number of elements and element spacing, the antenna side lobe level, directivity and direction of the main lobe can be modified by varying the

power and phase distribution for each element. Although directional antennae allow to accurately control the antenna pattern and thereby mitigate unwanted signals from directions other than the LOS direction, they are large in size and require significant additional signal processing techniques, making them difficult to use in most civilian applications (Sahmoudi and Landry 2008).

4.3.1.4 Summary

In summary, none of the state-of-the-art antenna techniques is able to mitigate multipath error sufficiently for all elevation angles. Mitigating the multipath error by antenna design is easier at high elevation angles than low elevation angles. Antenna-based techniques are summarised based on their strengths and weaknesses in Table 4.1.

Table 4.1: Comparison of antenna-based multipath mitigation techniques

Technique	*Strength*	*Weaknesses*
RHCP antenna	*Small in size and is applicable in all situations*	*Poor performance on reflected signals from low elevation*
	Does not need extra signal processing hardware in the receiver.	*Unable to effectively mitigate multiple reflected signals*
Choke Ring ground plane	*Excellent for reflected signals from the ground and low elevation angles*	*Removes low elevation LOS signals and is large in physical size*
	Does not need extra signal processing in the hardware	*Ground plane should be kept horizontal, which is not practical in some situations*
Directional antenna	*Good for both low and high elevation reflected signals*	*Large in size*
	Suppresses other interference signals from directions other than LOS direction	*Requires complex signal processing techniques, implemented in hardware*

4.3.2 SIGNAL-PROCESSING TECHNIQUES

Multipath errors that are not mitigated by antenna-based techniques can still be mitigated during the stage following the signal acquisition, i.e. during signal processing. In this section some of the main signal-processing techniques are presented, including the *narrow early-late correlator*, the *double delta correlator family* and the *multipath mitigation technique*. The weaknesses and strengths of each technique are discussed and compared.

4.3.2.1 Narrow early-late correlator

The *Narrow early-late correlator* is the simplest signal processing technique (Van Dierendonck 1992) in which a chip difference smaller than 1 (commonly 0.1) is used between the early and late code discriminator. Multipath distorts less near the peak area of the correlation function. Therefore, if the delay around the peak is tracked the effect of multipath can be reduced. A major drawback of this technique is that it is not able to track the signal for low signal to noise ratio scenarios. According to (Kaplan and Hegarty 2006), a narrow pre-correlation bandwidth (i.e. 4 MHz) with a narrow early-late Delay Lock Loop has little effect on multipath mitigation (Figure 4.2). Furthermore, it cannot improve the carrier phase multipath mitigation performance (Figure 4.3). This is due to the fact that this performance is a function of the shape of the correlator, which is the same for both narrow and wide correlators (Irsigler and Eissfeller 2001).

4.3.2.2 Double delta correlator family

The *double delta correlator* family uses two correlator pairs in the code discriminator function (Figure 4.4). It includes a number of widely-used code multipath error mitigation techniques, such as the *High Resolution Correlator* (HRC) and the *Early/Late Slope* (ELS) technique (McGraw and Braasch 1999). HRC performance is discussed here, as an example.

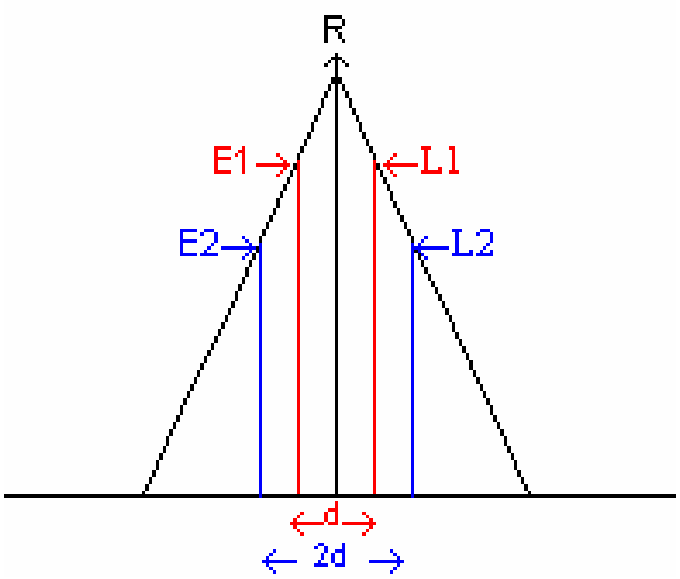

Figure 4.4**:** High Resolution Correlation function (Benachenhou et al. 2009)

In the HRC, if the space between E1 and L1 is d and the space between E2 and L2 is 2d, the code discriminator function can be obtained as:

$$D_{HRC} = (E_1 - L_1) - \frac{1}{2}(E_2 - L_2) \quad 4.12$$

The E1-L1 and E2-L2 can be interpreted as narrow correlators. Using this concept, the formula can be rewritten as follows:

$$D_{HRC} = Narow(d) - \frac{1}{2}\, Narrow\ (2d)$$

4.13

The Strobe Correlator is also a HRC with the following code discriminator function (Garin et al. 1996):

$$D_{STROBE} = 2.Narrow(d) - Narrow(2d) = 2D_{HRC}$$

4.14

Since code multipath is related to the shape of the code discriminator function and not to the linear combination of the correlator, the code multipath error envelope is the same for both HRC and Strobe Correlators. The carrier phase multipath error envelope is also the same for both cases because it depends on the shape of the signal autocorrelation function which is the same. The double delta correlator family is able to mitigate medium delay multipath errors (between 0.25 to 0.75 chips), more effectively than the narrow early late correlator. However, it has a similar impact as the narrow early late correlator on short delay multipath errors (i.e. shorter than 0.1 chips) (Weill 2003; Irsigler and Eissfeller 2001).

4.3.2.3 Multipath Estimation Delay Lock Loop

The Multipath Estimation Delay Lock Loop (MEDLL) is based on Maximum Likelihood (ML) estimation and was introduced in 1995. Using the MEDLL technique is like finding a set of reference correlation functions with a specific amplitude, phase and delay that fits more accurately the input signal.

This method allows improvements in the narrow-correlator performance by as much as 90% for one reflected path (Sahmoudi and Landry 2008). However, it cannot mitigate short delay multipath errors and, more importantly, requires high computational power.

4.3.2.4 Summary

Among the signal processing techniques, the maximum-likelihood techniques and double delta correlator family are able to mitigate medium and long delay carrier phase multipath errors. However, short delay code and carrier multipath errors are difficult to mitigate by signal-processing techniques alone. Table 4.2 summarises the strengths and weaknesses of the various *signal-processing* techniques discussed in this section.

Table 4.2: Signal processing techniques comparison

Technique	*Strength*	*Weakness*
Narrow early-late correlator	*Easy to implement*	*Not applicable in low SNR*
		Not effective on phase multipath error
		Unable to remove short delay multipath
Double delta correlator family	*Effective on medium delay code multipath error*	*Not effective on short and long delay multipath*
	Effective on medium delay carrier phase multipath error	
Maximum-Likelihood techniques	*Effective on code and carrier multipath error*	*High computational requirements*

4.3.3 MEASUREMENT-PROCESSING TECHNIQUES

Multipath errors that are not removed by antenna and signal processing techniques will contaminate the measurements obtained by the receiver. Therefore, measurement-based techniques, traditionally referred to as software techniques, are required to mitigate any residual multipath errors, especially for high accuracy positioning applications.

In this section, the six main categories of *measurement-processing* techniques for mitigating carrier phase multipath errors are discussed. These are the sidereal filtering, SNR-based multipath estimation technique, the simple elevation angle based stochastic

model, the sigma-ε stochastic model, the multiple antenna technique and the ray tracing technique.

4.3.3.1 Sidereal filtering

The orbital period of a GPS satellite is half a sidereal day (11 hours and 58 minutes). This results in a repeat in the geometry of each satellite every sidereal day. As the result, the same multipath condition will be created for a stationary receiver in the same environment. This is also true for the GLONASS constellation. Although, a GLONASS satellite geometry repeats every 8 days, there will be one satellite in the same spot of the sky after one sidereal day. This is because each orbital plane of the GLONASS constellation contains 8 satellites equally spaced.

The multipath repeating condition after one sidereal day can be exploited for multipath mitigation. Multipath mitigation based on *sidereal filtering* can be done in the measurement/observation as well as coordinate domains. In the former, firstly the final coordinates of a static antenna in double differenced mode are estimated after resolving all the ambiguities. Then the double differenced residual which includes double difference carrier multipath errors are obtained by taking back the ambiguities and the final coordinate estimates to the double differenced carrier phase model. Assuming that the sum of observed satellites single difference residuals are zero, the single differenced residuals can be recovered from the double differenced residuals. The single differenced

residual may pass through a low-pass filter to separate noise from the multipath error. Finally, single difference multipath model is achieved for each individual satellite and can be applied for the following days at the same time (Ye et al. 2014).

Sidereal filtering technique in coordinate domain can be done using a similar principle to the observation domain technique. In the coordinate domain, firstly, all the ambiguities are resolved. Then, coordinate residuals are calculated with respect to the long-term averaged coordinate of the antenna. The coordinate residuals are then subtracted from the processed coordinate of the following days at the same time (Ragheb et al. 2007).

Sidereal filtering in both observation and coordinate domains can be done only on static applications within the same environment. In addition, this technique also suffers from needing at least one sidereal day to form the multipath model. Most of the applications cannot tolerate such a long delay.

4.3.3.2 SNR-based multipath estimation technique

The carrier phase multipath error is directly related to SNR in the simple scenario where there is only one secondary path and the receiver is stationary (Bilich and Larson 2007). This relation can easily be derived using the phasor diagram shown in Figure 4.5.

In that figure, $A_m$and θ are the reflected signal amplitude and phase shift respectively, A_d and ϕ_d the direct path amplitude and phase respectively, A_c and ϕ_c the combined signal amplitude and phase respectively and ψ the carrier phase error.

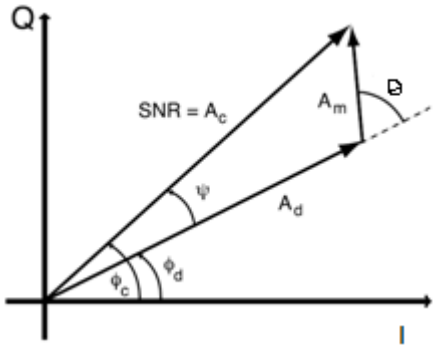

Figure 4.5: Phasor diagram for direct, reflected and combined signal (Lau and Cross 2006)

From the phasor diagram, the carrier multipath error can be obtained as:

$$\tan(\psi) = \frac{A_m sin\theta}{A_d + A_m cos\theta}$$

4.15

In the SNR based carrier multipath estimating technique A_m, θ and A_d are estimated from the SNR data and the carrier phase multipath error is calculated according to Equation 4.15. The SNR which is directly related to amplitude can be determined from the phasor diagram as:

$$SNR^2 \equiv A_C^2 = A_m^2 + 2A_d A_m cos\theta$$

4.16

The time varying nature of the phase shift θ results in a time varying SNR as well as phase error ψ. Consequently, the SNR data can be used to calculate the parameters required to estimate the carrier phase multipath error. In this technique, the multipath contaminated SNR (SNR_{MP}) is first separated from the nominal SNR (SNR_0). The nominal SNR can be estimated by fitting a polynomial of order 5 to 15 to the raw SNR. By subtracting the nominal SNR from the raw SNR, the multipath contaminated SNR can be extracted. In the next step, the amplitude and phase of the multipath contaminated SNR, which correspond to A_m and θ respectively according to the phasor diagram, are estimated. The angular frequency $\omega(t)$ of the SNR_{MP} is estimated first, for example, via the wavelet transform. After estimating the angular frequency of SNR_{MP}, the amplitude and phase of the SNR_{MP} are estimated as a function of time using an adaptive least squares approach. The carrier phase multipath error according to Equation 4.15 is dominated by $\sin(\theta)$ while the SNR is dominated by $\cos(\theta)$ resulted in a time lag between carrier multipath error and SNR. Therefore, the estimated θ from the SNR must be adjusted by $\frac{\pi}{2}$ before calculating the carrier phase multipath error:

$$\tan(\psi) = \pm k \frac{A_m \sin(\theta \pm \frac{\pi}{2})}{SNR_0 + A_m \cos(\theta \pm \frac{\pi}{2})} \quad 4.17$$

where k is the scale factor which determines the relationship between the SNR and multipath error in a specific receiver.

It is impossible to predict the correct sign for $\frac{\pi}{2}$ in equation 4.17. This sign ambiguity may lead to a 180 degree error in the carrier phase multipath estimation (Lau and Cross 2006).

Furthermore, the relationship between carrier phase multipath errors and the SNR discussed above is only valid in static modes. For dynamic scenarios, the carrier phase multipath error acts more like noise. Another limitation of the above method is that the number of reflectors needs to be known in order to be able to calculate the carrier phase multipath error. Additionally, separating the multipath contaminated SNR and nominal SNR from the raw SNR by a curve fitting approach cannot easily done in real time applications. Therefore, this technique is difficult to apply in dynamic real time scenarios.

4.3.3.3 Simple elevation angle based stochastic model

GNSS signals are attenuated by the atmosphere to a larger extent at lower elevation angles. Signals at low elevations are also more prone to multipath errors. Hence, observations at low elevation angles are less accurate than at high elevations (Liu 2001). Therefore, the elevation angle can be used to weigh GNSS measurements accordingly. In a simple elevation angle based stochastic model, a linear relationship between the GNSS signal quality and elevation is assumed. The cosine of the elevation angle is a simple parameter which can be used to define this relationship. For example, the standard deviation for the carrier phase measurement as function of elevation angle can be obtained as (Barnes et al. 1998):

$$\sigma = \sqrt{1 - (\sin E/1.001)^2}\,.\,\psi_m$$

4.18

where $\psi_m$is the maximum phase multipath error which can be approximated as 3 cm for the L1 frequency and E is the elevation angle.

This model is applicable for both dynamic and static situations and there is no need to know the number of reflected signals. However, using only the elevation angle as a weighting parameter is an oversimplification because in some cases a low elevation LOS signal gets low weight while a high elevation multipath signal gets a high weight in this model. According to (Lau and Cross 2007b) the application of simple elevation angle based stochastic methods results in slight improvements in the 3D position errors. The reason behind this small improvement is that the effects of the environment are not reflected on satellite elevation although there is strong correlation between observation accuracy and elevation angle (Liu 2001).

4.3.3.4 SIGMA-ε stochastic model

As discussed in Section 4.3.3.1, there is a correlation between the SNR and the carrier multipath error. This correlation is exploited based on Equation 4.19 in the *sigma-epsilon* model to assign a better standard deviation for the carrier phase measurements. The standard deviation of the carrier phase measurements is estimated as (Hartinger and Brunner 1999):

$$\sigma \quad = \sqrt{C.10^{-\frac{CNR}{10}}}$$

4.19

where C consists of carrier loop noise bandwidth and a term for converting from cycles to millimeters.

Since the CNR is effectively equivalent to the SNR, Equation 4.19 can be written in terms of the SNR as:

$$\sigma \quad = \sqrt{C.10^{-\frac{SNR}{10}}}$$

4.20

Similar to the *elevation angle-based* stochastic model, the *SIGMA-**ε*** model is applicable to dynamic and static scenarios. Knowledge about the number of multipath elements is not necessary (Lau and Cross 2007b) (Wieser and Brunner 2000). However, this model suffers from the same drawback as the elevation angle based stochastic model since the SNR is directly related to the elevation angle; i.e. a low elevation angle signal has a smaller SNR. Yet it is not always true that low elevation signals contain multipath. Moreover, the time lag between the SNR and carrier phase multipath error has a negative effect on any weighting technique based on the SNR.

4.3.3.5 Multiple antenna

The basic principle of the *multiple antenna* technique in multipath mitigation is based on exploiting the phase difference of reflected signals at different antennae. If the distance between the antenna elements is small (a few centimetres), the multipath errors are highly correlated and hence can be estimated if the geometry of the closely spaced antennae is known. In this technique, single differenced carrier phase measurements are first formed between the reference antenna *i* and each of the auxiliary antennae represented by *j*:

$$\Delta\Phi_f = \rho_{ij} - \lambda \ \ N_{ij,f} + m_{ij,f,\Phi} + \varepsilon_{ij,f,\Phi}$$

4.21

As a result of the single difference, all the correlated errors such as satellite and receiver clock errors are removed. As it has been discussed in Section 1.3.3.3 carrier phase measurement noise level is in order of mm which can be ignored. Due to the small separation distance between the antennae (few centimetres), the atmospheric errors are highly correlated which are almost eliminated by the differencing. If the range difference between the antennae is known and the ambiguities are resolved, single difference carrier multipath errors in radian (ψ) can be calculated as:

$$\lambda \ \ \psi_{ij} = \Delta\Phi_f - \rho_{ij} + \lambda \ \ N_{ij,f}$$

4.22

The single difference carrier multipath error is used to calculate the multipath parameters for each antenna element. Based on Equation 4.9, the differenced carrier multipath error is expressed as:

$$\psi_{ij} = \psi_j - \psi_i = \tan^{-1}\left[\frac{\alpha_j \sin\theta_j}{1 + \alpha_j \cos\theta_j}\right] - \tan^{-1}\left[\frac{\alpha_i \sin\theta_i}{1 + \alpha_i \cos\theta_i}\right]$$

4.23

where ψ_j is the phase multipath error in antenna j, $\psi_i$the phase multipath error in antenna i and θ the phase shift of the reflected signal relative to the direct signal.

Evaluating the above equation results in:

$$\psi_{ij} = \tan^{-1}\left[\frac{\alpha_j \sin\theta_j + \alpha_i\alpha_j \sin\theta_j \cos\theta_i - \alpha_i \sin\theta_i - \alpha_i\alpha_j \sin\theta_i \cos\theta_j}{1 + \alpha_i \cos\theta_i + \alpha_j \cos\theta_j + \alpha_i\alpha_j \cos\theta_i \cos\theta_j + \alpha_i\alpha_j \sin\theta_i \sin\theta_j}\right]$$

4.24

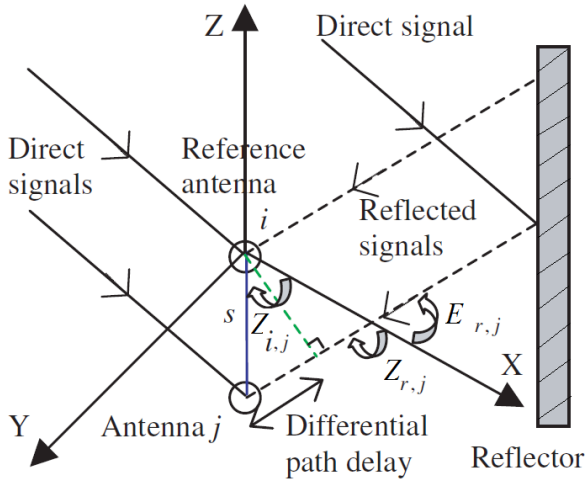

Figure 4.6: Multiple antenna geometry (Lau and Cross 2007b)

Assuming that the reflected signals arriving at the *antenna array* are parallel, the phase of the reflected signal in antenna j is equal to that in antenna i plus a differential path delay in radians:

$$\theta_j = \theta_i + \frac{2\pi}{\lambda_L}\Delta_d$$

4.25

where θ_j is the phase of the reflected signal in antenna j, θ_i the phase of the reflected signal in antenna i and Δd the differential path delay. Replacing Δd using geometrical operations, Equation 4.25 can be written as:

$$\theta_j = \theta_i - \frac{2\pi}{\lambda_L} s \cos\left(Z_{r,j} - Z_{ij}\right) cos\ E_{r,j}$$

4.26

where Z_{ij} is the azimuth of the line joining the antenna i (reference antenna) to the antenna j (auxiliary antenna), $Z_{r,j}$ the azimuth of the reflected signal to antenna j and $E_{r,j}$ the elevation angle of the reflected signal at the antenna j (Figure 4.6). Due to the small separation distance between antennae i and j related to the antenna reflector distance, it can be assumed that signals reaching the antennae from the reflector are parallel. Hence, the azimuth and elevation angles of the reflected signals are the same for both antennae. Therefore, $Z_{r,j}$ and $E_{r,j}$ are replaced by Z_r and E_r respectively in

Equation 4.26. Furthermore, it is assumed that all the reflected signals reaching different elements of the antenna are reflected from the same surface. Therefore, α_j is replaced by α_i in Equation 4.24. By evaluating Equations 4.24 and 4.26 the single difference phase multipath error can be written as:

$$\psi_{ij} = tan^{-1}\left[\frac{\alpha_i sin\left(\theta_i - \frac{2\pi}{\lambda_{L1}} s\cos(Z_r - Z_{ij})\, cos\, E_r\right) - \alpha_i sin\theta_i + \alpha_i^2\left(-\frac{2\pi}{\lambda_{L1}} s\cos(Z_r - Z_{ij})\, cos\, E_r\right)}{1 + \alpha_i cos\,\theta_i + \alpha_i cos\left(\theta_i - \frac{2\pi}{\lambda_{L1}} s\cos(Z_r - Z_{ij})\, cos\, E_r\right) + \alpha_i^2 cos\left(-\frac{2\pi}{\lambda_{L1}} s\cos(Z_r - Z_{ij})\, cos\, E_r\right)}\right] \quad 4.27$$

Equation 4.27 has four unknown parameters to be solved:

$$[\alpha_i\ \theta_i\ Z_r\ E_r]^T$$

where α_i is the damping factor, θ_i the phase shift of the reflected signal reaching antenna i, Z_r the azimuth of the reflected signal from the reflector r at the antenna array and E_r is the elevation of the reflected signal.

At least 5 antennae (i.e. 4 single difference equations), are required to calculate these parameters, using a standard least squares technique or Extended Kalman Filter. The phase shift at each antenna can then be calculated using Equation 4.26. In practice, to calculate the carrier multipath error at the reference antenna, only the damping factor and phase shift at the reference antenna are required.

In this technique, it is essential to accurately calculate the range difference between the various antenna elements. This can be done in a permanent stationary

reference station by computing the azimuth of the auxilary antennae to the reference antenna, while in kinematic applications this is very difficult due to the small separation between the antenna elements. Testing this technique in permanent stations showed a good approximation of the carrier multipath error (Lau and Cross 2007b). However, this technique is similar to the SNR technique in the sense that the number of reflected signals must be known. Furthermore, an *antenna array* is bulky which makes it difficult to be used in dynamic situations. These are serious limitations which make this technique impractical in real situations.

4.3.3.6 Ray tracing method

The geometry of the operational environment can be exploited to extract the required information for multipath error estimation. In this method, the carrier phase multipath error is estimated from known geometrical relationships between the satellite, reflector and receiver. Therefore, an accurate knowledge of the satellite-reflector-antenna geometry is essential. In addition, the reflection coefficient of the reflector material at the target frequency must be known.

By knowing the position of the corners of the reflector and the signal direction, any potential intersection point of the signal on the reflector can be determined. If an intersection exists, the phase shift of the reflected signal (θ) related to the LOS signal can be calculated as:

$$\theta = \frac{L_m - L_d}{\lambda} + \varphi_w \quad 4.28$$

where L_m is the distance of the multipath signal from the satellite to the antenna via the reflector, L_d the direct path, λ the wavelength and φ_W the phase wind-up error, which is negligible. By estimating the phase shift, the carrier phase multipath error can be calculated from Equation 4.9.

Testing the ray-tracing method for a set of data collected in a permanent station shows accurate calculation of carrier multipath error. However, this technique can be used for specular reflection only, with negligible penetration depth. In addition, the number of multipath signals and the satellite-reflector-antenna geometry should be known precisely, which is not possible in real situations.

4.3.3.7 Summary

The strengths and weaknesses of the measurement processing techniques discussed in Section 4.3.3 are presented in Table 4.3. Most of the measurement processing techniques are able to mitigate the residual carrier multipath error to varying degrees. Although some of the techniques (i.e. antenna array and ray tracing) are able to accurately estimate the carrier multipath error, serious limitations remain, which makes these techniques useful only for permanent stations or well controlled environments.

Hence mainly simple stochastic techniques such as the simple elevation or SNR based techniques are used in most of the applications.

Table 4.3: Comparison of measurement processing techniques

Technique	*Strengths*	*Weaknesses*
sidereal filtering	*Mitigates short delay and long delay multipath*	*Not applicable for dynamic scenarios*
		Not applicable in real time
SNR-based multipath estimation	*Mitigates short delay and long delay multipath*	*Number of multipath signals should be known*
		Not applicable for dynamic situations
		Sign error
Stochastic Models	*Applicable for dynamic and static situations*	*Ignore environmental effects*
	Mitigate short delay and long delay multipath	
Multiple antenna	*Mitigate short delay and long delay multipath*	*Number of multipath signals must be known*
		Not applicable for dynamic scenarios
Ray tracing	*Mitigate short delay and long delay multipath*	*Number of multipath signals must be known*
		Satellite-reflector-antenna geometry must be known

4.4 Summary

In this chapter, the GNSS signal models for direct and multipath-contaminated signals as well as the impact of multipath on the receiver measurements have been

presented. State-of-the-art techniques developed in the literature to mitigate the multipath effect on the code and carrier phase measurements were reviewed, including their characteristics, operational environments, advantages and limitations. Table 4.4 provides a summary of the different aspects of these techniques, classified into antenna-based, signal processing and measurement processing techniques. The review of the different multipath mitigation techniques presented in this chapter highlights their limitations in supporting high accuracy GNSS positioning in varying environments. From the discussion in this chapter and Table 4.4, it is clear that for high accuracy carrier-phase based positioning applications, residual carrier phase multipath errors in the measurements cannot sufficiently be mitigated using current techniques.

In high accuracy positioning, it is common to form linear combinations of measurements such as Ionosphere Free and Wide Lane combinations. If the residual carrier multipath error in the measurements is not mitigated effectively, the error is magnified in the combination. The main common weakness of the current techniques is that they are focusing on single frequency multipath mitigation, which is difficult to achieve. In order to address this deficiency, Chapter 5 investigates carrier phase multipath errors in linear combinations directly, and develops new ways to model the resulting errors and mitigate them.

Table 4.4: Comparison of multipath mitigation techniques

		Antenna techniques			Signal processing techniques			Measurement techniques					
		RHCP	Antenna array (beam forming)	Choke ring ground plane	Narrow early-late correlator	Double Delta correlator family	Maximum-Likelihood techniques	sidereal filtering	SNR-based multipath estimation	Simple Elevation angle Stochastic Model	SIGMA-ε stochastic Model	Multiple antenna	*Ray tracing*
Dynamic situations	Static	√	√	√	√	√	√	√	√	√	√	√	√
	Low dynamic	√			√	√	√		√	√	√		√
	Dynamic	√			√	√	√			√	√		√
Code multipath	Long delay	√	√	√	√	√		√	√	√	√	√	√
	Medium delay	√	√	√		√	√	√	√	√	√	√	√
	Short delay	√	√	√			√	√	√	√	√	√	√
Phase multipath	Long delay	√	√	√				√	√	√	√	√	√
	Medium delay	√	√	√		√	√	√	√	√	√	√	√
	Short delay	√	√	√			√	√	√	√	√	√	√
Environments	Unknown number of reflectors	√	√	√	√	√	√	√		√	√		
	Second reflection		√	√	√	√	√	√	√	√	√	√	√
	Low elevation reflection		√	√	√	√	√	√	√	√	√	√	√
	Low SNR	√		√				√	√	√		√	√
Efficiency	Simple calculation	√		√	√	√				√	√	√	
	Size	√			√	√		√	√	√	√		√
	Cost	√		√	√	√		√	√	√	√		√
	Problems			Excellent only for ground reflection				long processing delay	Sign error problem	Low weight for low elevation LOS signal	Low weight for low elevation LOS signal	Direction of antenna array should be known	*Needs for a good approximation of antenna and reflector position*

Chapter 5

CARRIER MULTIPATH MITIGATION IN LINEAR COMBINATIONS

Chapter 4 reviewed the current state-of-the-art GNSS multipath mitigation techniques. It concluded that current techniques are either unable to mitigate the residual carrier multipath errors to the level where high-accuracy positioning can be achieved or they are impractical for most applications targeted in this thesis.

The availability of multi frequency measurements provides new opportunities for ionospheric error mitigation by forming linear combinations of measurements, exploiting the dispersive nature of the ionosphere. However, when forming linear combinations of measurements at two or more frequencies, the carrier multipath error, which is typically at the centimetre level, can be magnified to decimetre level. Despite the fact that multipath error is frequency dependent, all existing multipath mitigation techniques attempt to correct the error at the single frequency level, even if linear combinations of measurements at multiple frequencies are formed. This thesis for the first time, attempts

to mitigate the carrier multipath error directly in linear combinations, utilising its dispersive nature.

Section 5.1 investigates the carrier multipath error in linear combinations in relation to that in individual frequencies. The carrier multipath error in linear combinations is then modelled in Section 5.2, based on a new observable referred to as Inter Frequency carrier Multipath (IFM) developed in this thesis. Section 5.3 discusses the process of deriving the IFM observable. Section 5.4 discusses the application of IFM observable. The chapter is concluded in Section 5.5.

5.1 Carrier multipath error in linear combinations

The carrier phase measurement (in units of length) obtained from the linear combination of measurements at two frequencies can be generalised as:

$$\Phi_c = \alpha\Phi_1 - \beta\Phi_2 \tag{5.1}$$

where Φ_1 and Φ_2 are the measurements in units of length at frequency 1 and 2 respectively and α and β are coefficients which define the weights of each observable. From Equation 5.1, errors and noise in the linear combination are obtained as:

$$V_c = \alpha V_1 - \beta V_2 \tag{5.2}$$

where $V_1$and V_2 represent the individual errors of each frequency signal in units of length, V_c is the error of the linear combination in units of length. According to Equation 5.2, the maximum carrier multipath error $m_{c,max}$ in a linear combination is obtained as:

$$m_{c,max} = \alpha m_{1,max} + \beta m_{2,max} \tag{5.3}$$

where $m_{1,max}$ and $m_{2,max}$ represent carrier multipath error in units of length at the respective frequency. From Equation 5.3, it is clear that the maximum error in the linear combination is higher than the error at each individual frequency for values of α and β greater than one. Examples of linear combinations include the Wide-Lane (WL) and Ionosphere-Free (IF) combinations. These are analysed in this thesis. According to Equation 2.25, the α and β values for IF combination in units of length are:

$$\alpha_{IF} = \frac{f_1^2}{f_1^2 - f_2^2} \approx 2.54$$
$$\beta_{IF} = \frac{f_2^2}{f_1^2 - f_2^2} \approx 1.54$$

For WL observable α and β values are obtained from Equation 3.20 as:

$$\alpha_{WL} = \frac{f_1}{f_1 - f_2} \approx 4.53$$
$$\beta_{WL} = \frac{f_2}{f_1 - f_2} \approx 3.53$$

Based on the α and β values and Equation 5.3, the maximum carrier multipath errors in the WL and IF are 0.43m and 0.21m respectively. This means that the error in WL is almost half of the WL wavelength and is larger than the L1 wavelength for IF combination, while carrier multipath error in single frequency measurement cannot exceed ¼ of the wavelength. This increase in the carrier multipath error in the WL observable makes ambiguity resolution more difficult. The increase in the error in the IF combination, causes a delay in the convergence time and a deterioration in the position accuracy. Therefore, modeling and mitigating carrier multipath errors in linear combinations is key to achieving high accuracy position solutions.

A simplified two dimensional geometry represented in Figure 5.1 is used to investigate the multipath error as a function of multipath delay.

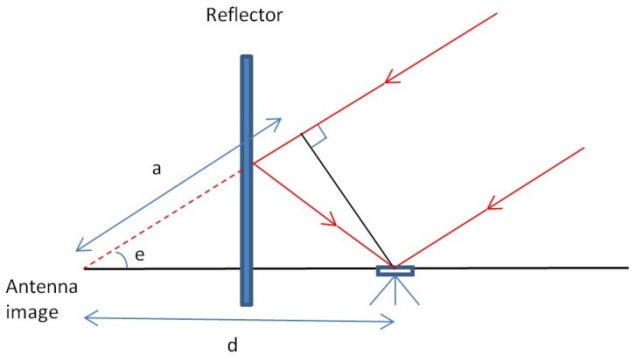

Figure 5.1: Simplified Multipath geometry

From Figure 5.1, the phase shift γ as a function of multipath delay *d* is:

$$\gamma = \frac{2\pi}{\lambda} d\ cos(e)$$

5.4

where *e* is the elevation angle. From the carrier multipath equation presented in Equation 4.15 and Equation 5.4, the carrier multipath error at each individual frequency is obtained as a function of the multipath delay as:

$$m = \tan^{-1}\left(\frac{\Gamma \sin\left(\frac{2\pi}{\lambda} d\ cos(e)\right)}{1 + \Gamma \cos\left(\frac{2\pi}{\lambda} d\ cos(e)\right)}\right)$$

5.5

Equation 5.5 is then used to illustrate the multipath error as a function of the multipath delay for each individual frequency together with the WL and IF combinations in Figures 5.2 and 5.3 respectively. The maximum possible carrier multipath error happens with a reflection coefficient of one. But having a reflection surface with such a reflection coefficient is rare in normal operational environments. Therefore, a reflection coefficient of 0.5 has been used to plot Figure 5.2 and Figure 5.3. Although the reflection coefficient of a surface is frequency dependent, for illustrative purposes it was assumed that GPS L1 and L2 have the same reflection coefficient (Najibi and Jin 2013). In the figures, the errors in the linear combinations have been generated by equation 5.2.

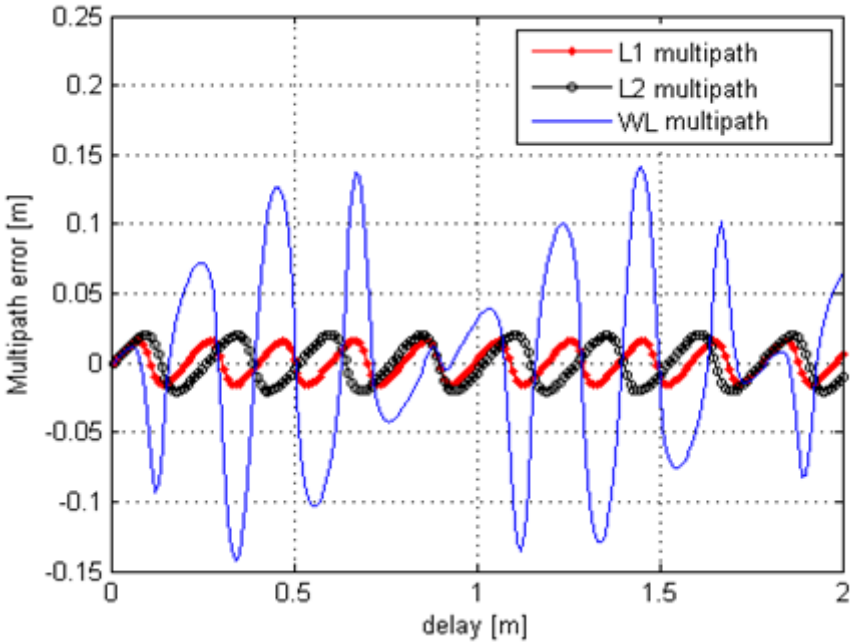

Figure 5.2: Relation between simulated multipath errors in L1, L2 and WL

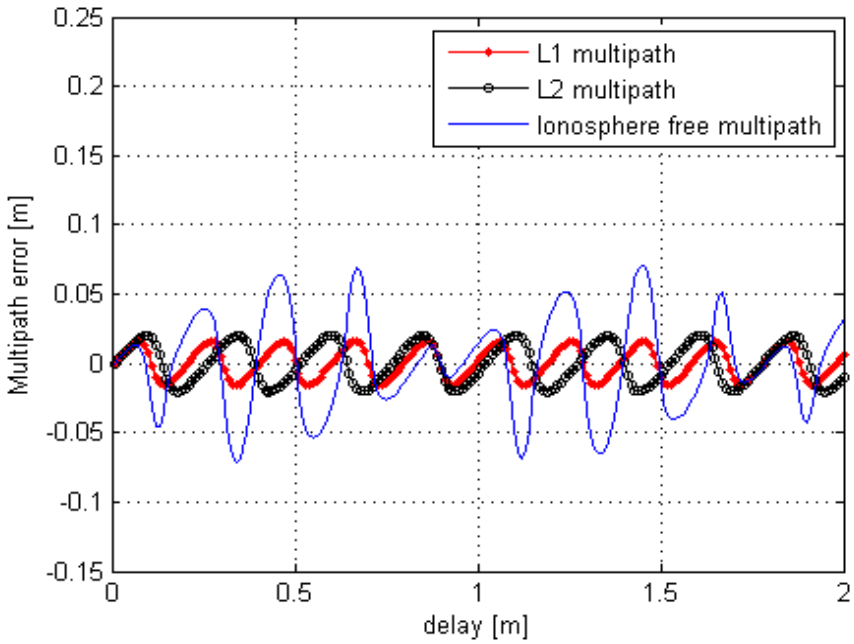

Figure 5.3: Relation between simulated multipath errors in L1, L2 and IF

Figure 5.2 and Figure 5.3 show that the WL and IF multipath errors are magnified where the errors at the different frequencies are out of phase. In the generating the figure, a reflection coefficient of 0.5 has been used. Therefore, the errors did not reach their maximum values.

5.2 Carrier multipath error modelling in linear combinations

Modeling errors is a prerequisite to the development of an effective mitigation technique. Unfortunately, modeling the multipath error is made difficult in real applications due to its dependency on the environment. Nonetheless, the dependency of the multipath error on the signal frequency can be exploited to model the error in linear combinations. Equation 5.2 for the carrier multipath error can be rewritten based on the β coefficient only. If x is the difference between the two coefficients α and β (i.e. $x = \alpha - \beta$) and m_c is the carrier multipath error in the linear combination, then:

$$\begin{aligned} m_c &= (\beta + x)m_{L1} - \beta m_{L2} \\ &= \beta(m_{L1} - m_{L2}) + x m_{L1} \end{aligned} \quad 5.6$$

The value in the parenthesis in Equation 5.6 is named the Inter-Frequency carrier Multipath error (IFM):

$$IFM = m_{L1} - m_{L2} \quad 5.7$$

Then the carrier multipath error in the linear combinations can be rewritten based on the IFM as:

$$m_c = \beta \cdot IFM + x \,.\, m_{L1} \tag{5.8}$$

It should be noted that the value of x (difference between α and β) in Equation 5.8 is 1 for WL and IF combinations. This means that if *IFM* can be estimated, a big part of the error in WL and IF combinations can be modeled, while the error in L1 remains unknown. The model of the carrier multipath error in linear combinations (Equation 5.8) forms the basis of the multipath mitigation techniques developed later in this thesis.

5.3 Estimating the IFM observable

The core of the carrier multipath model for linear combinations introduced by Equation 5.8 is the IFM observable. In this section, the IFM observable is estimated for different scenarios.

5.3.1 IFM IN DIFFERENT MODES

Depending on the targeted application, the IFM observable can be obtained in different modes, namely between-receivers, between-satellites and double-differenced modes as discussed below.

5.3.1.1 Between-receivers mode

The IFM observable in this mode is obtained in three steps. In the first step, the between-receiver single-difference of the carrier phase measurements is formed for each frequency:

$$\Delta\Phi_f^k = \Delta\rho^k - \Delta I_f^k + \Delta T^k - \lambda_f \Delta N_f^k + \Delta m_f^k + c\Delta t_r + \Delta B_f + \varepsilon$$

5.9

where Δ represents the differencing between receivers. This operation eliminates common errors between the two receivers and, for short baselines, decreases atmospheric errors significantly due to their correlation characteristics.

The single-difference measurements are then differenced across frequencies (i.e. L1-L2) in the second step to obtain geometry free combination. This eliminates the receiver clock errors and the geometric ranges:

$$\Delta\Phi_{\mathrm{L1}}^k - \Delta\Phi_{L2}^k = -\Delta I_{L1}^k + \Delta I_{L2}^k - \lambda_{L1}\Delta N_{L1}^k + \lambda_{L2}\Delta N_{L2}^k + \Delta m_{L1}^k - \Delta m_{L2}^k + \Delta B_{L1} - \Delta B_{L2} + \varepsilon'$$

5.10

These two steps significantly reduce the residual ionospheric error for short and medium baselines, as well as the rate of change of the residual ionospheric error. The residual ionospheric error in Equation 5.10 is the differenced inter-frequency ionospheric error (ΔIFI). If higher order ionospheric error is ignored, ΔIFI error can be expressed as

a function of the L2 ionospheric error using the relationship between the L1 ionospheric error (I_{L1}) and L2 ionospheric error (I_{L2}) as:

$$I_{L1} = \frac{f_2^2}{f_1^2} I_{L2} \tag{5.11}$$

$$\Delta IFI = \Delta I_{L2} - \frac{f_2^2}{f_1^2} \Delta I_{L2} = 0.39\, \Delta I_{L2} \tag{5.12}$$

The third step is designed to remove the residual ionospheric error, the ambiguity terms and the differential hardware delays between the L1 and L2 frequencies ($\Delta B_{L1} - \Delta B_{L2}$). Multipath errors tend to have sinusoidal patterns with zero mean (Ray and Cannon 1999). The ambiguity terms are constant assuming that cycle slips are detected and repaired. The differential hardware delays between the L1 and L2 frequencies, also known as Inter-Frequency Biases (IFB), are stable over long durations (of the order of days), and can therefore, be treated as constant (Gao et al. 1994). Hence the only remaining variable term in addition to the multipath errors after step two is the residual ionospheric error, which is the Inter-Frequency Ionospheric error (IFI). Given that the IFI can be assumed constant relative to the multipath error over a given time window, as justified in section 5.3.2.2, the multipath error can be extracted by removing the mean of the geometry free combination obtained by Equation 5.10 over the time-window, providing that the multipath has a mean value of zero over that time window. The IFM is then obtained as:

$$\text{IFM} = \Delta m_{L1}^{k} - \Delta m_{L2}^{k} \approx \Delta\Phi_{\text{L1}}^{k} - \Delta\Phi_{L2}^{k} - \frac{1}{N}\sum_{n=1}^{N}(\Delta\Phi_{\text{L1}}^{n} - \Delta\Phi_{L2}^{n})$$

5.13

where *N* is the number of epochs (time window) chosen in the computation of the mean. The optimum time window depends on the rate-of-change of IFI and IFM frequency. The relationship between these two parameters and their effect on the optimum time window are discussed in Section 5.3.2.

5.3.1.2 Between-satellites mode

The IFM observable between satellites is derived using an approach similar to that used for the between-receivers mode. The only difference is in the first step where measurements are differenced across satellites instead of across receivers. The method is applied to two satellites in close proximity, with similar elevation and azimuth angles. Signals from such satellites exhibit correlations between the ionospheric errors, which are mitigated by differencing across satellites. This mode is applicable to satellite combinations from different constellations only, given that satellites in the same constellation are separated from each other by large differences in elevation and azimuth angles. Although different constellations use different time frames, the IFM generation across constellations is unaffected because the satellite clocks are stable over long time periods and the inter-constellation time differences can therefore, be considered to be constant. Such constant biases are removed in the process of the IFM generation.

5.3.1.3 Double-differenced mode

The IFM observable in this mode is obtained in the same way as for the between-receivers mode. The only difference is in the first step where double differenced measurements are used instead of differenced measurement across receivers. Therefore, in the double differenced mode, receiver hardware delays are already removed by forming double differenced measurements while in the between receiver mode the receiver hardware delays form the IFB are removed in the step 3.

5.3.1.4 Impact of operational environment on IFM

The IFM observable characteristics vary with the environment (simple or complex reflections) and the application (static or dynamic). In urban environments, where a GNSS signal is reflected by several surfaces before reaching the antenna, the IFM observable may not exhibit a simple sinusoidal pattern, instead exhibiting a superposition of several sinusoidal patterns. In addition, in such environments typical reflections (i.e. multipath) occur also for satellites at high elevations. On the other hand, in open environments reflections typically come from the ground for satellites at low elevations and the number of reflecting surfaces tends to be limited. This tends to create relatively simpler sinusoidal IFM patterns.

The dynamics of the receiver also have a significant impact on the IFM observable. Increasing the speed of the receiver may change the IFM frequency and rate-of-change of IFI. Irrespective of the operational environment (simple or complex

reflections) and application type (static or dynamic), IFM in different modes can be estimated using the procedure explained above. The only impact of the environment and application factors is the optimum time window length. In this thesis, only stationary scenarios with reflection from the ground are considered (i.e. simple reflection), typical for most of the applications targeted in this thesis.

5.3.2 IFM SENSITIVITY TO TIME WINDOW

As discussed in Section 5.3.1.1, all the errors in the IFM, except the ionospheric and multipath errors, are constant over time. Therefore, the main factors driving the selection of the optimum time window are the time variability of the ionospheric error (differenced IFI) and multipath error (IFM). The IFM frequency and rate of change in IFI are investigated next.

5.3.2.1 IFM frequency

The carrier multipath frequency (v_f) for measurements at frequency f can be expressed as a function of the reflector distance (h) and satellite elevation angle (Rost and Wanninger 2010) as:

$$v_f = 2 * \frac{h}{\lambda} * \sin(z) * \left|\frac{dz}{dt}\right| \qquad 5.14$$

where *f* corresponds to GPS L1 and L2 in this thesis, z is the zenith angle (90 minus the elevation angle), and λ is the measurement wavelength. The IFM is obtained by subtracting two sinusoidal waves from each other ($\Delta m_{L1}^{k} - \Delta m_{L2}^{k}$). Hence, the IFM frequency is obtained as:

$$v_{IFM} = \frac{v_{L1} + v_{L2}}{2} \qquad 5.15$$

Equations 5.14 and 5.15 were used to calculate the IFM frequency (Figure 5.4) and period (Figure 5.5) as a function of the elevation angle and reflector distance. According to (Kaplan and Hegarty 2006) the elevation angle of a GPS satellite may change by up to $0.5°/min$ which is approximately $0.008°/second$. Therefore, in this analysis a rate of $0.008°/second$ in the elevation angle has been used. The highest rate of change in the elevation occurs at lower elevations, while at zenith the rate is zero. This means that the *IFM* observable has a lower frequency at higher elevation and hence needs a longer time window to be estimated. On the other hand, multipath error mainly occurs at low elevations where the rate of change in the elevation angle is at its highest. In addition in surveying, which is one of the main applications of this thesis, ground reflection at low elevation angles is very common. Therefore, it is justifiable to use a rate of change of $0.008°/second$ in elevation angle in this research.

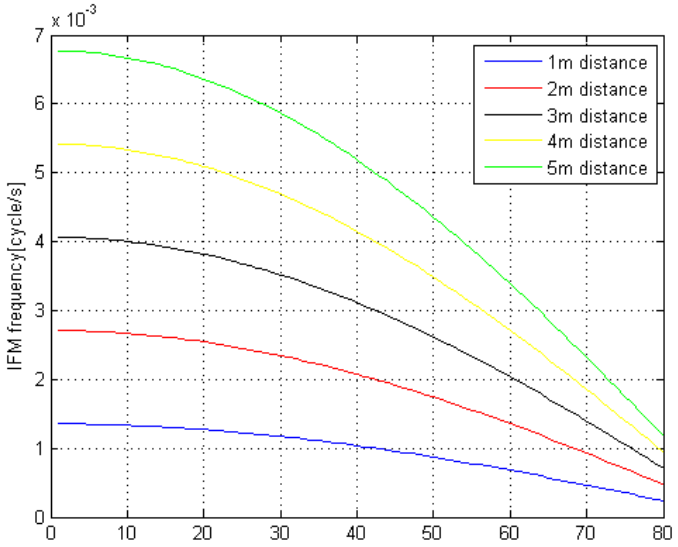

Figure 5.4: IFM frequency as a function of elevation angle for different reflector distances

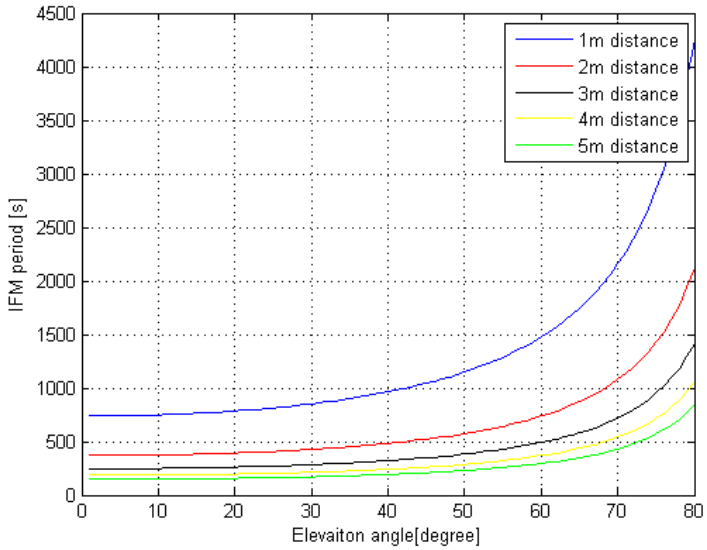

Figure 5.5: IFM period as function of elevation angle for different reflector distances

From Figure 5.4 and Figure 5.5, it is clear that a decrease in the reflector distance leads to a decrease in the IFM frequency. The frequency also decreases with increasing elevation angle. This change is faster for distant reflectors while with short reflectors (i.e. 1m), the IFM frequency is almost constant up to an elevation of 50 degrees. An understanding of the behaviour of the IFM frequency as a function of the elevation angle and reflector distance is key to choosing the correct strategy for the time window selection in Equation 5.13. This is because the best practice is to choose a time window which covers a multiple of IFM cycles. Otherwise, the assumption of a zero mean for the IFM may not be valid.

5.3.2.2 Changing rate of differenced IFI error

It is important that the differenced IFI error can be approximated as constant (relative to the IFM) during the selected time window. According to Figure 5.5, for reflections from objects distanced between 1 and 5 metres, the IFM period would be approximately between 200 to 4200 seconds. In this section, changes in the IFI error for 3 different time windows in this range (1000, 2000 and 3000 seconds) are examined as examples. To approximate changes in the IFI error for each of the windows, the time rate of changes in the differenced slant ionospheric delay ($\frac{d\Delta I}{dt}$) should be analysed. The time rate of change in the differenced slant ionopheric delay can be written as a combination of two different parts:

$$\frac{d\Delta I}{dt} = \frac{d\Delta I_a}{dt} + \frac{d\Delta I_b}{dt}$$

5.16

where $\frac{d\,\Delta I_a}{dt}$ is the change in the slant ionspheric delay over time due to changes in the differenced elevation angles between the two receivers.

$\frac{d\,\Delta I_b}{dt}$ is the change in the slant ionopheric delay over time due to changes in the elevation angle at each receiver. A change rate of 0.008 degree/s for the elevation angle was used. At low elevation angles, the error changes faster, making the extraction of the IFM more difficult. Therefore, to consider the worst case scenario, the starting elevation angle in a given time window is chosen to be as low as possible (e.g. 5 degrees).

Differences in the ionospheric errors between receivers due to difference in elevation angles between the two receivers were analysed in (Kaplan and Hegarty 2006) using:

$$\Delta I_f \approx \left| -\frac{baseline}{2 * 10^4} \cos(elevation) \frac{40.3}{f^2}\, TEC \right|$$

5.17

The relationship between the elevation angles change over time, and hence, the same formula can be used to analyse changes in the differenced slant ionospheric delays over time ($\frac{d\Delta I_a}{dt}$). To analyse $\frac{d\Delta I_a}{dt}$, it is assumed that the TEC value is the same at both receivers but changing as a function of the time of day. The spatial difference of the errors between the receivers are considered later in this section. Changes in the TEC

values over time are very slow at night and vary slowly during the day time (diurnal variation), with variations that hardly exceed 40 TECU. The maximum diurnal variation occurs typically during between 6am and 2pm local time (Perevalova et al. 2010). Therefore, the maximum diurnal variation rate is approximately 40TECU over 8 hours which is 0.0014 TECU/s ($1\ TECU\ =\ 10^{16}\ electrons/m^2$). This leads to up to 1.4, 2.8 and 4.2 TECU over 1000, 2000 and 3000 seconds respectively. Based on Equation 5.17, for each time window, the minimum and maximum differenced ionospheric errors are calculated respectively as:

$$\Delta I_{f,min} \approx \left| -\frac{1km}{2 * 10^4 km} \cos(\text{max elevation}) \frac{40.3}{f^2}\ TEC_{min} \right| \quad 5.18$$

$$\Delta I_{f,max} \approx \left| -\frac{1km}{2 * 10^4 km} \cos(\text{min elevation}) \frac{40.3}{f^2}\ TEC_{max} \right| \quad 5.19$$

where,

$$TEC_{min} = 50 * 10^{16} Electron/m^2 (typical\ value\ in\ temperate\ zones) \quad 5.20$$

$$TEC_{max} = TEC_{min} + diurnal\ variation \quad 5.21$$

Therefore, the change in the ionospheric error over a given time window is calculated as:

$$\delta\Delta I_f = \Delta I_{f,max} - \Delta I_{f,min}$$

5.22

where δ indicates the change in error over the time window. According to Equation 5.12, ΔIFI is $0.39\Delta I_{L2}$, therefore,

$$\delta\Delta IFI = 0.39\delta\Delta I_{L2} = 0.39(\Delta I_{L2,max} - \Delta I_{L2,min})$$

5.23

From Equations 5.18 to 5.23, the residual ionopheric errors for each time window ($\delta\Delta IFI$) are calculated and listed in Table 5.1.

Table 5.1: Changes in the residual ionospheric errors due to changes of elevation angle between the rover and base station

Time window (seconds)	*min elevation (degrees)*	*max elevation (degrees)*	$\delta\Delta IFI$ (mm/km)
1000	*5*	*13*	*0.01*
2000	*5*	*21*	*0.03*
3000	*5*	*29*	*0.05*

As depicted in Table 5.1, the changes in $\delta\Delta IFI$ are very small over all three time windows. For example, it reaches 5mm for a time window of 3000 seconds over a 100 km baseline. Therefore, this small variation in IFI can be considered as constant for baselines up to 100 km.

To analyse the second term in equation 5.16 ($\frac{d\Delta I_b}{dt}$), it is approximated that the differenced vertical ionopheric delay is increased by $2\,\frac{mm}{km}$ due to the spatial difference in TEC values (Kaplan and Hegarty 2006; Christie et al. 1998). Due to changes in the elevation angle over time (assuming the elevation angle is approximately the same in both receivers) the differenced slant delay due to the spatial difference also changes over time. The impact can be analysed using a function such as the single-layer mapping (SLM) function (Komjathy 1997). In this function, it is assumed that all the free electrons are concentrated in an infinitesimal spherical layer around the earth. The SLM is used to calculate the relation between vertical TEC and slant TEC values based on:

$$mapping\ function\ = \frac{1}{\cos(z')} \tag{5.24}$$

where z' is the geocentric zenith distance at the ionosheric pierce point. z' is obtained from the geocentric zenith distance at the height of the receiver (z) based on:

$$z' = \arcsin\left(\frac{R}{R+H} sin(z)\right) \tag{5.25}$$

$$\Delta I_{L2,min} = mapping\ function(max\ elevation) * 2mm \tag{5.26}$$

$$\Delta I_{L2,max} = mapping\ function(min\ elevation) * 2mm \tag{5.27}$$

From Equations 5.24 to 5.27 as well as Equation 5.22 and 5.23, the changes in the error over each time window ($\delta\Delta IFI$) are summarised in Table 5.2.

Table 5.2: Changes in residual ionospheric errors due to changes in elevation angle at each receiver

Time window (seconds)	*min elevation (degrees)*	*max elevation (degrees)*	$\delta\Delta IFI$ (mm/km)
1000	*5*	*13*	*0.26*
2000	*5*	*21*	*0.56*
3000	*5*	*29*	*0.81*

As shown in Table 5.2, for longer baselines, smaller time windows must be used to achieve a $\delta\Delta IFI$ that is sufficiently small compared to the multipath error. For example, over a 10 km baseline, the $\delta\Delta IFI$ is approximately 8 mm over a 3000s time window.

5.3.2.3 Minimum and maximum time window approaches

In this section two approaches are introduced for selecting the time window for IFM estimation, referred to as the minimum and maximum time window approaches. In the former, the time window is chosen to cover exactly one cycle of the IFM. This can be computed from Equations 5.14 and 5.15, based on a best estimate of the reflector distance from the antenna. However, in unknown operational environments, defining the effective

reflector and its distance from the antennas may not be achievable. Alternatively, a smart algorithm can be adapted to determine the IFM frequency during the process of the IFM estimation. Such an algorithm can be developed based on the Adaptive Notch Filter (ANF) which has been used in (Comp and Axelrad 1998) to extract the multipath frequency from SNR values.

In the maximum approach, the time window is chosen to be sufficiently long to contain several IFM cycles, with the expected $\delta\Delta IFI$ magnitude being smaller than the expected IFM magnitude. A potential approach is to progressively increase the time window to cover integer multiples of an IFM cycle (with at least one cycle), up to a level where the mean of the extracted IFM remains almost constant. If the number of complete IFM cycles in the time window exceeds this level, the IFM mean will deviate from the constant value due to ionospheric error contamination in the IFM. The benefit of maximum time window approach is that it is less sensitive to the accuracy of the estimated IFM period. On the other hand, this approach also increases the residual IFI in the estimated IFM observable. Due to the simplicity of the maximum time window, this approach is used in this thesis.

5.4 IFM applications

This section presents the different techniques which can be used to exploit the IFM observable. Although the IFM observable, by design, plays a key role in carrier multipath mitigation techniques, it may also be used for applications that exploit GNSS

multipath. The focus of this thesis is on the former, however, the latter is briefly discussed in Section 5.4.3.

5.4.1 IFM-BASED MASKING

The aim of IFM-based masking is to identify the level of carrier multipath error in each measurement and exclude from the solution calculation those measurements which exhibit high levels of carrier multipath errors. In this thesis IFM-based masking is introduced briefly as a potential application of IFM observable. It is not evaluated further because it is outside the scope of thesis and will be suitable in the future when there will be enough satellites available where excluding several 'bad' measurements does not result in a positioning outage.

IFM correlation with the measurements can be exploited to identify multipath level in the measurements. The IFM observable is correlated with carrier multipath error in linear combinations obtained from the carrier phase measurements at L1 and L2, such as the WL and IF combinations. The relationship between the IFM and the WL and IF combinations is shown in Figure 5.6, where the WL and IF carrier multipath errors were computed from Equation 5.2 and the IFM observable was computed from Equation 5.7.

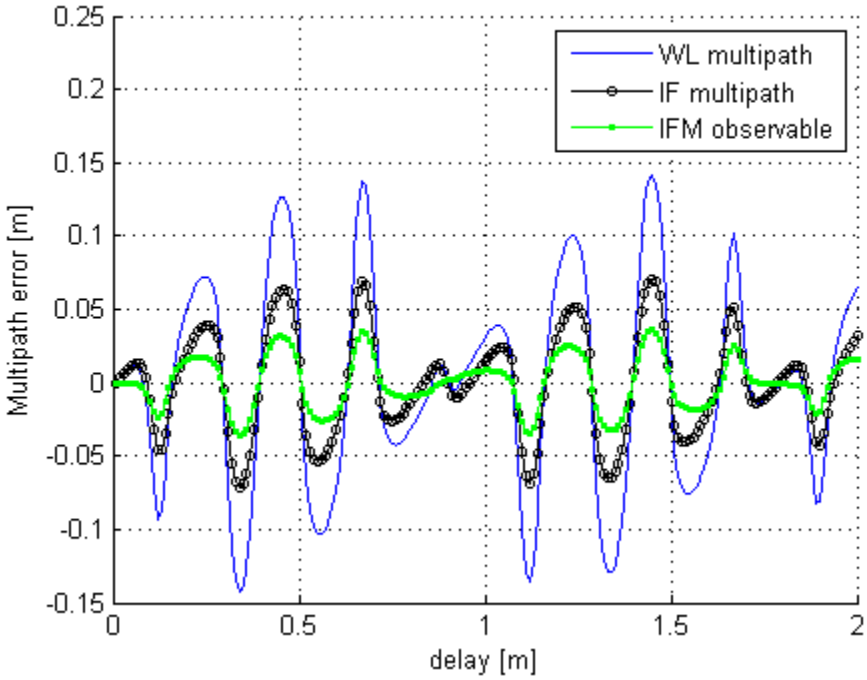

Figure 5.6: IFM, WL and IF carrier multipath as function of signal delay

As can be seen from Figure 5.6, the IFM observable is highly correlated with the WL and IF multipath errors. Therefore, the IFM peak magnitude over a span of time can be used as a multipath metric for the measurements in linear combinations. Using such carrier multipath metric, measurements with a high level of carrier multipath errors can be identified and excluded from the solution calculation. All three modes of IFM can be used for measurement masking. The IFM observable in between satellite mode is more suitable for measurement masking in positioning techniques which use only one receiver, such as in Precise Point Positioning (PPP). The double-differenced mode of IFM can be used for masking the measurements in applications which use double differenced

measurements such as RTK. The IFM observable in between-receivers mode can also be used for single satellite masking with high levels of multipath.

To use the multipath metric for measurement masking, a suitable threshold must be defined. An optimum multipath metric threshold depends on different factors such as the number of available satellites and satellite geometry. The average of the multipath metric for the selected time span is an important defining factor in the selection of the appropriate threshold. This means that if most of the measurements have high multipath metric values, obviously a higher threshold must be used to avoid too many exclusions and the resulting poor satellite geometry.

In addition to measurement masking, the IFM-based multipath metric can also be used for the selection of the reference satellite in double differencing. This enables the satellite with the smallest multipath metric to be selected as the reference satellite. Currently the most common approach to choosing the best satellite as a reference satellite in double differencing mode is based simply on the satellite elevation angle. In this technique it is assumed that the satellite with the highest elevation has the smallest levels of multipath and noise. However, this may not always be true, especially in urban environments where multipath errors may occur for signals from satellites at high elevations angles.

5.4.2 IFM-BASED MULTIPATH MITIGATION

The two IFM-based multipath mitigation techniques developed in this thesis, IFM-based multipath correction and IFM-based weighting, are discussed below.

5.4.2.1 IFM-based multipath correction

The linear combinations can be corrected with the known part of Equation 5.8. This results in replacing the carrier multipath error m_c by xm_{L1}, which corresponds to the carrier multipath error at the L1 frequency scaled by the difference between the α and β values. The corrected measurement in the linear combination is given by:

$$\widehat{\Phi}_c = \Phi_c - \beta \cdot IFM \tag{5.28}$$

where Φ_c is the combined measurement in units of length. The correction based on Equation 5.28 mitigates the carrier multipath error depending on the *x* value and equally mitigates Gaussian noise. This is because the noise exhibits the same zero-mean characteristics as the high frequency carrier multipath errors. After applying the correction based on Equation 5.28, the residual carrier multipath error depends on *x* and the m_{L1} values. For the WL and IF combinations, the *x* value is 1. Hence, the residual carrier multipath value in WL and IF will drop to the value in L1, which is significantly smaller (see Figure 5.2 and Figure 5.3). The IFM-based multipath correction technique is evaluated in Chapters 6 and 7.

5.4.2.2 IFM-based measurements weighting

The IFM can also be applied to weight the measurements. The elevation based stochastic technique is the most commonly applied to GNSS measurements. However, it

is oversimplified and does not accurately reflect the multipath effect on the measurements. By examining Figure 5.6, it is clear that there is very good correlation between the changes in carrier multipath errors in WL and IF and the IFM observable. This correlation can be shown by Equation 5.8 as well. According to Equation 5.8, the carrier multipath errors in the WL and IF combinations can be approximated as a function of the IFM observable as:

$$m_c \approx \beta(IFM) \tag{5.29}$$

where β is approximately 3.53 and 1.55 for the WL and IF combinations respectively.

This correlation may be used to build an IFM-based stochastic model to weigh the measurements of linear combination, which reflects the multipath condition of the measurements very accurately. In order to also take into account the effect of the elevation angle on the noise level, the IFM-based stochastic model combines the simple elevation based stochastic model with the IFM observable. The variance in this new model, σ_{IFM}^2, is obtained from the maximum expected variance of the measurements due to the noise (σ_{max}^2) as:

$$\sigma_{IFM}^2 = \left(1 - \left(\frac{\sin(E)}{1.001}\right)^2\right)(1 + C.|IFM|)\,\sigma_{max}^2 \tag{5.30}$$

where |.| denotes the absolute value, and C is a constant. The model presented by Equation 5.30 is simply a combination of simple elevation based weighting model (Equation 4.18 and IFM observable). According to Equation 5.30 when the IFM is zero, the elevation weight is applied. On the other hand, as the IFM magnitude increases the overall weight decreases. As it is not possible to determine the *C* value analytically, an empirical approach should be used. The value of *C* represents the relationship between elevation parameter and IFM observable in the model.

To further explain the impact of the IFM-based weighting technique on the measurements, the IFM observable, IFM-based weighting parameter (obtained from Equation 5.30) and the simple elevation based weighting parameter are plotted for a typical dataset in Figure 5.7, Figure 5.8 and Figure 5.9 respectively. The data set was collected in a relatively open environment with predominantly reflections from ground.

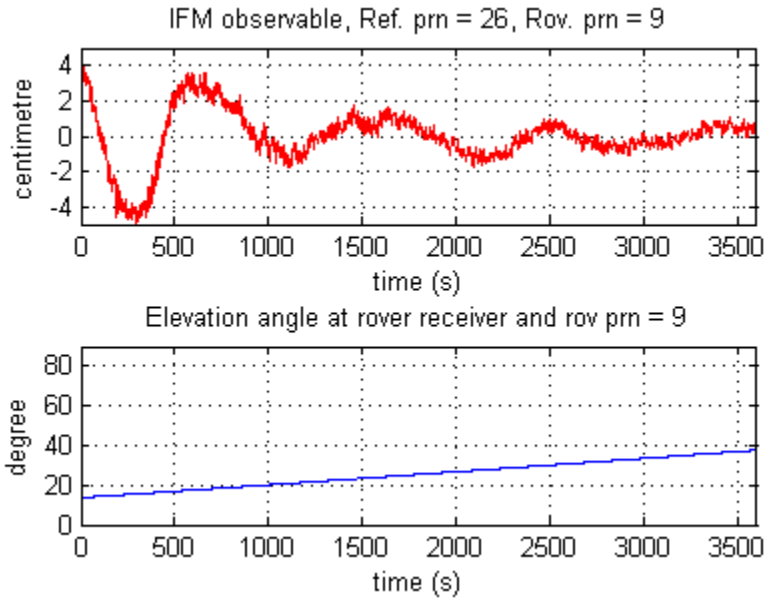

Figure 5.7: IFM observable (top) and elevation angle (bottom)

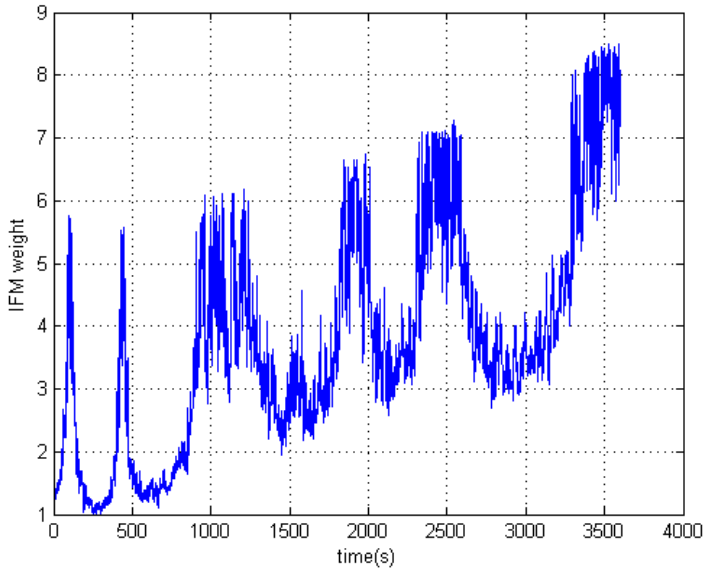

Figure 5.8: IFM-based weighting parameter for PRN 9 for the Silwood 1 dataset

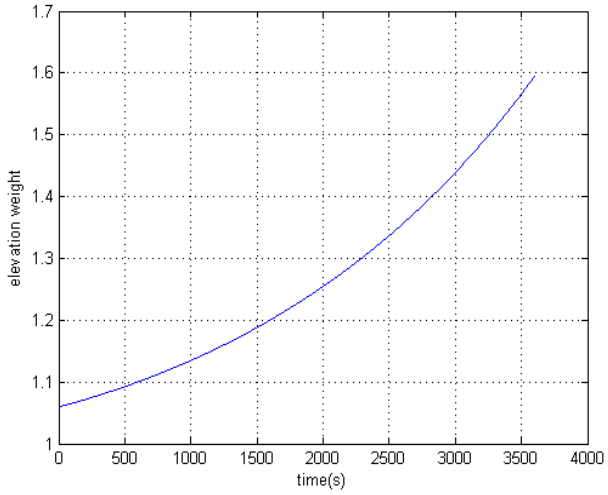

Figure 5.9: Simple elevation based weighting parameter for PRN 9 for the Silwood 1 dataset

As discussed in Chapter 4 and illustrated in Figure 5.9, the simple elevation based weighting considers a simple linear relation between the elevation and the weighting parameter and does not take into account the effect of the operational environment. This issue has been addressed by combining elevation angle with the IFM observable in the new model. Figure 5.8 shows that in the new weighting scheme the desirable characteristics below have been achieved:

- The general trend of weighting increases by increasing the elevation angle.
- During one IFM cycle:
    - The weighting parameter is at its minimum when IFM is at its minimum or maximum.
    - The weighting parameter is at its maximum at zero IFM.

To determine the best *C* value in the Equation 5.30, a range of values has been tested on IF combinations, with the one resulting in the best position accuracy selected. Figure 5.10 shows a comparison of the position accuracy obtained using three different *C* values in the IFM-based weighting scheme. In the figure, position errors resulting from the *C* values of 80, 100 and 120 are shown in red, blue and black respectively. As can be seen from the figure, the position accuracy for the *C* value of 100 is the best.

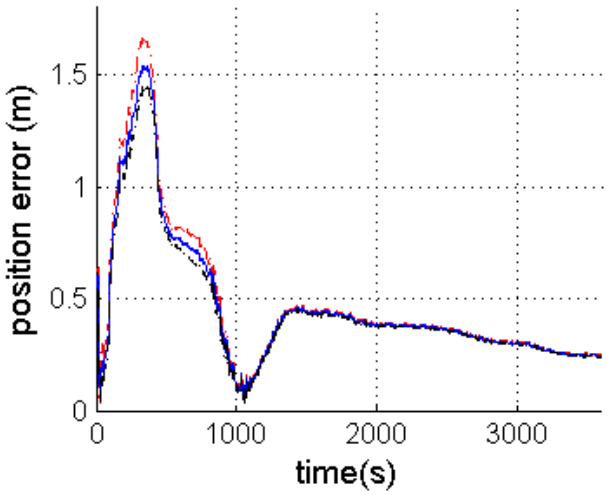

Figure 5.10: Position error using IFM-based weighting with *C* values of 80 (red), 100 (blue) and 120 (black)

From the analysis presented in the Figure and analyzing several other datasets it appears that the sensitivity of the position error to the *C* value is low. Using *C* values around 100 also provided the best ambiguity resolution results using the WL observable in most of the cases. Therefore, in this thesis a *C* value of 100 has been chosen for both IF and WL combinations.

5.4.3 IFM BASED MULTIPATH EXPLOITATION

GNSS multipath from the IFM observable contains a wealth of information about the environment surrounding the receiver which can be used in a number of applications. Examples include the measurement of snow depth and analysis of the soil moisture. Although this class of applications is not the focus of this thesis, the two examples above will be briefly discussed in the following subsections to highlight other potential applications of the IFM observable.

5.4.3.1 Snow depth measurements

Accumulation of snow on the ground in the vicinity of a GNSS antenna changes the effective reflector distance to the antenna. This results in changes in the multipath frequency. Past approaches have used the GNSS SNR as an indirect indicator of multipath frequency for snow depth measurement. These approaches have used the changes in the frequency of the (multipath contaminated) SNR as an indicator of changes in the distance between the reflector and receiver. However, the SNR variation is also a function of the elevation angle. Therefore, the impact of the elevation angle must be dissociated in order to extract the SNR variation resulting from multipath alone (Hefty and Gerhatova 2013).

On the other hand, the IFM observable is directly related to the carrier multipath error and is obtained from very high accuracy carrier phase measurements. Therefore, it provides an easier and more accurate means for measuring snow depth than the SNR

based approach. Such application, may use the IFM observable in between-receivers mode. If the two receivers are located close to each other, the ionosphere error will be eliminated almost completely and the IFM mean will remain constant over long periods of time. In the absence of ionospheric errors, the IFM can easily and accurately be estimated using the maximum time window approach. Performance analyses of using IFM for snow depth measurement is left for the experts in the relevant field.

5.4.3.2 Soil moisture analysis

The soil moisture is relevant amongst others in weather and climate forecasting, flood prediction and aquifer recharge studies. In the case of L-band signals, the surface reflectivity depends on the dielectric constant of the surface, which highly depends on the soil moisture and less so on soil type and vegetation. The amplitude of the multipath contaminated SNR is related to the reflection strength and hence to the moisture of the upper level of the soil. Therefore, the amplitude of the multipath contaminated SNR can be used in soil moisture analysis (Larson et al. 2008). However, using SNR for this purpose has the same limitations as for snow depth analysis. In addition, the amplitude of the multipath contaminated SNR is proportional to the multipath amplitude. The relationship between the two parameters may change from one receiver to another, depending on the applied SNR estimation process. On the other hand, the IFM observable is obtained from raw data and does not have this limitation. Therefore, the IFM can be used in between-receiver mode with two receivers located in close distance from each other. The amplitude of the IFM is related to the reflection strength and hence to the

moisture of the upper level of the soil. Performance analyses of using IFM for soil moisture analysis is left for the experts in the relevant field.

5.5 Summary

This chapter has analysed the carrier multipath error in linear combinations in relation to the error for single frequency measurements. It has shown that the error could be at the decimetre level for WL and IF combinations. Such error magnitudes will affect high accuracy carrier based positioning applications. The need for mitigating carrier multipath error in linear combinations was demonstrated and a model representative of carrier-multipath in such combinations developed, leading to a new type of observable: the IFM observable. On the basis of this new model two multipath mitigation techniques were developed: IFM-based multipath correction and IFM-based measurement weighting. Although, IFM observable was primarily invented for multipath mitigation, its use for various other indirect applications has been discussed also.

The IFM-based multipath correction and IFM-based measurement weighting methods introduced in this chapter are tested and validated with real data in the next two chapters. Chapters 6 and 7 apply the IFM-based multipath mitigation techniques to carrier phase IF and WL combinations respectively.

Chapter 6

CARRIER MULTIPATH MITIGATION IN IONOSPHERE-FREE COMBINATION

In the previous chapter a new approach to isolating the carrier multipath error for linear combinations of signals at two frequencies was developed, leading to the formulation of the IFM observable. Different applications of this observable were introduced, including multipath mitigation applications: IFM-based masking, IFM-based multipath correction and IFM-based measurement weighting. In this chapter IFM-based multipath correction and IFM-based measurement weighting techniques are applied to the IF combination on the basis of real data. The position accuracies achieved by each technique are compared with those obtained by simple elevation weighting.

The data collection campaigns are discussed in section 6.1, experimental setup and data collection process are presented, with the test cases outlined in Section 6.2. Sections 6.3 and 6.4 discuss the application of the multipath correction and measurement weighting techniques to the datasets and the evaluation of the positioning performance.

Section 6.4 concludes the chapter with a comparison of the two mitigation techniques and the elevation based weighting and the identification of the optimal technique for IF combinations.

6.1 Data collection campaigns

To test the techniques developed in this thesis it is ideal to use real data rather than simulated data. At an early stage of the research several data collection campaigns where conducted in urban environments and also in environments with shadowing effects (i.e. surrounded by tress). In surveying applications reflection from ground is very common. Therefore, eventually it was decided to focus on simple reflection rather than complex multipath environment conditions. For this purpose, several data collection campaigns with different settings were conducted. Among these, the three most relevant are presented below:

- Hyde Park 1 campaign: Collection of 4 hours data using two receivers next to a lake to capture short delay multipath (Figure 6.1).
- Hyde Park 2 campaign: Collection of 4 hours data using two receivers at a distance of approximately 5m from the lake to capture medium delay multipath.
- Silwood Park 1 campaign: Collection of 4 hours data using 2 receivers beside an aluminium reflector (1 by 2 metre in size) for two successive days at the same time to capture repeating multipath condition (Figure 6.2).

- Silwood Park 2 Campaign: Collection of 4 hours data using two receivers in an open field with no artificial reflector to capture reflection from ground (Figure 6.3).

Figure 6.1: Hyde Park 1 campaign setup

Figure 6.2: Silwood Park 1 campaign setup

In Hyde Park 1 and 2 campaigns, the expectation was to capture a specular reflection from the smooth surface of the water with the appropriate satellite-reflector-receiver geometry. However, subsequent analysis revealed no significant carrier multipath error due to the inappropriate geometry.

The Silwood Park 1 campaign was also not successful in capturing enough carrier multipath errors, partly due to the same reason as Hyde Park 1 and 2 campaigns. In addition, due to using a vertical reflector some of the satellites were blocked by the reflector.

The Silwood Park 2 campaign, however, resulted in clear high level defuse reflections for a period of the time. The presence of carrier multipath error in the datasets collected in this campaign was proved by analyzing the IFM observable. Therefore, the Silwood Park 1 campaign was used in this thesis in addition to a dataset from a reference station, mainly for two reasons. Firstly, specular reflection is very rare in real life applications and secondly defuse reflection from the ground is a major problem in surveying which is one of the main application of this thesis.

In the next section the setup used for data collection in the Silwood Park 2 campaign is discussed in more detail.

6.2 Experimental setup and test case definition

Two datasets, each of one hour duration, were collected using two Leica GS15 receivers in May 2012 at the Imperial College London Silwood Park campus (Silwood 1

and Silwood 2). The data were collected in a relatively open area with no vertical reflective surfaces in the vicinity of the antenna using the setting shown in Figure 6.3 and Figure 6.4. The main source of reflection was the ground covered with wet grass. On the west side of the baseline, there was a sloping terrain below antenna level, which could create forward scatter reflections for low elevation satellites with an azimuth of approximately 270 degrees. Forward scatter occurs when the signal is reflected from a horizontal surface below antenna level. Additionally, a dataset was obtained from FARB a surveyed permanent station approximately 17km apart from the Silwood 1 and Silwwod 2 stations. FARB is operated by Ordnance Survey agency at the southern part of England. The positions of the Ordnance Survey stations are generally given with standard errors better than 0.008m and 0.020m in plan and height respectively (OS 2014).

Figure 6.3: Receiver stations for the Silwood 1 and Silwood 2 data capture

Figure 6.4: Satellite view of the Silwood 1 and Silwood 2 stations (from Google map)

In this thesis, the validation of the multipath mitigation techniques has covered two main scenarios: short baseline (i.e. 20m) and medium baseline (>10km) scenarios. The short baseline scenario aimed at simplifying the assessment process and minimising the effect of the ionospheric error on the IFM estimation. The medium baseline scenario aimed at including the effect of the ionospheric and hence simulating real life scenarios.

Therefore, three test cases were defined:

- Case1: Differencing between Silwood 1 and Silwood 2 with an approximate baseline of 20m to cover the short baseline scenario.
- Case 2: Differencing between Silwood 1 and FARB, with an approximate baseline of 17km to cover the medium baseline scenario.
- Case 3: Differencing between Silwood 2 and FARB, with an approximate baseline of 17 km to cover the medium baseline scenario.

The three test cases are used throughout the remainder of this thesis to test the new multipath mitigation techniques.

The reference positions for the Silwood 1 and Silwood 2 receivers were obtained in static mode using the GrafNav software (NovAtel 2014) in RTK mode with FARB as the reference station. The position accuracies obtained with the Grafnav software are 1.4 cm and 4.8 cm SEP (Spherical Error Probable) for Silwood 1 and Silwood 2 respectively. This level of accuracy for the reference positions is assumed to be satisfactory given that the aim is mitigation of decimetre level carrier multipath error in linear combination. The CEP (Circular Error Probable) values for Silwood 1 and Silwood 2 are 0.9 and 3 cm

respectively. For each test case, one station was used as the reference and the other as a rover, and the solutions were calculated epoch by epoch. The iNsight project (www.insight-gnss.org) POINT software was used to test the new methods developed in this thesis. The advantage of using the POINT software was twofold. Firstly, the accessibility to its source code. Secondly, the availability of a built-in RTK function with the option of using different types of measurements and linear combinations of measurements. This enabled the integration of the developed multipath mitigation techniques into the POINT software. In this chapter, IF code and carrier combinations are used for positioning calculation. According to Equation 2.23 in Chapter 2, ambiguities in the carrier phase IF combination do not have integer characteristics. Therefore, float solution is used in this chapter.

6.2.1 IFM ESTIMATION

The IFM observables (Equation 5.7 in Chapter 5) for the between-receivers and double-differenced modes were generated for the three test cases defined in the previous section. The time window used for the IFM estimation was chosen to be one hour. According to Figure 5.5 (Chapter 5), such a time window contains multiple of IFM cycles even for short signal delays (e.g. 1 metre) at low elevation angles, required to fulfil the maximum time window condition (see Section 5.3.2.3).

The IFM observable is affected by cycle slips. If a jump due to a cycle slip is detected it can be corrected in the IFM observable easily by subtracting the jump magnitude from the observables after the detected point. As discussed in, Section 5.3, the

IFM observable consists of multipath, residual ionospheric error and noise. Multipath error and hence, the IFM observable and ionospheric error are highly correlated between epochs (i.e. over one second). Therefore, changes in the IFM observable between two epochs are dominated by the noise levels between the two IFM epochs. According to the Leica receiver datasheet, carrier phase noise is less than 0.5mm. Hence, the noise level in the IFM observable in both the between receiver and the double differenced modes should be less than 1cm. Therefore, in this thesis discontinuities larger than 1 cm in the IFM observable were assumed to be the result of cycle slips and were accordingly corrected. Figure 6.5, Figure 6.6 and Figure 6.7 illustrate the IFM observable for the between-receivers mode for test cases 1, 2 and 3 respectively. Figure 6.8, Figure 6.9 and Figure 6.10 illustrate the IFM observable for the double-differenced mode for test cases 1, 2 and 3 respectively. The (a) part of each of the figures shows the IFM observable and elevation angles for satellites with relatively high-level multipath as a function of time. The (b) part of each of the figures shows the corresponding results for satellites with relatively low-level multipath.

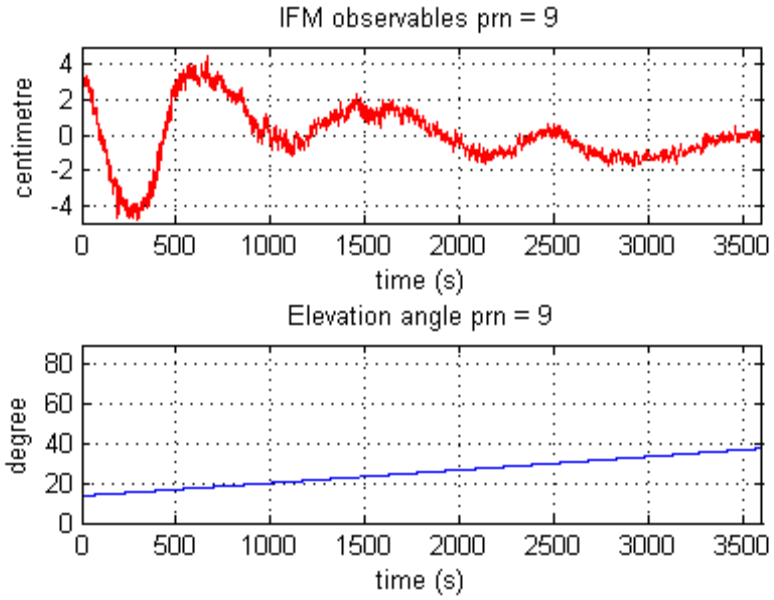

(a) Satellite with high multipath level

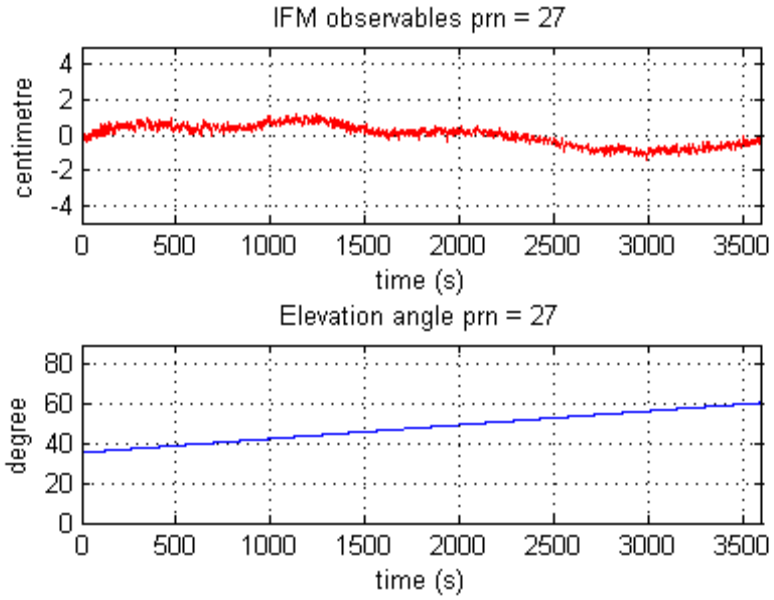

(b) Satellite with low multipath level

Figure 6.5: IFM observed and elevation angle in between-receiver mode for test case 1

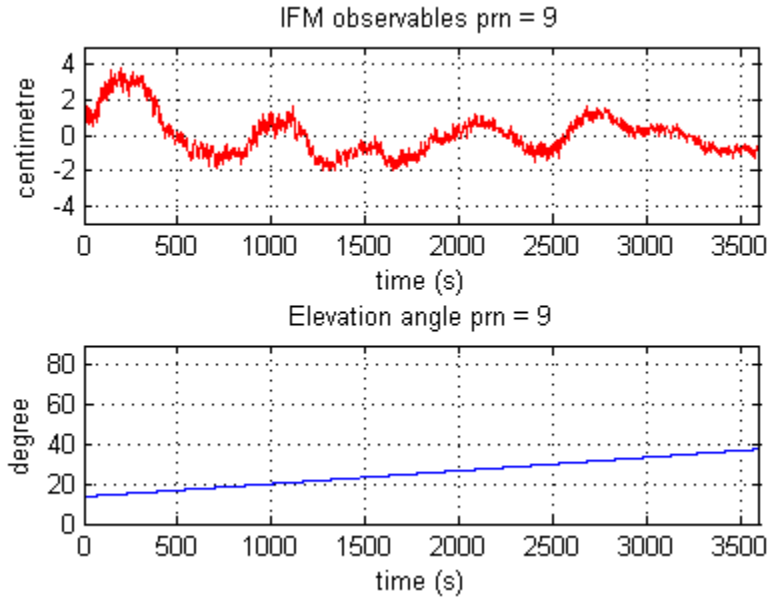

(a) Satellite with high multipath level

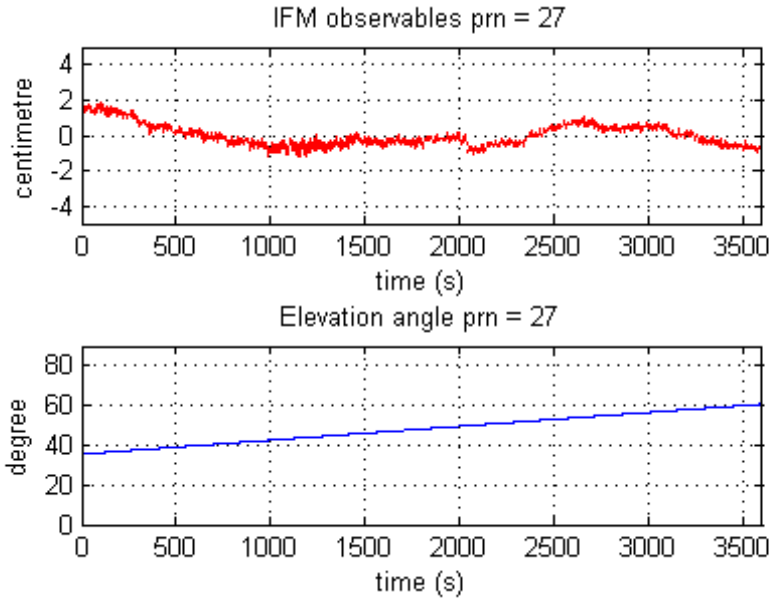

(b) Satellite with low multipath level

Figure 6.6: IFM observed and elevation angle in between-receiver mode for test case 2

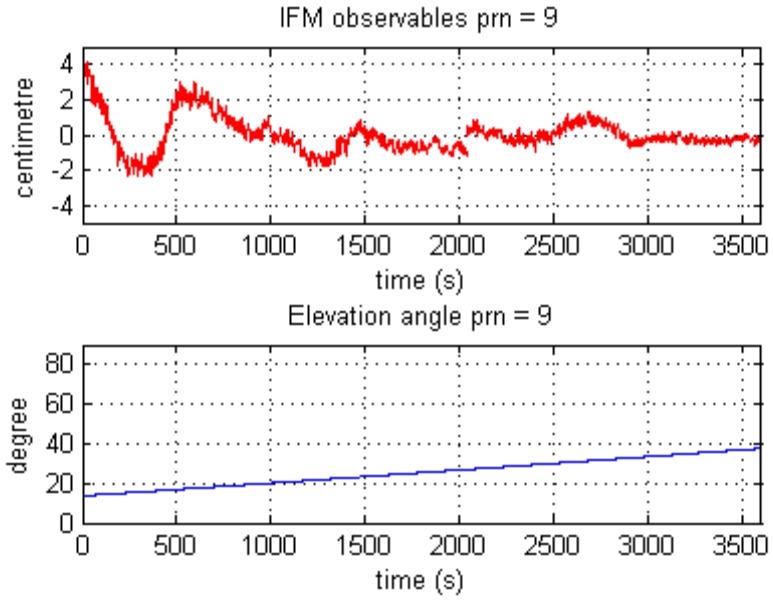

(a) Satellite with high multipath level

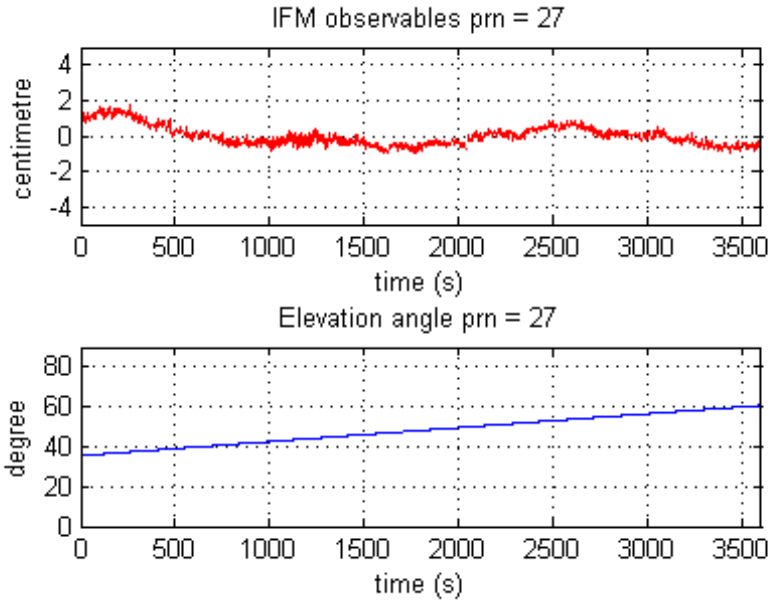

(b) Satellite with low multipath level

Figure 6.7: IFM observed and elevation angle in between-receiver mode for test case 3

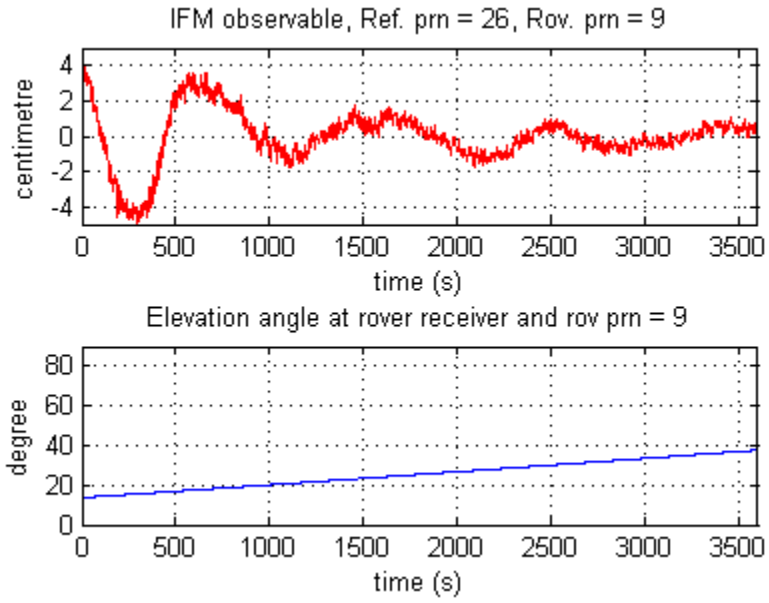

(a) Satellites with high multipath level

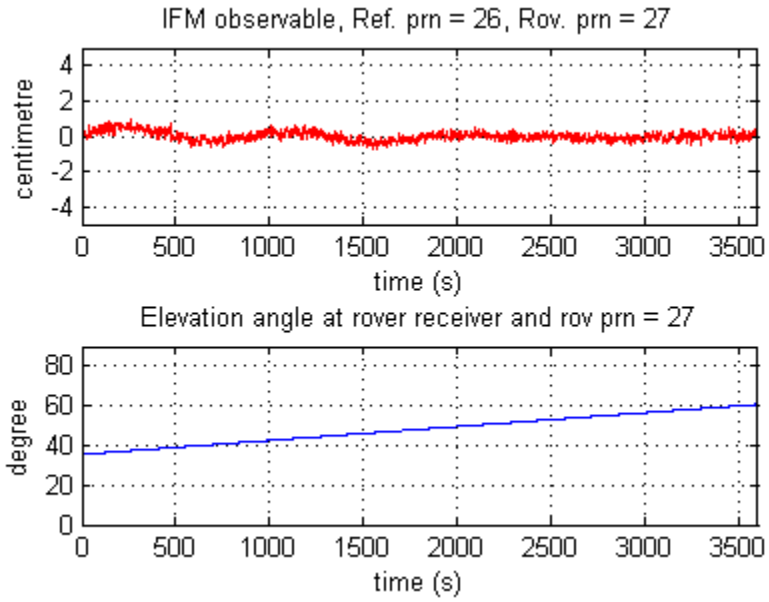

(b) Satellites with low multipath level

Figure 6.8: IFM observed and elevation angle in double-differenced mode for test case 1

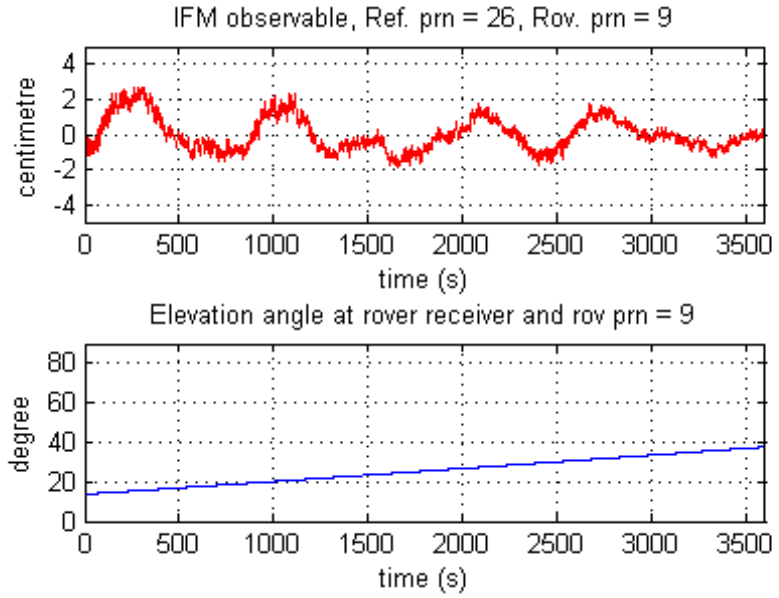

(a) Satellites with high multipath level

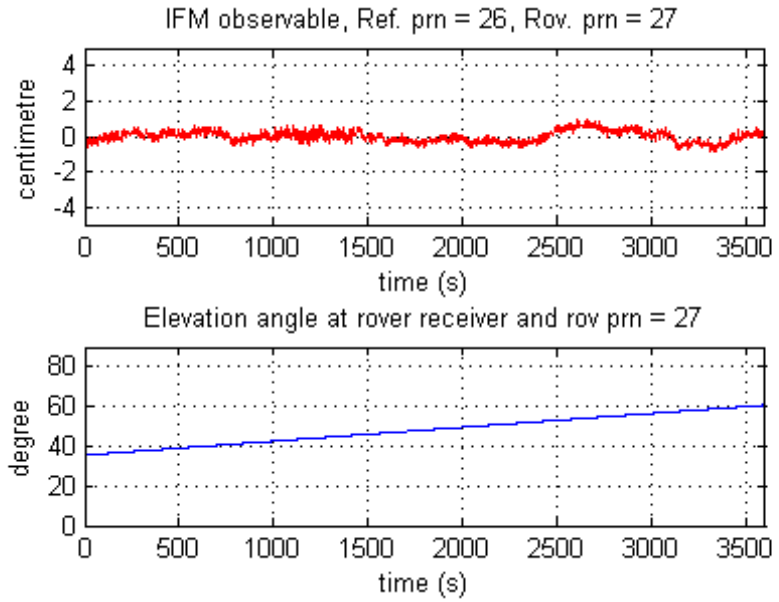

(b) Satellites with low multipath level

Figure 6.9: IFM observed and elevation angle in double-differenced mode for test case 2

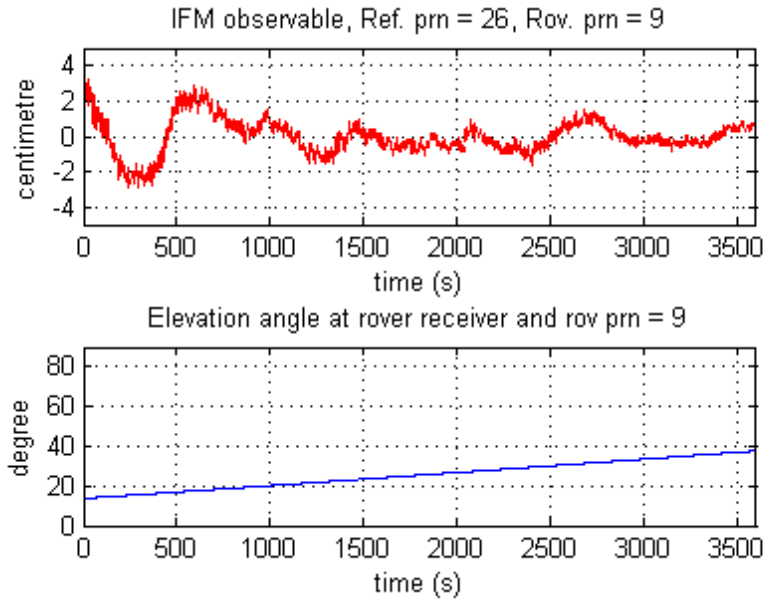

(a) Satellites with high multipath level

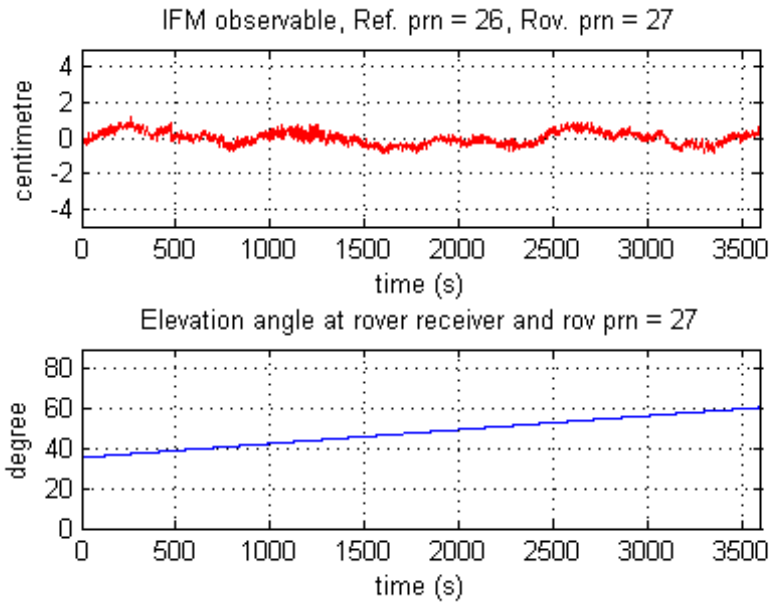

(b) Satellites with low multipath level

Figure 6.10: IFM observed and elevation angle in double-differenced mode for test case 3

The IFM observables illustrated in the figures exhibit a sinusoidal pattern with stable mean, in line with expectations. It can be seen from the IFM figures that the mean values remain almost constant for the whole period, even for test case 3 with a 17 km baseline, indicating that the $\delta\Delta IFI$ is negligible relative to the IFM observable, a key requirement in using the maximum time window approach (see Section 5.3.2.3). The figures also show that the observables are similar for the between-receiver and double-differenced modes. This suggests that the IFM observable in double-differenced mode was dominated by multipath in the secondary satellite (prn 9). This is also in line with expectations because in double-differenced mode, the satellite with the highest elevation angle was chosen as the reference satellite, which is typically less prone to multipath errors. In addition the chosen window time covers several IFM cycles in all the scenarios, which means the chosen time window is suitable for the current datasets.

6.3 IFM based multipath correction

The IFM observable in double differenced mode has been used to correct carrier phase measurements in IF combinations. The IFM-based multipath correction model defined in Section 5.4.2.1 (Equations 5.28) has been applied to the carrier phase IF combination to compute the position. The horizontal position errors for test cases 1, 2 and 3 are illustrated in Figure 6.11, Figure 6.12 and Figure 6.13 respectively. The vertical blue line in each of the Figures shows the point where the difference between the results obtained before and after the correction reaches the threshold of 7cm and stays within this

threshold for the rest of the dataset. The reason for choosing this threshold is that the difference between the two results after convergence in most of the cases stays below it and that it is within the accuracy requirement of the applications relevant to this thesis. The horizontal RMS errors and horizontal mean errors, obtained for the period before the threshold, are summarised in Table 6.1 and Table 6.2 respectively.

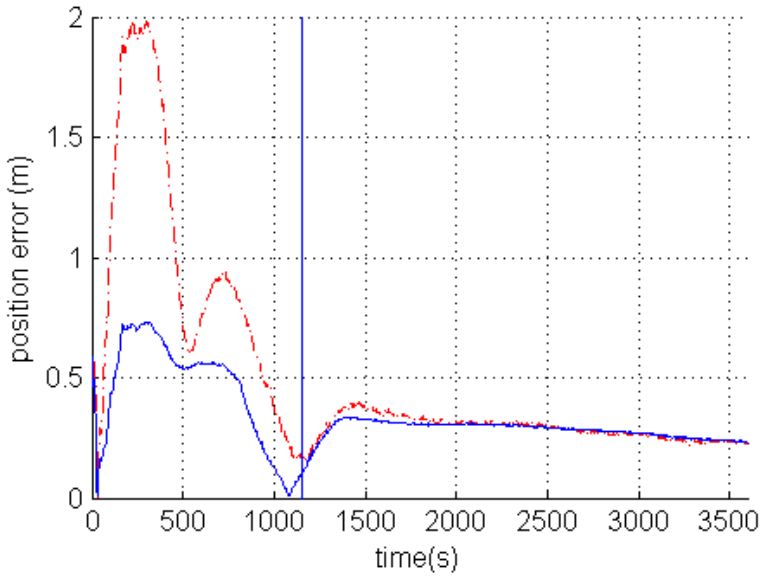

Figure 6.11: Case 1: horizontal position errors obtained before IFM-based correction (red) and after IFM-based correction (blue)

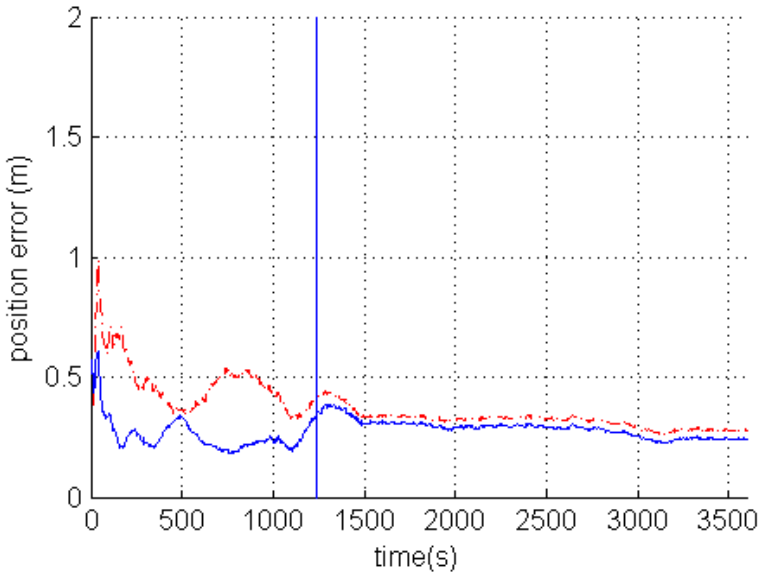

Figure 6.12: Case 2: horizontal position errors obtained before IFM-based correction (red) and after IFM-based correction (blue)

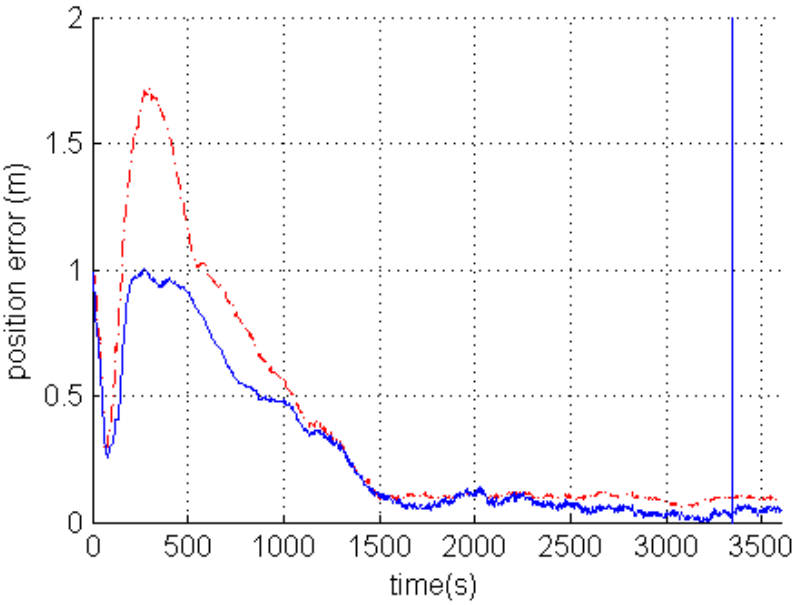

Figure 6.13: Case 3: horizontal position errors obtained before IFM-based correction (red) and after IFM-based correction (blue)

Table 6.1: Improvement in Horizontal RMS error using IFM-based multipath correction technique for test cases 1, 2 and 3

Test case	*Base line (km)*	*Horizontal RMS Error (m)*		*Improvement %*
		Before correction	*After correction*	
1	*0.02*	*1.110*	*0.499*	*55.1*
2	*17*	*0.488*	*0.271*	*44.4*
3	*17*	*0.620*	*0.429*	*30.8*

Table 6.2: Improvement in Horizontal mean error using IFM-based multipath correction technique for test cases 1, 2 and 3

Test case	*Base line (km)*	*Horizontal mean error (m)*		*Improvement %*
		Before correction	*After correction*	
1	*0.020*	*0.952*	*0.447*	*53.0*
2	*17*	*0.474*	*0.261*	*44.9*
3	*17*	*0.410*	*0.293*	*28.51*

The results in Figure 6.11, Figure 6.12, Figure 6.13, Table 6.1 and Table 6.2 show that the application of the IFM-based multipath correction significantly improves the position accuracy for IF combinations. The most significant improvement was achieved for the shortest baseline. This could be due to the relatively smaller ionosphere error in the estimated IFM observable due to the shorter baseline and the relatively higher

multipath levels, given that the permanent station is, by design, expected to be less affected by multipath.

6.4 IFM based weighting

In this section the IFM-based weighting model (Equation 5.30) defined in Section 5.4.2.2 is applied to the IF carrier phase measurements and the results are compared with the elevation based weighting Figure 6.14, Figure 6.15 and Figure 6.16 for test cases 1, 2 and 3 respectively. The vertical blue line in each of the Figures shows the point where the difference between the results obtained before and after the correction reaches the threshold of 7cm and stays within this threshold for the rest of the dataset. The horizontal RMS errors and horizontal mean errors, obtained for the period before the threshold, are shown in Table 6.3 and Table 6.4 respectively.

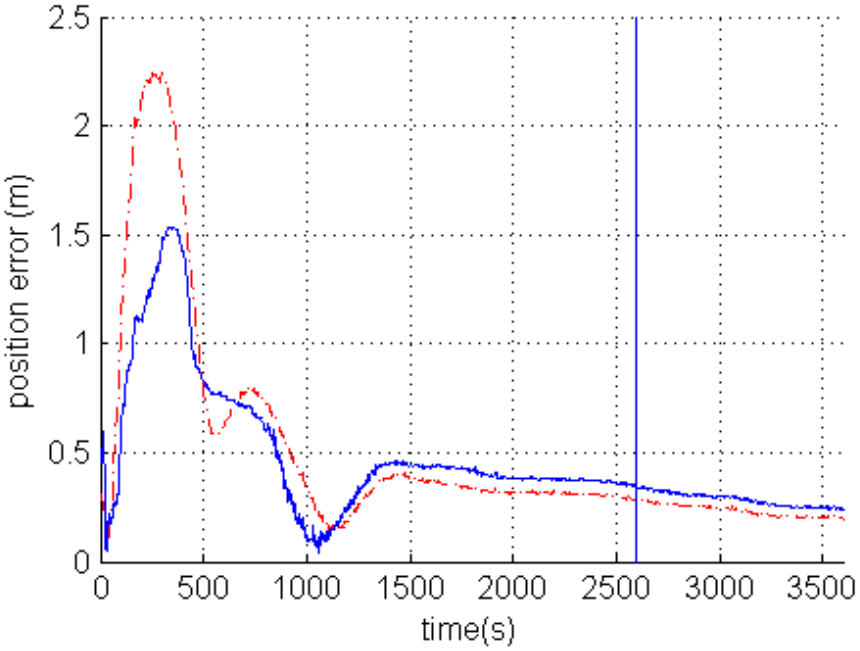

Figure 6.14: Case 1 horizontal position errors obtained using the eleva\tion-based weighting (red) and IFM-based weighting (blue)

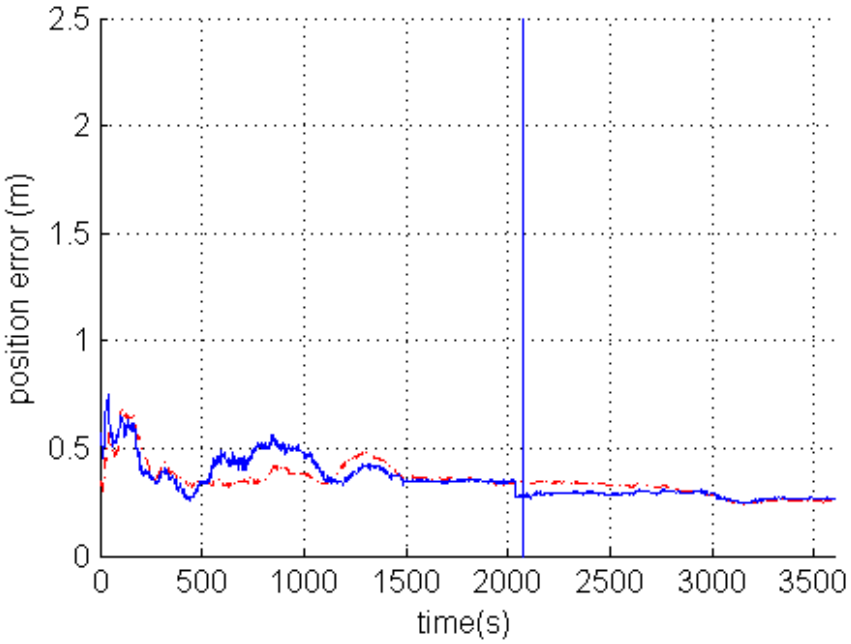

Figure 6.15: Case 2 horizontal position errors obtained using the elevation-based weighting (red) and IFM-based weighting (blue)

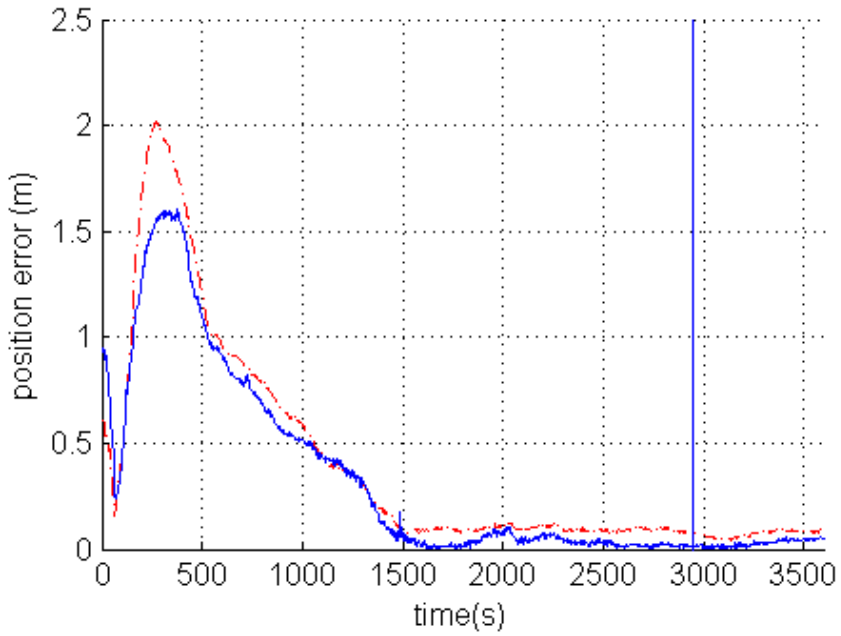

Figure 6.16: Case 3 horizontal position errors obtained using the elevation-based weighting (red) and IFM-based weighting (blue)

Table 6.3: Improvement in Horizontal RMS error using IFM-based weighting technique for test cases 1, 2 and 3

Test case	*Base line (km)*	*Horizontal RMS Error (m)*		*Improvement %*
		Before correction	*After correction*	
1	*0.020*	*0.826*	*0.628*	*23.9*
2	*17*	*0.398*	*0.415*	*-4.3*
3	*17*	*0.715*	*0.616*	*13.8*

Table 6.4: Improvement in Horizontal mean error IFM-based weighting for test cases 1, 2 and 3

Test case	*Base line (km)*	*Horizontal mean error (m)*		*Improvement %*
		Before correction	*After correction*	
1	*0.020*	*0.609*	*0.532*	*12.6*
2	*17*	*0.391*	*0.406*	*-3.8*
3	*17*	*0.470*	*0.394*	*16.1*

The above results show that the IFM-based weighting technique improved the horizontal position accuracies in two cases out of 3. In case 2, it had a slightly negative effect on the position accuracy. The improvements achieved in cases 1 and 3 can mainly be attributed to a decrease in the peak position error around epoch 300. This peak error is probably due to peak IFM observable value in satellite 9 (Figure 6.8). Although the peak position error around epoch 300 decreased, it does not disappear. This suggests that either the estimated IFM was not accurate enough or there are other factors responsible for the peak error such as code multipath error, or L1 carrier multipath error. The new stochastic technique is more effective than elevation based weighting in the presence of a high level of IFM, while at lower IFM it is less effective. This is in line with expectations because, based on the carrier multipath model introduced in Chapter 5 Equation 5.6, carrier multipath errors in IF comprises scaled IFM observable plus carrier multipath error in L1. Since the IFM-based weighting model reflects mainly the IFM observable and has no direct impact on the carrier multipath errors in L1, the IFM-based weighting is expected

to deliver better results when the IFM magnitude is high relative to L1 multipath. According to Figure 6.14 (case 1), the horizontal position after the vertical blue line is converging to a value that is relatively less accurate when applying the IFM-based weighting. The difference in the convergence is less than the selected threshold (7cm) which could be associated with the inaccuracies of the reference positions used for the Silwood 1 and Silwood 2 stations. In case 2 and 3 the positioning of the reference receiver (FARB) was known more accurately. Therefore, the apparent inaccuracy in case 1 is not present in cases 2 and 3.

6.5 Summary

This section discusses the relative strengths of the various IFM-based multipath mitigation techniques tested in this chapter on the IF carrier. Table 6.5 and Table 6.6 compare the horizontal RMS error and horizontal mean errors obtained with these techniques with those obtained with a simple elevation weighting technique.

Table 6.5: Horizontal RMS error comparison between elevation based weighting with IFM-based multipath mitigation techniques

Test scenario	*Base line (km)*	*Horizontal RMS error (m)*			*Improvement over elevation weighting %*	
		Elevation weighting	*IFM-based correction*	*IFM-based weighting*	*IFM-based correction*	*IFM-based weighting*
1	*0.020*	*0.826*	*0.499*	*0.628*	*39.6*	*24.0*
2	*17*	*0.398*	*0.271*	*0.415*	*32.0*	*-4.3*
3	*17*	*0.715*	*0.429*	*0.616*	*40.0*	*13.8*

Table 6.6: Horizontal mean error comparison between elevation based weighting with IFM-based multipath mitigation techniques

Test scenario	*Base line (km)*	*Horizontal mean error (m)*			*Improvement over elevation weighting %*	
		Elevation weighting	*IFM-based correction*	*IFM-based weighting*	*IFM-based correction*	*IFM-based weighting*
1	*0.020*	*0.609*	*0.447*	*0.532*	*26.6*	*12.6*
2	*17*	*0.391*	*0.261*	*0.406*	*33.2*	*-3.8*
3	*17*	*0.470*	*0.293*	*0.394*	*37.6*	*16.2*

Based on the results in Table 6.5 and Table 6.6, it can be concluded that IFM-based weighting technique resulted in improvements over the simple elevation based technique in two cases out of three. The IFM-based multipath correction technique resulted in better position accuracies in all 3 test cases. The IFM-based correction was able to mitigate the peak errors around epoch 300 much better than the IFM-based weighting technique. This suggests that IFM-based multipath correction is more effective than IFM-based weighting in IF combinations for high levels of carrier multipath error.

In the next chapter, the IFM-based multipath mitigation techniques are applied to the WL observable and their performance evaluated in terms of the ambiguity resolution time.

Chapter 7

CARRIER MULTIPATH MITIGATION IN WIDE LANE OBSERVABLE

In the previous chapter IFM-based multipath mitigation techniques were tested for the IF combination. In this chapter the IFM-based multipath mitigation techniques are applied to the WL combination, with the aim of decreasing the ambiguity resolution time. The real data and test cases presented in Chapter 6 are also used here to assess the performance of the IFM-based mitigation techniques for the WL combination. The aim is to improve the ambiguity resolution by mitigating carrier multipath error in WL. For ambiguity validation throughout this chapter, the Ratio Test (Euler and Schaffrin 1991) has been used based on:

$$\frac{R_2}{R_1} \geq k$$

7.1

where R_2 is the residual of the second best integer ambiguity candidate vector, R_1 is the residual of the first best candidate vector and k is the threshold. A threshold of 3 is used in this thesis. In all the experiments in this thesis, the single frequency ambiguities are always fixed at the same epoch as the WL ambiguities

In Sections 7.1 and 7.2, the multipath correction and measurement weighting techniques are evaluated respectively. Section 7.3 concludes with a comparison of the IFM-based multipath mitigation techniques with the traditional elevation-based weighting. The most effective technique for WL combination are then identified.

7.1 IFM-based multipath correction

The IFM observable in double-differenced mode was used to correct the carrier multipath error in the double differenced WL observable. Correcting the WL observable with the model provided in Section 5.4.2.1 changes the correlation between the WL and L1 and L2 carrier phase measurements. In order to analyse the impact of the multipath correction on the WL combination, and dissociate the results from the impacts of changes in the measurement correlations, the WL was used as the only carrier phase measurement in the first experiment. After applying the corrections to the WL, the remaining WL multipath errors are correlated with the L1 carrier phase multipath errors, which are treated as noise by the Kalman filter. This noise correlation results in a non-optimal estimator of the Kalman filter (Ma et al. 2010). Therefore, in the second experiment, the

L2 carrier phase measurement is added to the observation vector instead of the L1, in order to increase position accuracy.

7.1.1 EXPERIMENT 1

In this experiment, L1 code phase and WL carrier phase measurements are used for position estimation, which is done using KF. WL ambiguity resolution is attempted.

The horizontal position errors before and after applying carrier phase multipath correction are shown in Figure 7.1, Figure 7.2 and Figure 7.3 for test cases 1, 2 and 3 respectively. The ambiguity resolution times and the improvements following multipath correction are summarised in Table 7.1.

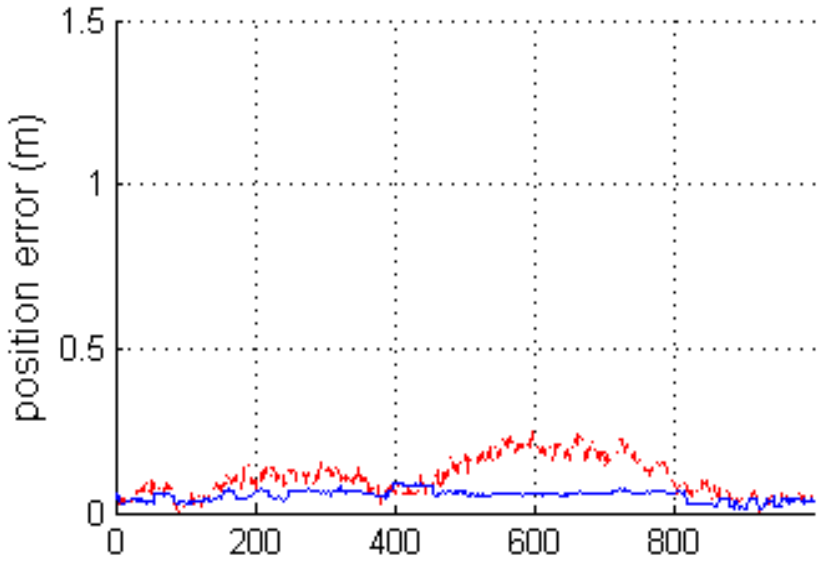

Figure 7.1: Case 1 horizontal position errors before multipath correction (red) and after IFM-based multipath correction (blue)

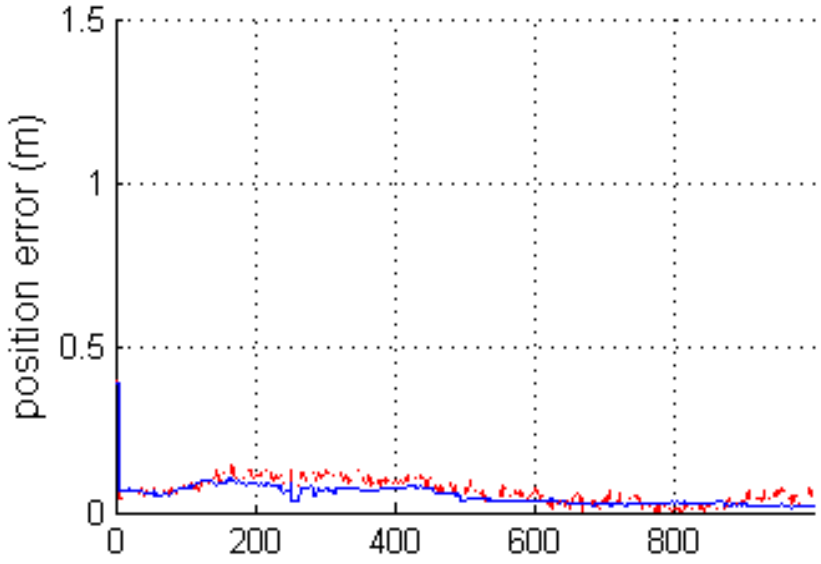

Figure 7.2: Case 2 horizontal position errors before multipath correction (red) and after IFM-based multipath correction (blue)

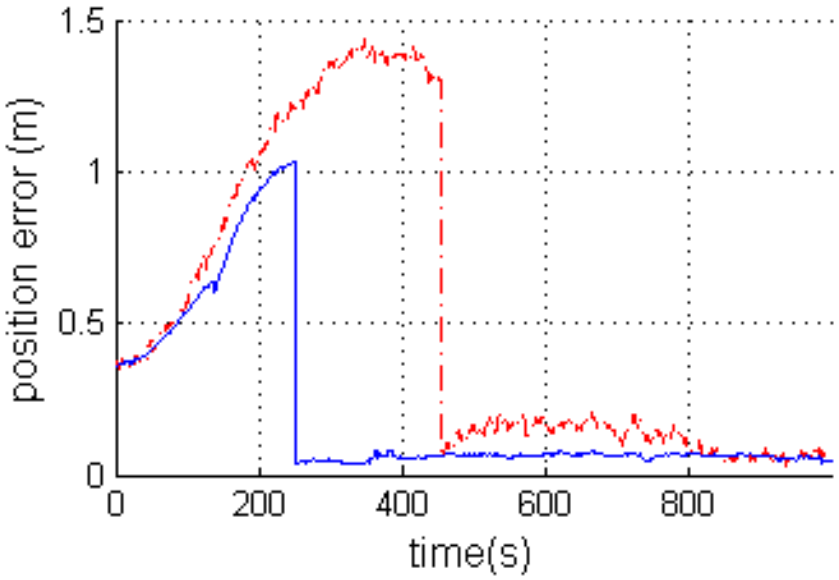

Figure 7.3: Case 3 horizontal position errors before multipath correction (red) and after IFM-based multipath correction (blue)

Table 7.1: Improvement in ambiguity fixing time using IFM-based multipath correction for test cases 1, 2 and 3 in Experiment 1

Test case	*Baseline (km)*	*Time To Ambiguity Fixing (TTAF) (seconds)*		*Improvement in TTAF*	
		Before correction	*After correction*	*(Seconds)*	*%*
1	*0.020*	*47*	*25*	*22*	*47*
2	*17*	*7*	*6*	*1*	*14*
3	*17*	*455*	*252*	*203*	*45*

The results above show that by using the proposed method, the ambiguity fixing time has been reduced in all three cases. In case 3, the ambiguities are fixed at a point

where the position error is larger than at prior epochs. This may occur when biases are absorbed by the ambiguities at an early stage in the ambiguity resolution process. Case 2 has a considerably shorter fixing time than case 3 prior to and after multipath correction. This difference appears to be associated with the difference in the multipath magnitude between the two cases especially during the early epochs. As can be seen from top panels of Figure 6.8 Figure 6.7 and Figure 6.8, the IFM value in the first epoch is 4.6cm for Case 1, -1cm for Case 2 and 3.5cm for Case 3. Among all three cases, multipath errors are largest for Case 1. At the same time, due to the shorter baseline, the estimated IFM is the most accurate. Therefore, case 1 achieves the best improvement.

The small discontinuity in the position error around 800 seconds in case 1 is the result of a change in the number of satellites. Using only the WL carrier phase observable results in a noisy position solutions (as shown in Figure 7.1, Figure 7.2 and Figure 7.3). Following the multipath correction, the effects of noise and multipath errors are decreased significantly, which results in having a smoother position.

7.1.2 EXPERIMENT 2

In this experiment, L1 code phase, L2 carrier-phase and WL carrier phase measurements are used for position estimation, which is done using KF. The horizontal position errors before and after carrier phase multipath correction are shown in Figure 7.4, Figure 7.5 and Figure 7.6 for test cases 1, 2 and 3 respectively. The ambiguity resolution times and the improvements following multipath correction are summarised in Table 7.2.

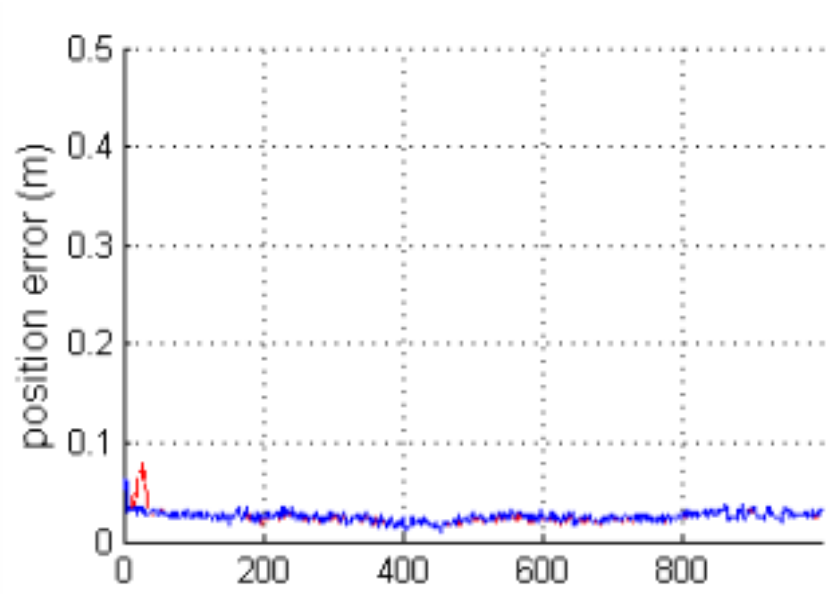

Figure 7.4: Case 1 horizontal position errors before multipath correction (red) and after IFM-based multipath correction (blue)

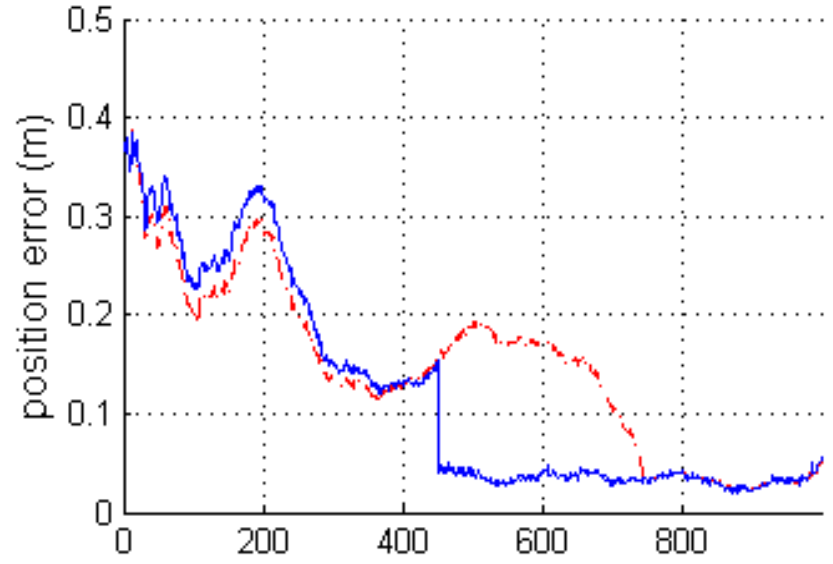

Figure 7.5: Case 2 horizontal position errors before multipath correction (red) and after IFM-based multipath correction (blue)

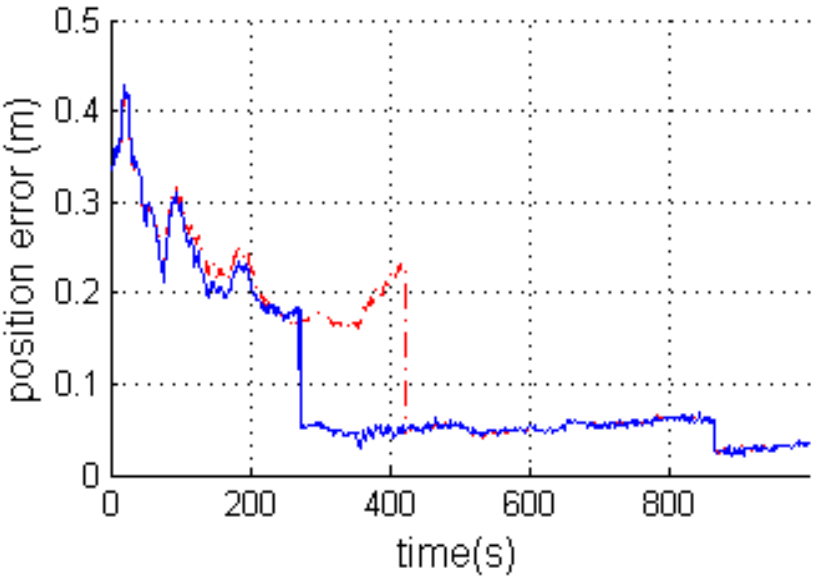

Figure 7.6: Case 3 horizontal position errors before multipath correction (red) and after IFM-based multipath correction (blue)

Table 7.2: Improvement in ambiguity fixing time using IFM-based multipath correction for test cases 1, 2 and 3 in Experiment 2

Test case	*Baseline (km)*	*Time to ambiguity fixing (TTAF) (seconds)*		*Improvement in TTAF*	
		Before correction	*After correction*	*(Seconds)*	*%*
1	*0.020*	*34*	*6*	*28*	*82*
2	*17*	*744*	*452*	*292*	*39*
3	*17*	*424*	*273*	*151*	*36*

The above results show that in this experiment, as in the previous experiment, applying the multipath correction technique results in faster ambiguity fixing. However, results in Figure 7.5 show that correcting multipath errors in the WL may also increase position errors. This correction changes the correlation between the L2 and WL carrier phase measurements, potentially affecting the position error. In Figure 7.6, there is a small discontinuity in the position error after 800 seconds, which is due to a change in the number of satellites.

7.1.3 EXPERIMENT 3

As discussed in Section 5.4.2.1, the WL observable corrected based on the IFM observable is highly correlated with the L1 carrier measurements. Therefore, it is suggested to use the corrected WL observable with L2 carrier phase measurements. However, L2 carrier phase measurements have higher noise and ionospheric errors relative to L1 carrier phase measurements. Hence, the use of L1 carrier phase measurements is expected to result in a faster ambiguity resolution. Therefore, an interesting comparison is the ambiguity resolution time using L2 carrier phase measurements with the corrected WL with the resolution time using L1 carrier phase measurements and the original WL observable. Horizontal position errors before and after carrier phase multipath correction are shown in Figure 7.7, Figure 7.8 and Figure 7.9 for test cases 1, 2 and 3 respectively. The ambiguity resolution times and the improvements following multipath correction are summarised in Table 7.3.

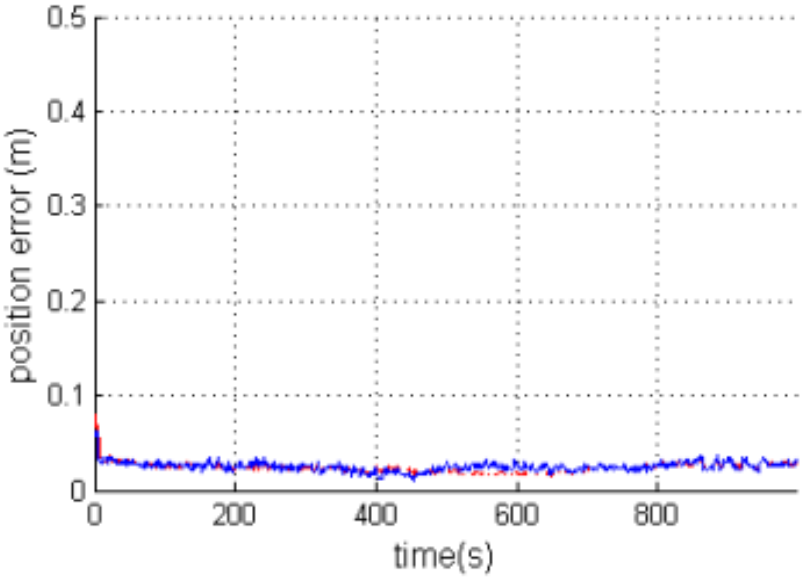

Figure 7.7: Case 1 horizontal position errors using L1 code and phase and WL (red) and L1 code, L2 phase and corrected WL (blue)

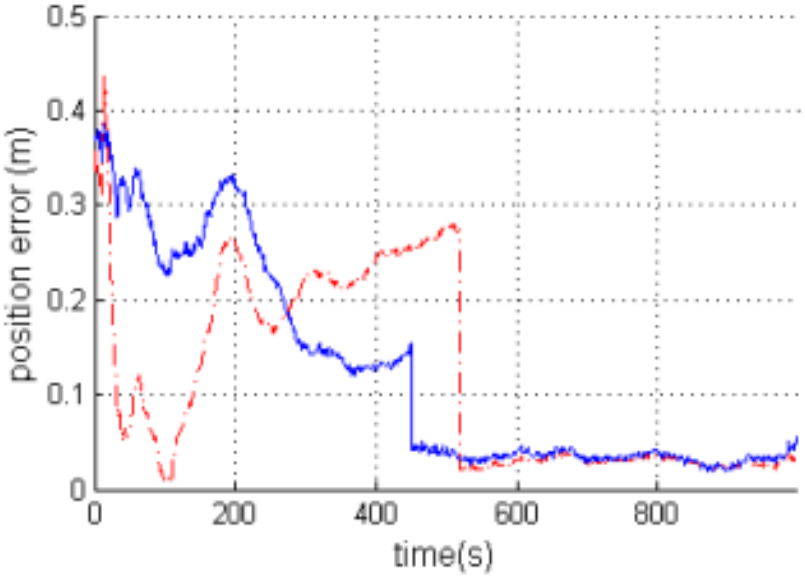

Figure 7.8: Case 2 horizontal position errors using L1 code and phase and WL (red) and L1 code, L2 phase and corrected WL (blue)

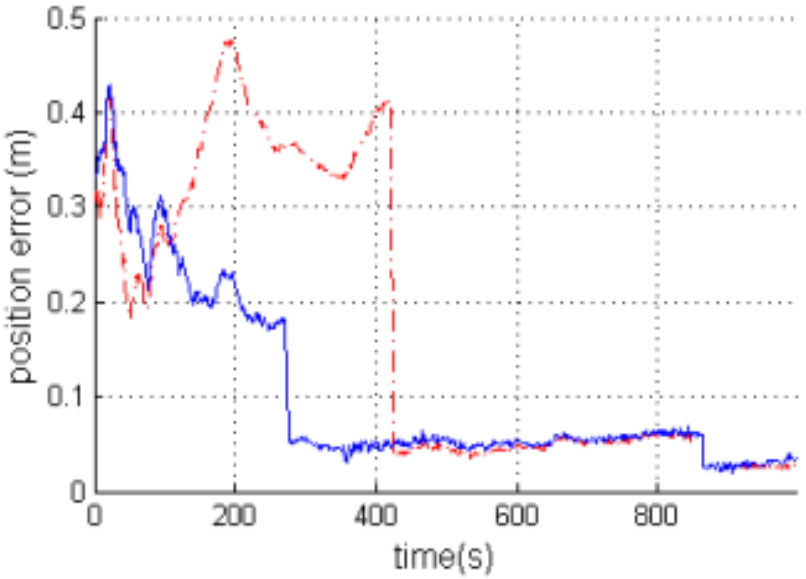

Figure 7.9: Case 3 horizontal position errors using L1 code and phase and WL (red) and L1 code, L2 phase and corrected WL (blue)

Table 7.3: Improvement in ambiguity fixing time using IFM-based multipath correction for test cases 1, 2 and 3 in Experiment 3

Test case	*Baseline (km)*	*Time To Ambiguity Fixing (TTAF) (seconds)*		*Improvement in TTAF*	
		Using L1 code and phase and WL	*Using L1 code, L2 phase and corrected WL*	*(seconds)*	*(%)*
1	*0.020*	*8*	*6*	*2*	*25*
2	*17*	*520*	*452*	*68*	*13*
3	*17*	*425*	*273*	*152*	*35*

A comparison of the results in this experiment with those obtained in experiment 2 shows that using the L1 carrier phase measurement instead of the L2 carrier phase measurement speeds up the ambiguity resolution, as expected. Nonetheless, the use of the IFM-based corrected WL observable with L2 carrier phase provides better results compared with using L1 with uncorrected WL. This is despite the fact that L1 carrier phase measurement has better quality than L2 carrier phase measurement.

7.1.4 SUMMARY

To conclude, when using the IFM-based correction technique, ambiguity resolution is faster if WL is used as the only carrier phase measurement. This could be due to high levels of multipath in the single frequency observations. Therefore, it is better to use the WL observable as the only carrier phase measurements before ambiguity fixing. After fixing WL ambiguity, L1 or L2 carrier phase measurements can be added to improve position accuracy.

7.2 IFM-based weighting

In this section, the IFM-based weighting technique is applied to the WL observable, with the aim of improving the ambiguity resolution time. The result is compared with legacy elevation based weighting techniques. The IFM observable in double-differenced mode is used, in line with the use of double differenced measurements. In order to analyse the impact of the new stochastic model and dissociate

any impacts of correlations between different carrier phase measurements, the WL is used as the only carrier phase measurement in the first experiment. In the second and third experiments, the L1 and L2 carrier phase measurements are added respectively to the observation vector in order to improve position accuracy.

7.2.1 EXPERIMENT 1

In this experiment, L1 code phase measurements and WL carrier phase observables are used. The horizontal position errors using elevation based weighting and IFM based weighting are shown in Figure 7.10, Figure 7.11 and Figure 7.12 for test cases 1, 2 and 3 respectively. The ambiguity resolution times and the improvements following IFM based weighting are summarised in Table 3.

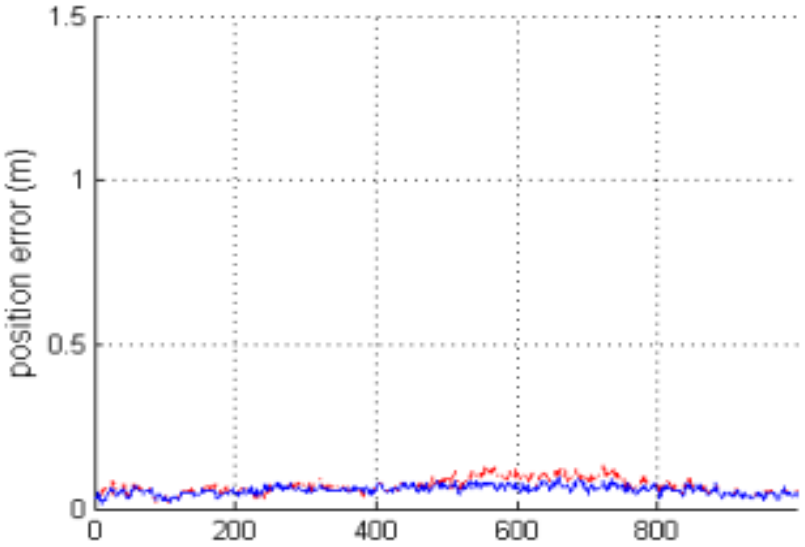

Figure 7.10: Case 1 horizontal position errors obtained using elevation based weighting (red) and IFM-based weighting (blue)

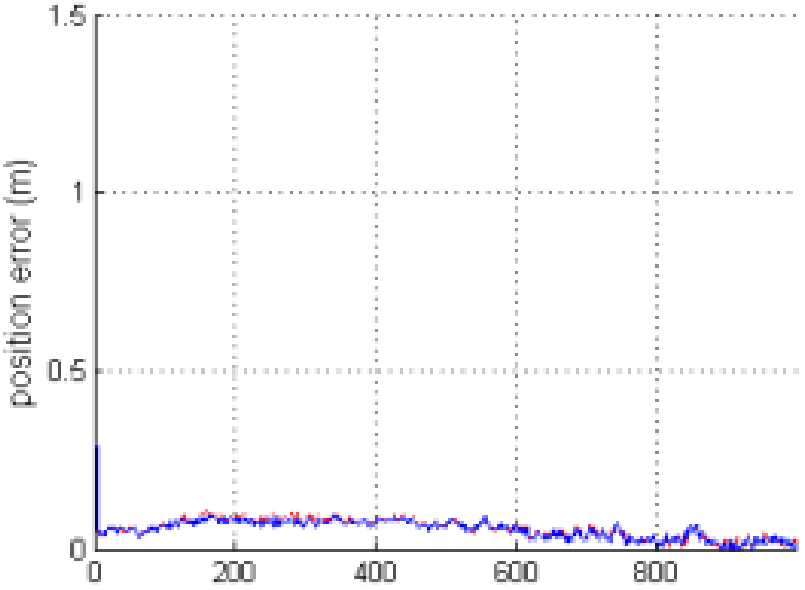

Figure 7.11: Case 2 horizontal position errors obtained using elevation based weighting (red) and IFM-based weighting (blue)

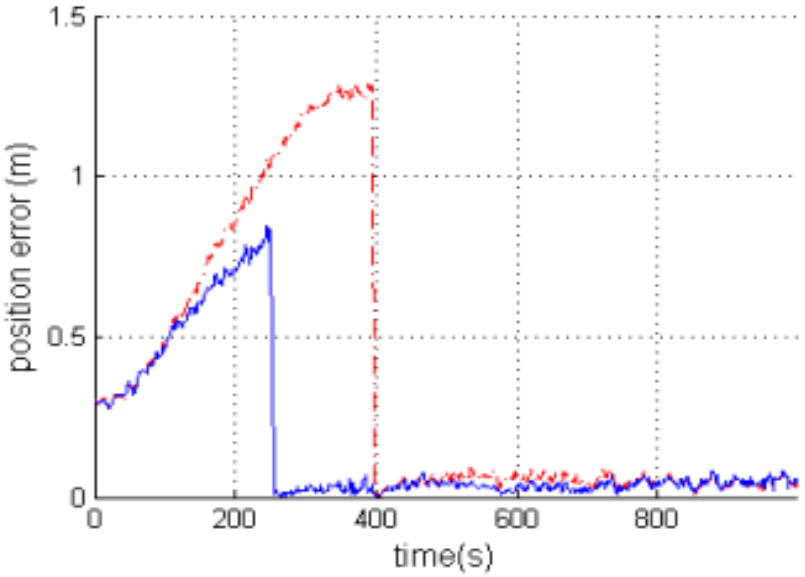

Figure 7.12: Case 3 horizontal position errors obtained using elevation based weighting (red) and IFM-based weighting (blue)

Table 7.4: Improvement in ambiguity fixing times using IFM-based weighting for test cases 1, 2 and 3 in Experiment 1

Test case	*Baseline (km)*	*Time To Ambiguity Fixing (TTAF) (seconds)*		*Improvement in TTAF*	
		Using elevation weighting	*Using IFM-based weighting*	*(Seconds)*	*(%)*
1	*0.020*	*27*	*6*	*21*	*78*
2	*17*	*6*	*6*	*0*	*0*
3	*17*	*397*	*252*	*145*	*37*

The above results suggest that by using the IFM-based weighting scheme, the ambiguity fixing time can be reduced in two cases out of three. The improvement in case

1 is best where the ambiguity is fixed at the 6s (the minimum time for attempting ambiguity fixing defined in the Software configuration). The highest improvement in case 1 is attributed to higher multipath levels for this case compared to the other two cases, where one set of measurements is from a surveyed permanent station, with significantly lower levels of multipath.

Using only the WL carrier phase observable results in significant noise in the position estimation. The IFM-based weighting scheme does not have a significant effect on the WL noise level, contrary to the IFM-based correction technique (Section 7.1.1), which decreases the WL noise level significantly.

7.2.2 EXPERIMENT 2

In this experiment, carrier phase measurements at the L1 frequency were used in addition to the WL carrier phase measurements to test the elevation based technique. The mathematical correlation between the L1, L2 and WL observables can be calculated using the Gauss's propagation of error law. Based on this law, if two vectors of quantities Z and Y are related to each other deterministically, their covariance matrixes are also related to each other. In other words if vector Z is obtained from vector Y:

$$Z = XY \tag{7.2}$$

then the covariance matrix of Z (C_z) can be obtained from the covariance matrix of Y (C_y) as:

$$C_z = X\, C_y X^T$$

7.3

Accordingly, the covariance matrix for the observable vector containing the L1 and WL carrier phase measurements is obtained as:

$$\begin{bmatrix} \sigma_{L1}^2 & \sigma_{L1}^2 \\ \sigma_{L1}^2 & \sigma_{L1}^2 + \sigma_{L2}^2 \end{bmatrix}$$

7.4

where σ_{L1}^2 and σ_{L2}^2 are the carrier phase variances of the L1 and L2 observations respectively. Applying elevation based weighting on the L1 and L2 observations affects the diagonal as well as the off diagonal elements of the covariance matrix. On the other hand, the IFM based weighting technique can be applied only to the WL carrier phase measurements because it provides no information on the carrier phase measurements at each of the individual frequencies. By weighting only the WL observable, the off diagonal elements in the covariance matrix are no longer valid. In other words, the IFM based stochastic model cannot be applied in the presence of off-diagonal elements. Therefore, in this experiment, the result of the elevation-based technique applied to the L1 and L2 measurements (and hence WL) is compared with the result of the IFM based weighting technique obtained in the previous experiment (using L1 code and corrected WL). By making this comparison it should become clear which strategy is better; using

L1 and WL carrier phase measurements with elevation angle-based weighting or using WL measurement as the only carrier phase measurement weighted based on IFM observable.

The horizontal position errors obtained from the elevation based weighting and IFM based weighting technique are shown in Figure 7.16, Figure 7.17 and Figure 7.18 for test cases 1, 2 and 3 respectively. The ambiguity resolution times and the improvements following the application of the IFM based weighting are summarised in Table 7.6.

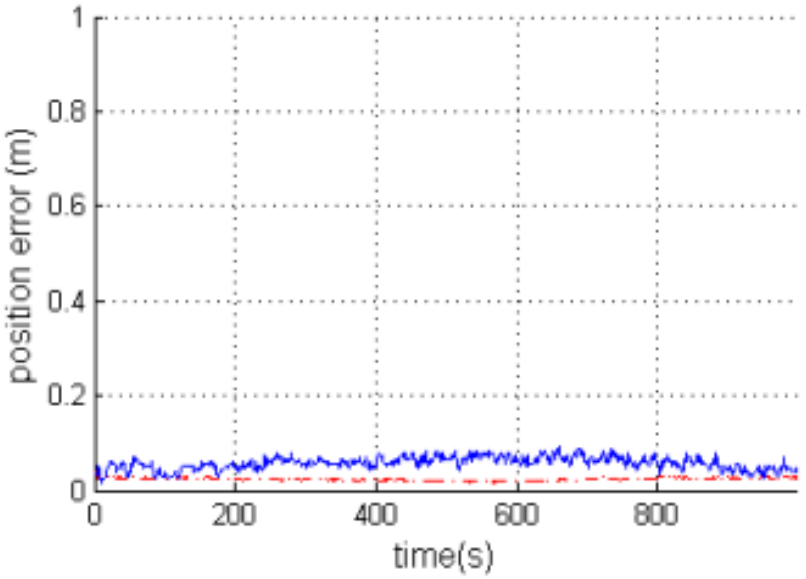

Figure 7.13: Case 1 horizontal position errors obtained using elevation based weighting (red) and IFM-based weighting (blue)

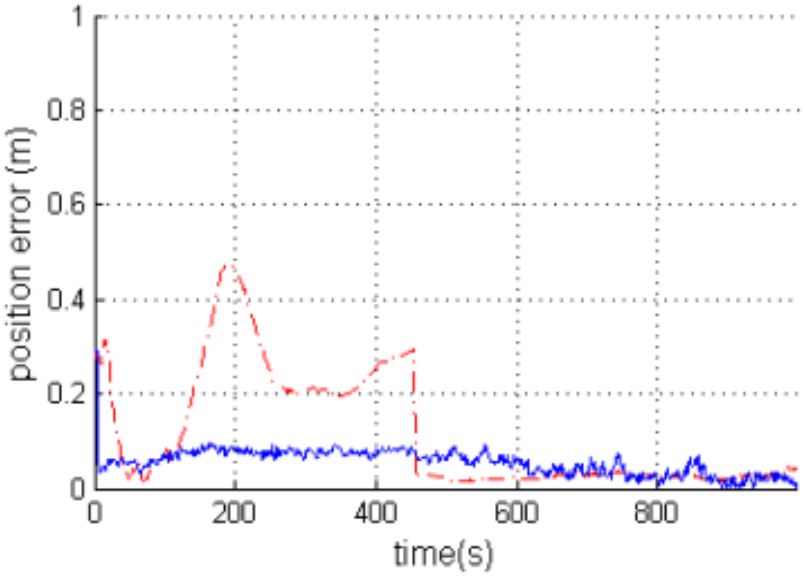

Figure 7.14: Case 2 horizontal position errors obtained using elevation based weighting (red) and IFM-based weighting (blue)

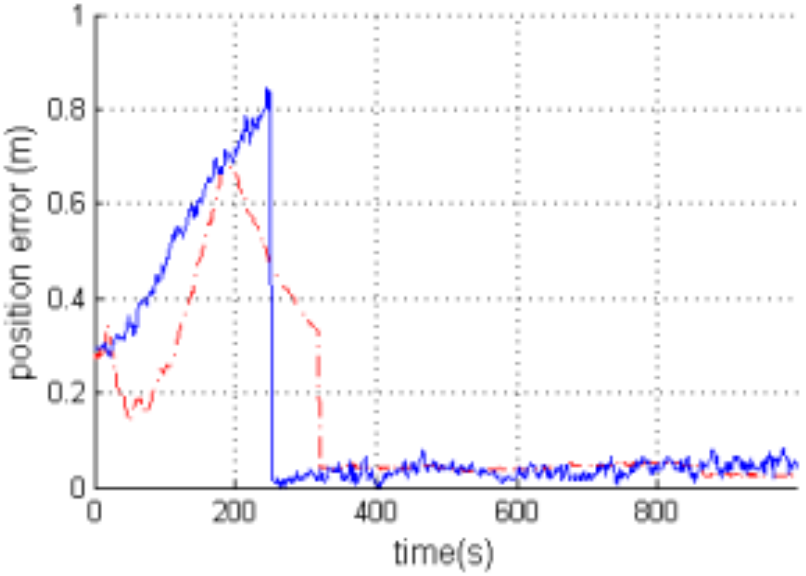

Figure 7.15: Case 3 horizontal position errors obtained using elevation based weighting (red) and IFM-based weighting (blue)

Table 7.5: Improvement in ambiguity fixing times using IFM-based weighting for test cases 1, 2 and 3 in Experiment 2

Test case	*Baseline (km)*	*Time To Ambiguity Fixing (TTAF) (Seconds)*		*Improvement in TTAF*	
		Using elevation weighting	*Using IFM-based weighting*	*(Seconds)*	*(%)*
1	*0.020*	*6*	*6*	*0*	*0*
2	*17*	*457*	*6*	*451*	*99*
3	*17*	*320*	*252*	*68*	*21*

The above results show that the IFM-based weighting applied to the WL observable as the only carrier achieved better results for long baselines (case 2 and 3) than the elevation based weighting using L1 and WL carrier phase measurements. However, using the L1 carrier phase measurements results in less noise in the position domain. Therefore, after fixing the ambiguities with the IFM-based weighting technique, it is useful to add the L1 carrier phase measurement to achieve a less noisy position solution.

7.2.3 EXPERIMENT 3

Typically, L1 carrier phase measurements are expected to be superior to L2 carrier phase measurements. Therefore, an interesting comparison would be to apply the IFM-based weighting to WL and compare the achieved resolution time to the time achieved using raw WL and L2 carrier phase measurement instead of L1 carrier phase measurements. In this experiment, for the same reasons as in experiment 2, the WL observable is used as the only carrier phase measurement when the IFM-based weighting is applied (see results in Section 1.3 experiments 1 and 2).

The horizontal position errors obtained from the elevation based weighting and IFM based weighting techniques are shown in Figure 7.16, Figure 7.17 and Figure 7.18 for test cases 1, 2 and 3 respectively. The ambiguity resolution times and the improvements following the application of the IFM based weighting are summarised in Table 7.6.

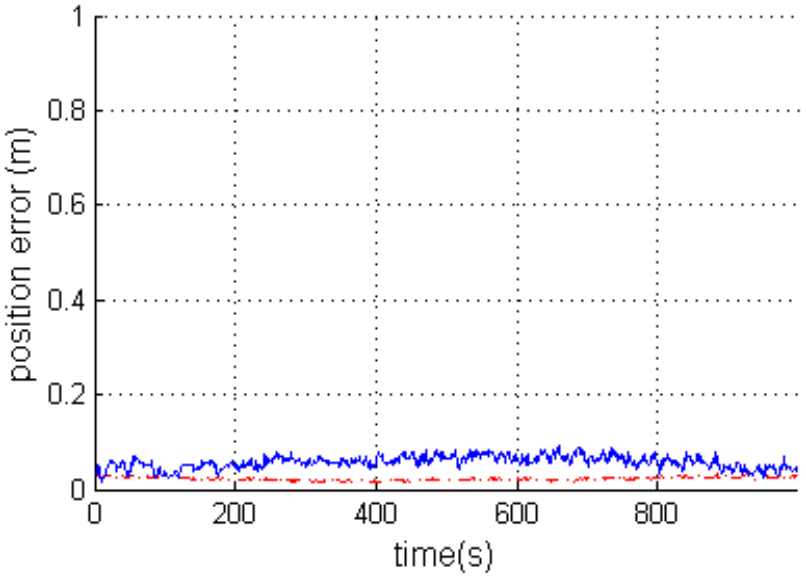

Figure 7.16: Case 1 horizontal position errors obtained using elevation based weighting (red) and IFM-based weighting (blue)

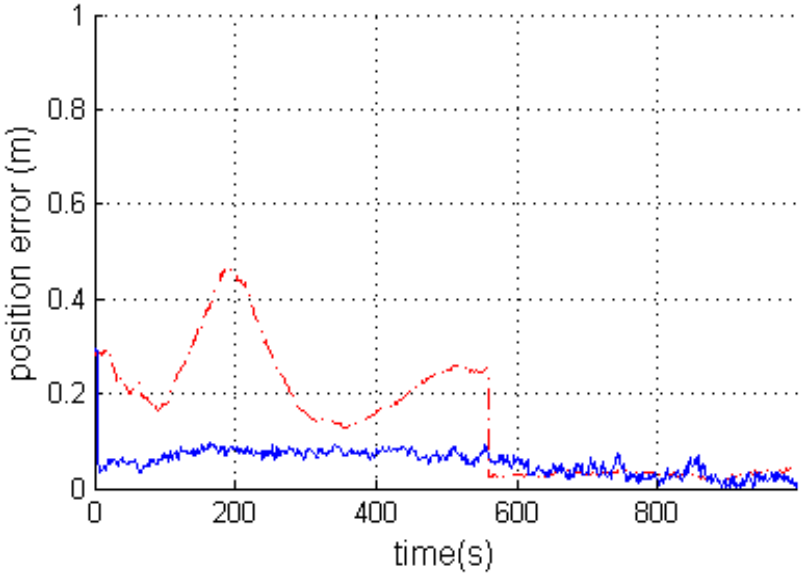

Figure 7.17: Case 2 horizontal position errors obtained using elevation based weighting (red) and IFM-based weighting (blue)

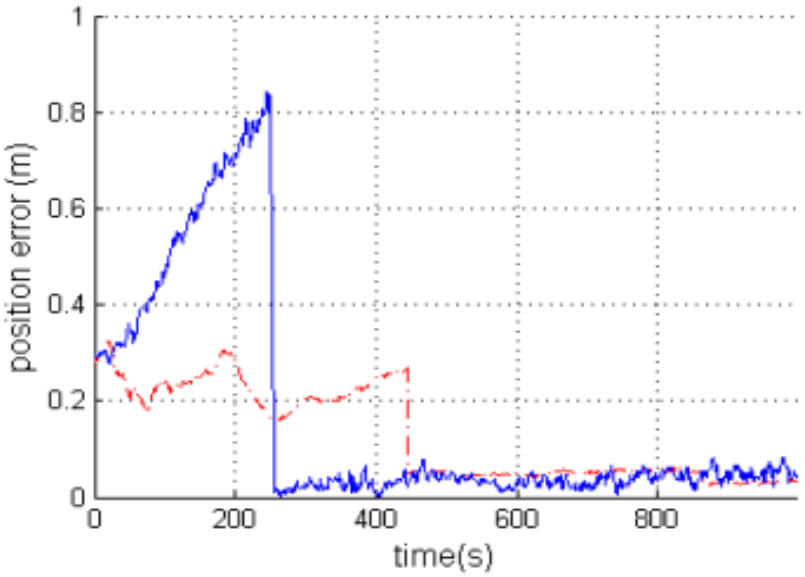

Figure 7.18: Case 3 horizontal position errors obtained using elevation based weighting (red) and IFM-based weighting (blue)

Table 7.6: Improvement in ambiguity fixing time using IFM-based weighting for test cases 1, 2 and 3 in Experiment 3

Test case	*Baseline (km)*	*Time to ambiguity fixing (TTAF) (Seconds)*		*Improvement in TTAF*	
		Using elevation weighting	*Using IFM-based weighting*	*(Seconds)*	*%*
1	*0.020*	*6*	*6*	*0*	*0*
2	*17*	*561*	*6*	*555*	*99*
3	*17*	*445*	*252*	*193*	*43*

As expected, using L2 carrier phase measurements instead of L1 results in delayed ambiguity resolution for those cases with long base lines (Case 2 and 3) and hence, is inferior to the results obtained by IFM-based weighting.

The new IFM-based weighting technique applied to the WL observable as the only carrier phase measurement is able to achieve faster ambiguity resolution time than elevation based weighting. However noise levels in the position with the new weighting scheme are high due to using the WL observable as the only carrier phase measurement. Therefore, after fixing the WL ambiguities, carrier phase measurements at single frequencies must be added to improve position accuracy.

7.3 Summary

Table 7.7 compares the results from the elevation based weighting technique with those from the two IFM-based multipath mitigation techniques developed in this thesis. The comparison focuses on identifying which technique is most effective in improving ambiguity resolution times.

Table 7.7: Improvement in ambiguity resolution times for test cases 1, 2 and 3

Test case	*Base line (km)*	*TTAF for best experiments (seconds)*			*Improvement in TTAF over elevation weighting %*	
		Elevation weighting	*IFM-based correction*	*IFM-based weighting*	*IFM-based correction*	*IFM-based weighting*
1	*0.020*	*27*	*25*	*6*	*7.4*	*77.8*
2	*17*	*6*	*6*	*6*	*0*	*0*
3	*17*	*397*	*252*	*252*	*36.5*	*36.5*

From Table 7.7 it can be concluded that IFM-based weighting delivers better results than either the elevation based weighting or IFM-based correction methods.

An interesting conclusion can be drawn by comparing the results in this chapter with those for the IF observable in the previous chapter. For the IF combination, the best mitigation technique is the IFM-based correction, while for the WL observable, it is the IFM-based weighting. This difference most probably is due to inaccuracies in the estimated IFM observable in both chapters. It seems that ambiguity resolution is very sensitive to the accuracy of the corrections applied. Float solutions with long convergence times, typically used for the IF observables, are less sensitive to the accuracy of the corrections. Therefore, it is safer to use IFM-based weighting for ambiguity resolution.

CHAPTER 8

CONCLUSIONS, IMPMEMENTAION AND FUTURE WORK

This chapter presents the conclusions drawn from the research conducted in this thesis. In addition, it discusses a number of implementation aspects of the novel techniques developed in this thesis and identifies the relevant future work.

8.1 Conclusions

Overall, the thesis has achieved its objectives formulated in Chapter One. This is evidenced by following the conclusions drawn from the work presented.

Following the detailed literature review, applications that require centimetre level positioning accuracy have been identified, and the need to employ carrier-phase measurements with novel carrier multipath mitigation techniques highlighted.

1. From the review of the literature on high accuracy positioning techniques, it has been determined that the main limitation to achieving the required accuracy is carrier multipath error especially in linear combinations such as wide-lane (WL) and ionosphere-free (IF) combinations.

2. From the extensive review of the literature on measurements processing based multipath mitigation techniques, it has been shown that all the existing techniques are either inaccurate or impractical. All the existing techniques target the multipath error in each individual frequency independently of the error in other frequencies even when a linear combination of measurements is intended to be formed.

3. In this thesis and for the first time, carrier multipath error in the linear combination measurements has been targeted directly for different reasons. Firstly, the carrier multipath error in a linear combination is much higher than the error in a single frequency making it easier to detect and model. Secondly, and conversely the carrier multipath error in a linear combination is more complex compared to the error in a single frequency. Thirdly, the carrier multipath error has a dispersive nature which may be used for modelling similar to the ionospheric error. This new approach to tackling multipath error has resulted in the development of a new model for error mitigation in linear combinations.

4. A new observable named Inter Frequency carrier Multipath (IFM) observable has been introduced which is obtained from carrier phase measurements in two different frequencies. The IFM observable is a combination of the error in the two

frequencies. This new observable has applications in different fields including carrier multipath mitigation.

5. New carrier multipath mitigation techniques have been developed by utilizing the error modelling and IFM observable developed in this research. The mitigation techniques are applicable to linear combinations. The mitigation based on the new techniques can be achieved by multipath correction and measurement weighting.

6. The new multipath mitigation techniques have been validated using real data achieving better positioning accuracy than the elevation weighting technique obtained by the IF combination. The new techniques also achieved faster ambiguity resolution time than the elevation weighting technique using WL combination.

7. A significant achievement of this thesis is the opening of a new research direction in carrier multipath mitigation techniques by utilizing the dispersive nature of the error, targeting the error in linear combinations and introducing the IFM observable.

8.2 Implementation

The validation of the IFM-based techniques developed in Chapter 5 has been performed in Chapter 6 and 7 in post-processing mode. This is by estimating the IFM observable in post processing in a Matlab environment. Then the estimated IFM has been applied to the POINT software for position solution calculations. Ultimately, the IFM-based techniques should be applied in real time by automating the whole process from

IFM estimation to multipath mitigation. This can be done by modifying any GNSS software capable of processing dual frequency carrier phase measurements. This section proposes methods for including the IFM-based multipath mitigation capability in a GNSS software.

8.2.1 IFM-BASED MASKING

To add the IFM-based multipath detection capability to the target software, a module with a few basic operations is required. Such a module must be able to save carrier phase measurements in two frequencies for an expected maximum length of one IFM period and estimate the IFM observable according to its model. For multipath detection, the IFM observable can be estimated at a much lower rate than the measurements. In fact the rate of the IFM observable required in calculating the multipath metric is directly proportional to the multipath frequency. Low frequency multipath needs a lower rate of the IFM observable to be used in multipath metric calculation and *vise versa*.

By decreasing the rate of the IFM observable, less memory and processing power are consumed and hence, efficiency is increased. The processing power and memory usage can be further reduced by calculating the multipath metric only for those satellites which are more prone to high levels of multipath. The elevation angle could be used to identify such satellites. A better strategy is to calculate the multipath metric at a very low rate of the IFM continuously. If a high level of multipath is detected, the rate can then be increased to get a more reliable multipath metric. The detected satellite with a high level

of carrier multipath error can then be excluded easily by giving its measurement a very low weight. At the same time the multipath level must be monitored continuously. If the multipath error level becomes acceptable, the measurements are then given a corresponding higher weight. Therefore, IFM-based masking does not require significant modifications to the satellite exclusion in the software.

8.2.2 IFM-BASED CORRECTION

In the POINT software linear combinations of measurements are formed and the IFM-based correction applied based on the appropriate correction model. The correction applied to the measurements in this way must be at the same rate as the measurement.

This process can be automated easily by introducing modified IF or WL observables having less multipath errors instead of using conventional IF or WL observables and then correcting the observables. If this is possible, the correction process does not need extra implementation. In this section it is attempted to derive a modified version of IF and WL observables contaminated with the same level of multipath as measurements after applying the correction technique introduced in this work. These new combinations are named as Multipath Free IF (MFIF) and Multipath Free WL (MFWL) observables.

8.2.2.1 Multipath Free IF observable

To obtain the MFIF, the conventional IF formula is written as:

$$\varphi_{if(cycle)} = \frac{f_1^2}{f_1^2 - f_2^2}\varphi_{L1(cycle)} - \frac{f_2^2}{f_1^2 - f_2^2}\varphi_{L1(cycle)} + B$$

8.1

where

$$B = \frac{f_2^2}{f_1^2 - f_2^2}\varphi_{L1(cycle)} - \frac{f_1\ f_2}{f_1^2 - f_2^2}\varphi_{L2(cycle)}$$

Equation 8.1 is the same as the original IF equation with addition and subtraction of a common term. If all the carrier phase errors in L1 and L2 frequencies are named as E_1 and E_2 respectively, the B part of equation 8.1 can be expanded as:

$$B = \frac{f_2^2}{f_1^2 - f_2^2}\varphi_{L1(cycle)} - \frac{f_1\ f_2}{f_1^2 - f_2^2}\varphi_{L2(cycle)}$$

$$= \frac{f_2^2}{f_1^2 - f_2^2}\left(\frac{f_1}{c}\rho \quad - N_{L1} + E_1\right) - \frac{f_1\ f_2}{f_1^2 - f_2^2}\left(\frac{f_2}{c}\rho \quad - N_{L2} + E_2\right)$$

$$= \frac{f_1 f_2^2}{c(f_1^2 - f_2^2)}\rho \quad - \frac{f_2^2}{f_1^2 - f_2^2}N_{L1} + \frac{f_2^2}{f_1^2 - f_2^2}E_1 \ - \frac{f_1 f_2^2}{c(f_1^2 - f_2^2)}\rho$$

$$+ \frac{f_1\ f_2}{f_1^2 - f_2^2}N_{L2} - \frac{f_2^2}{f_1^2 - f_2^2}E_2$$

8.2

After eliminating the common terms B can be written as:

$$B = \frac{f_1\ f_2}{f_1^2 - f_2^2}N_{L2} - \frac{f_2^2}{f_1^2 - f_2^2}N_{L1} + \frac{f_2^2}{f_1^2 - f_2^2}E_1 - \frac{f_1\ f_2}{f_1^2 - f_2^2}E_2 = C + V$$

where C consists of all constant terms and V all the variable terms.

Based on the analysis made for IFM estimation in chapter 5, the only variable terms in B are carrier multipath errors (with zero mean) and ionospheric error (differenced IFI). It was also shown in Section 5.3.2 that differenced IFI can be assumed approximately constant (relative to the multipath error) for some time window depending on the baseline. Therefore, using the mean of B in equation 8.1 eliminates a large part of the carrier multipath. MFIF is then obtained as:

$$\varphi_{MFIF(cycle)} = \frac{f_1^2}{f_1^2 - f_2^2}\varphi_{L1(cycle)} - \frac{f_2^2}{f_1^2 - f_2^2}\varphi_{L1(cycle)} + \overline{B} \qquad 8.3$$

or

$$\varphi_{MFIF(cycle)} = \varphi_{L1(cycle)} + \overline{B} \qquad 8.4$$

The optimum time window in the MFIF observable follows the same rule as the time window used for IFM estimation discussed in chapter 5. The multipath level of MFIF is the same as IF measurements corrected based on the IFM-based multipath correction. This can be shown by expressing the MFIF observable in the units of length. Therefore, applying the IFM-based correction on IF and using the MFIF observable provide the same performance.

8.2.2.2 Multipath Free WL observable

Similar to the MFIF combination, the MFWL is introduced in this section which contains much less multipath error compared to the conventional WL observable. To obtain the MFWL, the conventional WL formula is written as:

$$\varphi_{WL(cycle)} = \varphi_{L1(cycle)} - \frac{f_2}{f_1}\varphi_{L1(cycle)} + B \qquad 8.5$$

where

$$B = \frac{f_2}{f_1}\varphi_{L1(cycle)} - \varphi_{L2(cycle)}$$

Equation 8.5 is the same as the original WL equation with addition and subtraction of a common term. If all the carrier phase errors in L1 and L2 frequencies are referred to as E_1 and E_2 respectively, the B part of equation 8.5 can be expanded as:

$$B = \frac{f_2}{f_1}\varphi_{L1(cycle)} - \varphi_{L2(cycle)} = \frac{f_2}{f_1}\left(\frac{f_1}{c}\rho - N_{L1} + E_1\right) - \left(\frac{f_2}{c}\rho - N_{L2} + E_2\right)$$
$$= \frac{f_2}{c}\rho - \frac{f_2}{f_1}N_{L1} + \frac{f_2}{f_1}E_1 - \frac{f_2}{c}\rho + N_{L2} - E_2 \qquad 8.6$$

After eliminating the common terms, B can be written as:

$$B = N_{L2} - \frac{f_2}{f_1} N_{L1} + \frac{f_2}{f_1} E_1 - E_2 = C + V$$

8.7

where C consists of all constant terms and V all the variable terms.

Based on the analysis made for IFM estimation in chapter 5, the only variable terms in B are carrier multipath errors (with zero mean) and ionospheric error (differenced IFI). It was also shown in Section 5.3.2 that differenced IFI can be assumed approximately constant (relative to the multipath error) for some time window depending on the baseline. Therefore, using the mean of B in equation 8.5 eliminates a big part of carrier multipath. MFWL is obtained as:

$$\varphi_{MWL(cycle)} = \varphi_{L1(cycle)} - \frac{f_2}{f_1} \varphi_{L1(cycle)} + \overline{B}$$

8.8

or

$$\varphi_{MWL(cycle)} = 0.221 * \varphi_{L1(cycle)} + \overline{B}$$

8.9

The optimum time window in the MFWL observable follows the same rule as the time window used for IFM estimation discussed in chapter 5. The MFWL observable has the same level of multipath as the corrected WL observable based on the IFM observable. This can be shown by expressing the MFWL observable in units of length. Therefore, both techniques have the same level of performance.

Introducing the MFIF and MFWL in this section significantly facilitates the implementation of IFM-based multipath correction in available software. When using these new observables, the only parameter which needs to be identified is the window length. This could be done based on a minimum or maximum window length strategy discussed in IFM estimation in chapter 5.

8.2.3 IFM-BASED WEIGHTING

The IFM-based stochastic model introduced in this thesis is a combination of the simple elevation weighting model and the IFM observable. Therefore, the IFM-based weighting can be implemented as complementary to the simple elevation based weighting techniques. IFM-based weighting must be applied at the same rate as the measurement. Therefore, the amount of extra memory and processing power is similar to the IFM-based correction technique.

8.3 Recommendations for future works

8.3.1 MULTIPLE REFLECTION EFFECT ON MULTIPATH MITIGATION

Reflection from the ground is very common in high accuracy applications such as surveying. Such reflections are difficult to mitigate by existing techniques due to having short delay relative to the direct signal. Therefore, real data used in this thesis were collected in relatively open environment and the dominant multipath was due to

reflection from ground. On the other hand, reflection from one dominant surface creates a relatively simple sinusoid signature in the IFM observable. This simplifies estimating the IFM observable and hence simplifies IFM-based multipath mitigations. However, in some applications the reflection might happen from different reflection surfaces. In such a scenario the IFM observable becomes more complex and contains several zero mean sinusoidal signals superimposed on top of each other. Since the complex IFM observable still exhibits a zero mean characteristic, the IFM-based multipath mitigation techniques developed in this thesis can be applied on the multipath error caused from several reflections. By increasing number of reflections multipath will tend more towards random noise. In other words the IFM frequency is higher in such environments and hence a shorter time window is needed for the IFM estimation. Further work is required on the validation of IFM-based multipath mitigation techniques for complex environments which have multiple reflector surfaces in the vicinity of the antenna.

8.3.2 DYNAMICITY EFFECT ON MULTIPATH MITIGATION

In some of the main high accuracy positioning applications such as surveying it is sufficient to perform positioning in static mode. Therefore, the real data used in this thesis were collected in the static mode. Fortunately, the multipath error has a simple signature in static mode compared to the dynamic mode. However, performing high accuracy positioning in a dynamic situation may also be necessary in some applications. For example, in surveying dynamic positioning can save time and money. Therefore, it is beneficial to assess the IFM-based multipath mitigation techniques for dynamic

situations. With increasing movement of the antenna it is expected that the frequency of IFM increases and it becomes more like Gaussian noise. A similar effect can be seen on SNR analysed in (Lau and Cross 2007b). However, according to the analysis in Chapter 4 SNR is not directly correlated to carrier multipath error. Hence, it cannot be used for multipath modelling and multipath mitigation in dynamic situations. On the other hand, if changes in the surrounding environment make the IFM observable completely like noise, it still represents the carrier multipath error. Therefore, the IFM-based multipath mitigation techniques are applicable for such situations. It should be noted that the high frequency IFM observable requires a shorter time window to be estimated which makes the process even easier. Future work should address the performance of the IFM-based mitigation techniques for dynamic applications.

8.3.3 SMART IFM CYCLE DETECTION

It has been determined in this thesis that the desirable time window to estimate the IFM observable is the minimum time which contains approximately one cycle of the IFM observable. Calculating the IFM cycle requires good estimation of the reflector distance from the antenna. Such information may not be always available. Therefore, it is desirable to develop a smart algorithm which defines the phase of IFM at each epoch and hence detect the IFM cycle. As discussed in Chapter 5, this can be done by applying an adaptive notch filter similar to the SNR based multipath estimation technique proposed in (Lau and Cross 2007b) .

8.3.4 INTER MULTIPLE FREQUENCY CARRIER MULTIPATH OBSERVABLE

In this research, the IFM observable has been estimated for linear combination of measurements obtained from two frequencies (i.e. IF and WL). With the increasing number of available GNSS frequencies many new possible linear combinations will emerge. The common problem of such combinations is the possible increase in the level of noise and multipath errors. Hence, the approach used for carrier multipath error mitigation in IF and WL can be extended to the measurements formed from more than two frequencies. For future work it is suggested to investigate the prospect of introducing Inter Multiple Frequency carrier Multipath (IMFM) error and developing carrier multipath model for the new combinations based on IMFM. Such a model may have several benefits including carrier multipath mitigation.

8.3.5 CODE MULTIPATH DETECTION

The IFM observable has been introduced in this research for carrier phase measurements and the corresponding mitigation techniques were developed to mitigate the error in carrier phase measurements. The application of the IFM-based mitigation techniques to code phase measurements depends on the characteristics of the code multipath error. It has been shown that the code multipath mean deviates from zero with increasing multipath delay (Ray 2000). The deviation is larger for strong reflections. On the other hand, estimating the IFM observable based on the process used in this research requires multipath error with zero mean. Therefore, if the same process is applied for

code measurements, the IFM observable will not represent the multipath error correctly. However, the mean value does not affect the peak to peak values of the errors. Therefore, the IFM observable obtained from code measurements can be used in multipath metric calculation in the same way as used in carrier phase measurements to develop the IFM-based masking technique. Further investigation is required into the IFM observable estimation for code measurements and validation of IFM-based masking using code measurements.

REFERENCES

Angrisano A, Gaglione S, Gioia C, Massaro M, Robustelli U, Santamaria R (2011) Ionospheric models comparison for single-frequency GNSS positioning. ENC 2011

Barnes J, Ackroyd N, Cross P (1998) Stochastic modelling for very high precision real-time kinematic GPS in an engineering environment. In: XXI Congress of the International Federation of Surveyors, 1998. pp 61 - 76

BDS (2014) BeiDou Navigation Satellite System. http://en.beidou.gov.cn.

Benachenhou K, Sari E, Hammadouche M (2009) Multipath mitigation in GPS/Galileo receivers with different signal processing techniques. In: IEEE: 5th International conference: Sciences of Electronic, Technologies of Information and Telecommunications, 2009. pp 1-8

Bidaine B, Warnant R (2011) Ionosphere modelling for Galileo single frequency users: illustration of the combination of the NeQuick model and GNSS data ingestion. Advances in Space Research 47 (2):312-322

Bilich A, Larson KM (2007) Mapping the GPS multipath environment using the signal-to-noise ratio (SNR). Radio Science 42 (6):RS6003

Borre K, Akos DM, Bertelsen N, Rinder P, Jensen SH (2007) A software-defined GPS and Galileo receiver: a single-frequency approach. Springer,

Christie J, Pervan B, Enge P, Powell J, Parkinson B, Ko P (1998) Analytical and experimental observations of ionospheric and tropospheric decorrelation effects for differential satellite navigation during precision approach. In: Proc. ION GPS, 1998. Institute of Navigation, pp 739-748

Comp CJ, Axelrad P (1998) Adaptive SNR-based carrier phase multipath mitigation technique. Aerospace and Electronic Systems, IEEE Transactions on 34 (1):264-276

DoD (2008) Global Positioning System Standar Positioning Service Performance Standard. fourth edn. Department of Defence (Dod) USA, USA

ESA (2002) Mission High Level Definition. European commision,

Euler H-J, Schaffrin B (1991) On a measure for the discernibility between different ambiguity solutions in the static-kinematic GPS-mode. In: Kinematic Systems in Geodesy, Surveying, and Remote Sensing. Springer, pp 285-295

GALA (2000) Galileo Overall Architecture Study: Preliminary User Requirements. Ref: GALA-Racalcs-003 Report

Galuscak–OM6AA R, Hazdra P (2006) Circular polarization and polarization losses. DUBUS,

Gao Y, Heroux P, Kouba J (1994) Estimation of GPS receiver and satellite L1/L2 signal delay biases using data from CACS. Paper presented at the Proceedings of the International Symposium on Kinematic Systems in Geodesy, Geomatics and Navigation, Banff, Canada,

Garin L, van Diggelen F, Rousseau JM (1996) Strobe & edge correlator multipath mitigation for code. In, 1996. pp 657-664

GPSWold (2011) GLONASS Modernization. GPS World. http://gpsworld.com/glonass-modernization-12232/.

Groves P (2008) Principles of GNSS, Inertial and Multisensor Integrated Navigation Systems. Artech House

Hannah BM (2001) Modelling and simulation of GPS multipath propagation.

Hartinger H, Brunner F (1999) Variances of GPS Phase Observations: The SIGMA-Model. GPS solutions 2 (4):35-43

Hefty J, Gerhatova Ľ (2013) Using GPS multipath for snow depth sensing-first experience with data from permanent stations in slovakia.

Irsigler M, Eissfeller B (2001) Comparison of multipath mitigation techniques with consideration of future signal structures. In, 2001. pp 2584-2592

Jenkins B, Caswell I (2007) GNSS Evolution Next Enhancement of System Infrastructures (GENESI), Forcast of mid and long term users' needs. Technical report.

Kaplan ED, Hegarty CJ (2006) Understanding GPS: principles and applications. Artech house,

Komjathy A (1997) Global ionospheric total electron content mapping using the Global Positioning System. PhD Dissertation, University of New Brunswick, CANADA

Komjathy A, Langley R (1996) An assessment of predicted and measured ionospheric total electron content using a regional GPS network. In: Proceedings of the National Technical Meeting of the Institute of Navigation, 1996. pp 615-624

Kouba J, Heroux P (2000) GPS Precise Point Positioning using IGS orbit products. GPS solutions 5 (2):12-28

Kubo N, Yasuda A (2003) How multipath error influences on ambiguity resolution. In, 2003.

Kunysz W (2003) A three dimensional choke ring ground plane antenna. In, 2003. pp 9-12

Larson KM, Small EE, Gutmann E, Bilich A, Axelrad P, Braun J (2008) Using GPS multipath to measure soil moisture fluctuations: Initial results. GPS Solutions 12 (3):173-177

Lau L, Cross P (2006) A New Signal-to-Noise-Ratio Based Stochastic Model for GNSS High-Precision Carrier Phase Data Processing Algorithms in the Presence of Multipath Errors.

Lau L, Cross P (2007a) Development and testing of a new ray-tracing approach to GNSS carrier-phase multipath modelling. Journal of Geodesy 81 (11):713-732. doi:10.1007/s00190-007-0139-z

Lau L, Cross P (2007b) Investigations into Phase Multipath Mitigation Techniques for High Precision Positioning in Difficult Environments. Journal of Navigation 60 (03):457-482. doi:10.1017/S0373463307004341

Leick A (2004) GPS satellite surveying. 3rd edn. Wiley. com, Canada

Lim W, Jang H, Yu J (2010) New method for back lobe suppression of microstrip patch antenna for GPS. In, 2010. IEEE, pp 679-682

Liu X (2001) A comparison of stochastic models for GPS single differential kinematic positioning. In: Proceedings of the 15th International Technical Meeting of the Satellite Division of The Institute of Navigation (ION GPS 2002), 2001. pp 1830-1841

Ma L, Wang H, Chen J (2010) Analysis of Kalman Filter with Correlated Noises under Different Dependence. Journal of Information & Computational Science 7 (5):1147-1154

Mannucci A, Wilson B, Yuan D, Ho C, Lindqwister U, Runge T (1998) A global mapping technique for GPS-derived ionospheric total electron content measurements. Radio Science 33 (3):565-582

McGraw G, Braasch M (1999) GNSS multipath mitigation using gated and high resolution correlator concepts. In, 1999. pp 333-342

Mendes V, Langley R (1998) Tropospheric zenith delay prediction accuracy for airborne GPS high-precision positioning. In: Proceedings of The Institute of Navigation 54th Annual Meeting, 1998. pp 337-347

Moernaut GJK, Orban D (2008) Basics Of GPS Antennas.

Najibi N, Jin S (2013) Physical Reflectivity and Polarization Characteristics for Snow and Ice-Covered Surfaces Interacting with GPS Signals. Remote Sensing 5 (8):4006-4030

Notarpietro R, Cucca M, Bonafoni S (2012) GNSS Signals: A Powerful Source for Atmosphere and Earth's Surface Monitoring.

NovAtel (2014). http://www.novatel.com/products/software/grafnav/.

OS (2014) Ordnance Survey. http://www.ordnancesurvey.co.uk/about/.

Perevalova N, Polyakova A, Zalizovski A (2010) Diurnal variations of the total electron content under quiet helio-geomagnetic conditions. Journal of Atmospheric and Solar-Terrestrial Physics 72 (13):997-1007

Puchrik L, Svabensky O, Pospisil L, Weigel J (2014) New velocity analysis in geodynamic network Sneznik based on GNSS measurement processing using reprocessed IGS product. ACTA Geodynamica Et Geomaterialia 11 (1):17-22

Ragheb A, Clarke P, Edwards S (2007) GPS sidereal filtering: coordinate-and carrier-phase-level strategies. Journal of Geodesy 81 (5):325-335

Rao GS (2010) Global Navigation Satellite Systems: with Essentials of Satellite Communications. Tata McGraw Hill,

Ray J, Cannon M (1999) Characterization of GPS carrier phase multipath. In: Proc. ION-NTM-1999, San Diego, CA, January 25 - 27 1999. pp 343 - 352

Ray JK (2000) Mitigation of GPS code and carrier phase multipath effects using a multi-antenna system. University of Calgary,

Rim H, Schutz B (2002) Precision orbit determination (POD). Algorithm Theoretical Basis Document, Center for Space Research, The University of Texas at Austin, Austin, Tex, USA

Rizos C (1997) Principles and practice of GPS surveying. University of New South Wales,

Rost C, Wanninger L (2010) Carrier phase multipath corrections based on GNSS signal quality measurements to improve CORS observations. In: Position Location and Navigation Symposium (PLANS), 2010 IEEE/ION, 4-6 May 2010 2010. pp 1162-1167. doi:10.1109/plans.2010.5507235

Sabatini MR, Palmerini GB (2008) Differential Global Positioning System (DGPS) for Flight Testing.

Sahmoudi M, Landry RJ (2008) Multipath Mitigation techniques using maximum-likelihood principle. Inside GNSS 3(8):24-29

Samama N (2008) Global positioning: Technologies and performance, vol 7. John Wiley & Sons,

Schaer S (1999) Mapping and predicting the Earth's ionosphere using the global positioning system. PhD Dissertation, University of Bern,

SDCM (2012). http://www.sdcm.ru/index_eng.html.

Segall P, Davis JL (1997) GPS applications for geodynamics and earthquake studies. Annual Review of Earth and Planetary Sciences 25 (1):301-336

Swatschina P Geowissenschaftliche mitteilungen.

Teunissen P (1995) The least-squares ambiguity decorrelation adjustment: a method for fast GPS integer ambiguity estimation. Journal of Geodesy 70 (1):65-82

Teunissen P, De Jonge P, Tiberius C (1996) The Volume of the GPS Ambiguity Search Space and its Relevance for Integer Ambiguty Resolution. In: PROCEEDINGS OF ION GPS, 1996. Citeseer, pp 889-898

Teunissen P, Joosten P, Tiberius C (2002) A comparison of TCAR, CIR and LAMBDA GNSS ambiguity resolution. In: Proceedings of ION GPS, 2002. pp 24-27

Wanninger L, Wallstab-Freitag S (2007) Combined processing of GPS, GLONASS, and SBAS code phase and carrier phase measurements. In: Proc. ION GNSS, 2007. pp 866-875

Weill LR (2003) Multipath Mitigation. GPS World,

Wieser A, Brunner FK (2000) An extended weight model for GPS phase observations. Earth planets and space 52 (10):777-782

Ye S, Chen D, Liu Y, Jiang P, Tang W, Xia P (2014) Carrier phase multipath mitigation for BeiDou navigation satellite system. GPS Solutions:1-13